NEANDC(E)-322-U Vol. V
INDC(Ger)-36/LN+Special
KfK 4953

PROGRESS REPORT ON NUCLEAR DATA RESEARCH IN THE FEDERAL REPUBLIC OF GERMANY

for the Period April 1, 1990 to March 31, 1991

July 1991

Edited by
S. Cierjacks
Kernforschungszentrum Karlsruhe
Institut für Materialforschung
Federal Republic of Germany

NEANDC(E)-322-U Vol. V
INDC(Ger)-36/LN+Special
KfK 4953

PROGRESS REPORT ON NUCLEAR DATA RESEARCH IN THE FEDERAL REPUBLIC OF GERMANY

for the Period April 1, 1990 to March 31, 1991

July 1991

Edited by
S. Cierjacks
Kernforschungszentrum Karlsruhe
Institut für Materialforschung
Federal Republic of Germany

PREFACE

This report has been prepared to promote the exchange of nuclear data research information between the Federal Republic of Germany and other member states of NEA and IAEA. It includes for the first time also contributions from laboratories of the previous Democratic Republic of Germany. Thus it brings together progress reports from KfK Karlsruhe, KFA Jülich, ZfK Rossendorf, ZfI Leipzig the Universities of Dresden, Hannover, Köln, Mainz, München and Stuttgart, as well as from PTB Braunschweig and FIZ Karlsruhe. As in previous years, the emphasis of the work reported here is on measurement, compilation and evaluation of application-oriented nuclear data, such as those relevant to fission- and fusion-reactor technologies, development of intense neutron sources, astrophysics research, cosmogenic and meteoritic investigations, production of medically important radioisotopes, etc.

Each contribution is presented under the laboratory heading where the work was done. When the work is relevant to requests in the World Request List for Nuclear Data, WRENDA 83/84 (INDC(SEC)-88/URSF), the corresponding request identification numbers are given in the headings of the respective laboratory reports.

Karlsruhe, July 1991 S. Cierjacks

CONTENTS

ABTEILUNG NUKLEARCHEMIE
UNIVERSITÄT ZU KÖLN
AND
ZENTRALEINRICHTUNG FÜR STRAHLENSCHUTZ
UNIVERSITÄT HANNOVER

Page

KERNFORSCHUNGSZENTRUM KARLSRUHE
INSTITUT FÜR KERNPHYSIK

1. ^{87}Rb: *s*-PROCESS NUCLEOSYNTHESIS AT N = 50

D. Neuberger and F. Käppeler

^{87}Rb is one of the neutron magic nuclei with N = 50, which are characterized by particularly small cross sections. Therefore, these isotopes are efficiently produced in the *s*-process, so that their *s*-abundances exceed by far the respective *r*-process contributions. The mass range at N = 50 is important because of the fact that two different *s*-processes - commonly addressed as *weak* and *main* *s*-process component (1) - contribute about equally to the observed abundances. For a detailed discussion of *s*-process nucleosynthesis in the mass region $84 < A < 90$ it is, therefore, necessary to start with accurate cross sections for these critical nuclei. The present study of the ^{87}Rb cross section continues a program for the investigation of neutron magic nuclei (2).

The stellar neutron capture cross section of ^{87}Rb has been measured by the activation technique. Neutrons were produced by the ^{7}Li(p,n)^{7}Be reaction at a proton energy of 1912 keV. The resulting neutron spectrum allows directly to determine the stellar cross section for a thermal energy of kT = 25 keV (3,4). Natural Rb_2SO_4 samples with thicknesses between 0.7 and 70 mg/cm^2 were sandwiched between gold foils during the irradiations in order to use the gold cross section as a standard. After irradiation, the induced activity was measured by detecting the beta decay electrons of ^{88}Rb in a 4π Si(Li) spectrometer.

In addition, 1.5 and 2 mm thick self-supporting Rb_2SO_4 tablets were irradiated as well. In these cases, the induced activity was determined with a HPGe detector via the intense gamma-ray lines at 898 and 1836 keV. With both methods, consistent cross sections were obtained. The present result for a thermal energy of kT = 25 keV is compared in Fig. 1 with previous values (5 - 8). Note that the uncertainties achieved in the present work are more than two times smaller than those of the existing data. Agreement within the quoted uncertainties is obtained with the recent measurements of Beer and Macklin (7) and of Jaag (8). This holds also for the calculated cross section of Harris (5), but this value carries an uncertainty of at least 50%. The astrophysical consequences of the improved ^{87}Rb cross section are presently investigated.

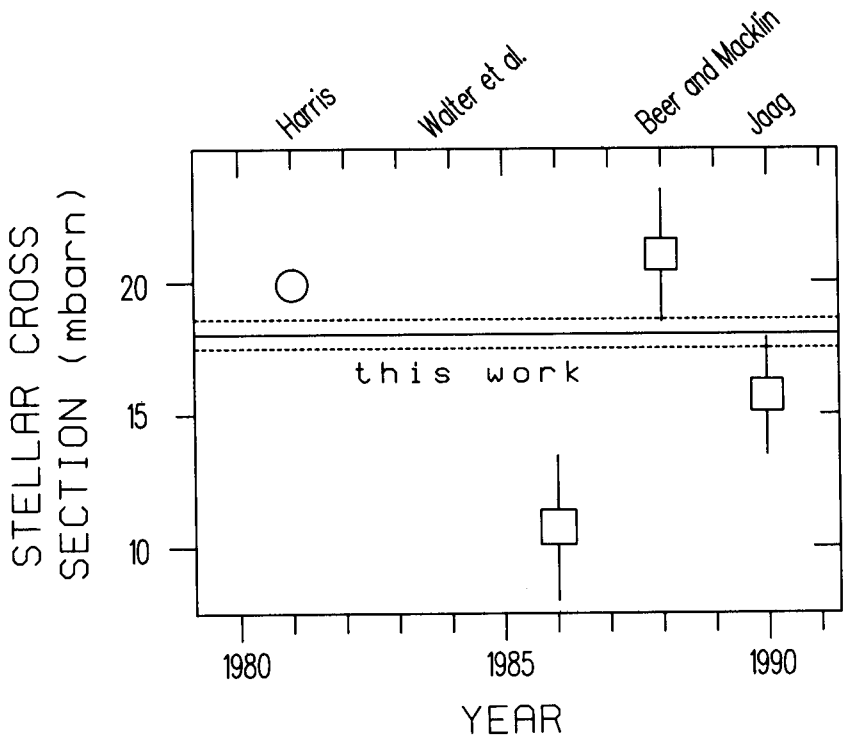

Fig. 1. Comparison of the present stellar ^{87}Rb cross section with previous results.

(1) F. Käppeler, H. Beer, and K. Wisshak, Rep. Prog. Phys. 52, 945 (1989).
(2) F. Käppeler, W. R. Zhao, H. Beer, and U. Ratzel, Ap. J. 355, 348 (1990).
(3) H. Beer and F. Käppeler, Phys. Rev. C 21, 534 (1980).
(4) W. Ratynski and F. Käppeler, Phys. Rev. C 37, 595 (1988).
(5) M. J. Harris, Ap. Space Sci. 77, 357 (1981).
(6) G. Walter, H. Beer, F. Käppeler, and R.-D. Penzhorn, Astron. Astrophys. 155, 247 (1986).
(7) H. Beer and R. L. Macklin, Ap. J. 339, 962 (1989).
(8) S. Jaag, Dipl. thesis, University of Karlsruhe (1990).

2. THE STELLAR CROSS SECTIONS OF ^{120}Sn, ^{121}Sb, ^{123}Sb, AND ^{128}Te – A STUDY OF POSSIBLE s-PROCESS BRANCHINGS AT A = 121, 122

W. Schanz, G. Rupp, F. Käppeler

The *s*-process neutron capture flow in the mass region 120 < A < 126 is characterized by possible branchings at A = 121, 122 (Fig. 1). Due to the short half-lives of the branch point isotopes ^{121}Sn and ^{122}Sb, these branchings are significant only for the comparably high neutron densities predicted by stellar models. In that case, the *s*-only isotopes ^{122}Te and ^{123}Te would be partly bypassed by the neutron capture flow, and only the

third *s*-only isotope, ^{124}Te, would experience the total exposure. The importance of accurate Te cross sections for the definition of these branchings is addressed in the following contribution. In addition, improved cross sections of other relevant nuclei were required for a quantitative branching analysis.

The stellar cross sections of ^{120}Sn, ^{121}Sb, ^{123}Sb, and ^{128}Te were determined in a series of activation measurements. The irradiations were carried out in the neutron field obtained via the ^{7}Li(p,n)^{7}Be reaction at a proton energy of 1912 keV, that is known to yield the proper stellar average cross section for a thermal energy of kT = 25 keV (1,2). Repeated activations with different experimental parameters (neutron flux, sample thickness and diameter) allowed for investigation of systematic uncertainties. In case of the Sb isotopes, the induced activities were determined by gamma counting via the decay lines at 564 keV (^{122}Sb) and at 603 keV (^{124}Sb) with a calibrated HPGe detector. Since no gamma-rays are emitted in the decay of the other isotopes, the induced activities had to be measured via the beta decay electrons, instead. Accordingly, thin samples of isotopically enriched material were irradiated, which were then counted in a 4π electron spectrometer with an efficiency of 97%. An example of such an electron spectrum is given in Fig. 2. By the simultaneous irradiation of appropriate gold foils, all cross sections were measured relative to the standard cross section of ^{197}Au (2). For the final results, experimental uncertainties between 2.7 and 3.8 % could be achieved. The comparison with previous data shows large discrepancies of up to 50%.

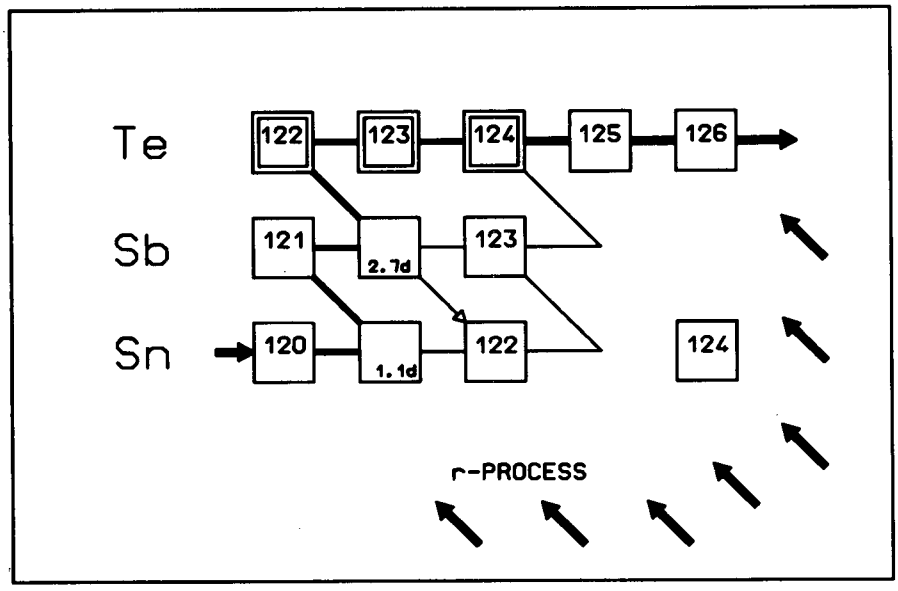

Fig. 1 The *s*-process flow between ^{120}Sn and ^{126}Te with the possible branchings at A = 121, 122.

The description of the *s*-process in the mass range $120 < A < 126$ with the classical approach (3) yields practically no branchings at A = 121, 122, thus confirming the σN equality for the *s*-only isotopes ^{122}Te, ^{123}Te, and ^{124}Te predicted by the 'local approximation'. However, the currently best stellar model for the *s*-process, i.e. for helium shell burning in low mass AGB stars of low metallicity (Ref. 4 and references therein) leads, indeed, to significant branchings, resulting in 5% lower σN values for ^{122}Te and ^{123}Te than for ^{124}Te. The consequences of this discrepancy between the classical approach and the stellar model are discussed in the next contribution.

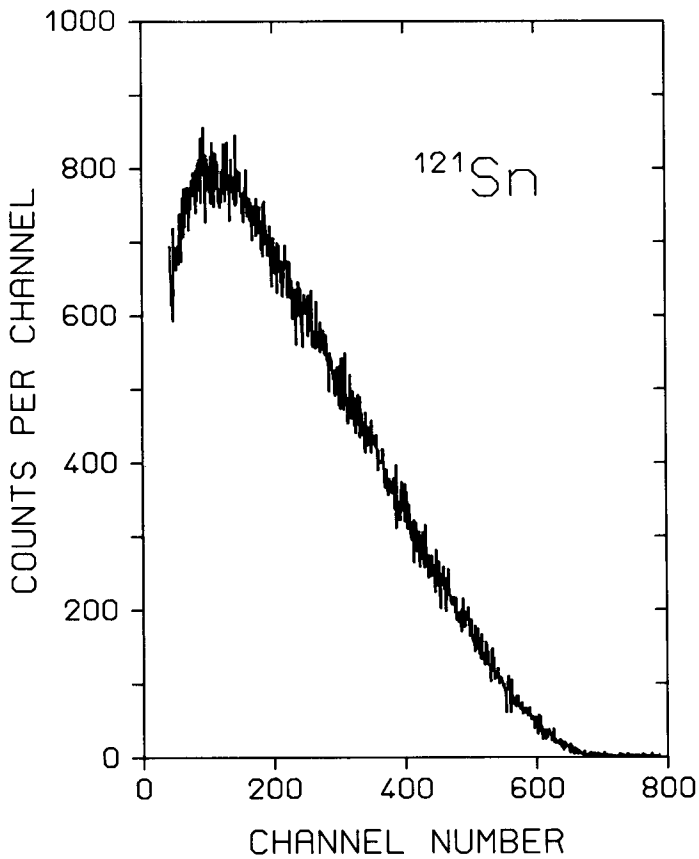

Fig. 2 The electron spectrum from the decay of ^{121}Sn ($t_{1/2}$ = 27 h) measured with the 4π electron spectrometer

(1) H. Beer and F. Käppeler 1980, Phys. Rev. C, 21, 534.
(2) W. Ratynski and F. Käppeler 1988, Phys. Rev. C, 37, 595.
(3) F. Käppeler, H. Beer, and K. Wisshak, 1989, Rep. Prog. Phys., 52, 945.
(4) R. Gallino 1989, *The Evolution of Peculiar Red Giants*, IAU Symposium No. 106, eds. H. Johnson and B. Zuckerman (Cambridge, Cambridge University Press) p. 176.

3. MEASUREMENT OF THE keV NEUTRON CAPTURE CROSS SECTIONS OF ^{122,123,124,125,126}Te WITH THE KARLSRUHE 4π BaF_2 DETECTOR

K. Wisshak, F. Voß, F. Käppeler and G. Reffo*.

The neutron capture cross sections of ^{122,123,124,125,126}Te have been measured in the neutron energy range from 10 to 200 keV using the Karlsruhe 4π BaF_2 detector for the registration of capture gamma-ray cascades. Neutrons were produced via the ^{7}Li(p,n)^{7}Be reaction by bombarding metallic Li targets with the pulsed proton beam of a 3.75 MV Van de Graaff accelerator. The neutron energy was determined by time of flight. The flight path of the experiment was 78 cm, the time resolution 1 ns. The cross sections were determined relative to the standard cross section of gold.

Three independent runs have been performed with maximum neutron energies of 70, 100 and 200 keV, respectively. While runs with low maximum neutron energies offer optimum signal to background ratio in the most important energy region around 30 keV (see below), the data measured around 200 keV gave optimum accuracy for the absolute normalization of the cross section ratio. The threshold in the sum energy of the 4π detector was varied between 1.8 and 2.5 MeV. In case of the low threshold, the absolute efficiency for capture events was larger than 95% for the even and larger than 98% for the odd tellurium isotopes. Highly enriched metallic samples were used with masses between 0.5 g (^{123}Te) and 4 g (^{126}Te).

Preliminary data for the capture cross sections of ^{122,123,124}Te are given in Fig.1. The experimental cross section ratios have been converted into absolute values using the gold standard cross section from literature as described in Ref. (1). The statistical uncertainty of the cross sections for the energy bins of Fig. 1 is about 1 % above 20 keV. The systematic uncertainties are not yet evaluated completely but are expected to be well below 1 % for the cross section ratios. The uncertainty of the gold cross section is 1.5 % (see Ref. 1).

The isotopes of tellurium play an important role in s-process studies. It is the only element with three s-only isotopes, i.e. ^{122,123,124}Te. Since the isotopic abundances are known with uncertainties of 0.1 %, accurate stellar cross sections of these isotopes offer the possibility to check the 'local approximation' predicted by the classical s-process model which means that the product of s-abundance and stellar cross section is constant for neighboring isotopes. A preliminary evaluation of the Maxwellian averaged cross sections at kT=30 keV was made using the data of Fig. 1, the result of our

experiments with Moxon-Rae detectors in the energy range from 1 to 10 keV (see next contribution) as well as the data of Macklin and Winters above 200 keV (Ref. 2). The ratios $N\sigma(^{122}Te)/N\sigma(^{124}Te)$ and $N\sigma(^{123}Te)/N\sigma(^{124}Te)$ found in this way agreed with the prediction of the classical model to better than 1 %. Since the present uncertainties are about five times smaller than those of previous experiments, this result is significant and - if finally confirmed - would rule out stellar s-process models with comparably high neutron fluxes. These models lead to branchings of the s-process path at ^{121}Sn and ^{122}Sb, which would reduce the $N\sigma$ -values of $^{122,123}Te$ by about 5 % compared to ^{124}Te.

* Comitato Nazionale dell'Energia Nucleare e dell'Energie Alternative, Bologna, Italy

(1) K. Wisshak, F. Voß, F. Käppeler and G. Reffo, Phys. Rev. C42, 1731 (1990).
(2) R.L. Macklin and R.R. Winters report ORNL-6561 Oak Ridge National Laboratory (1989).

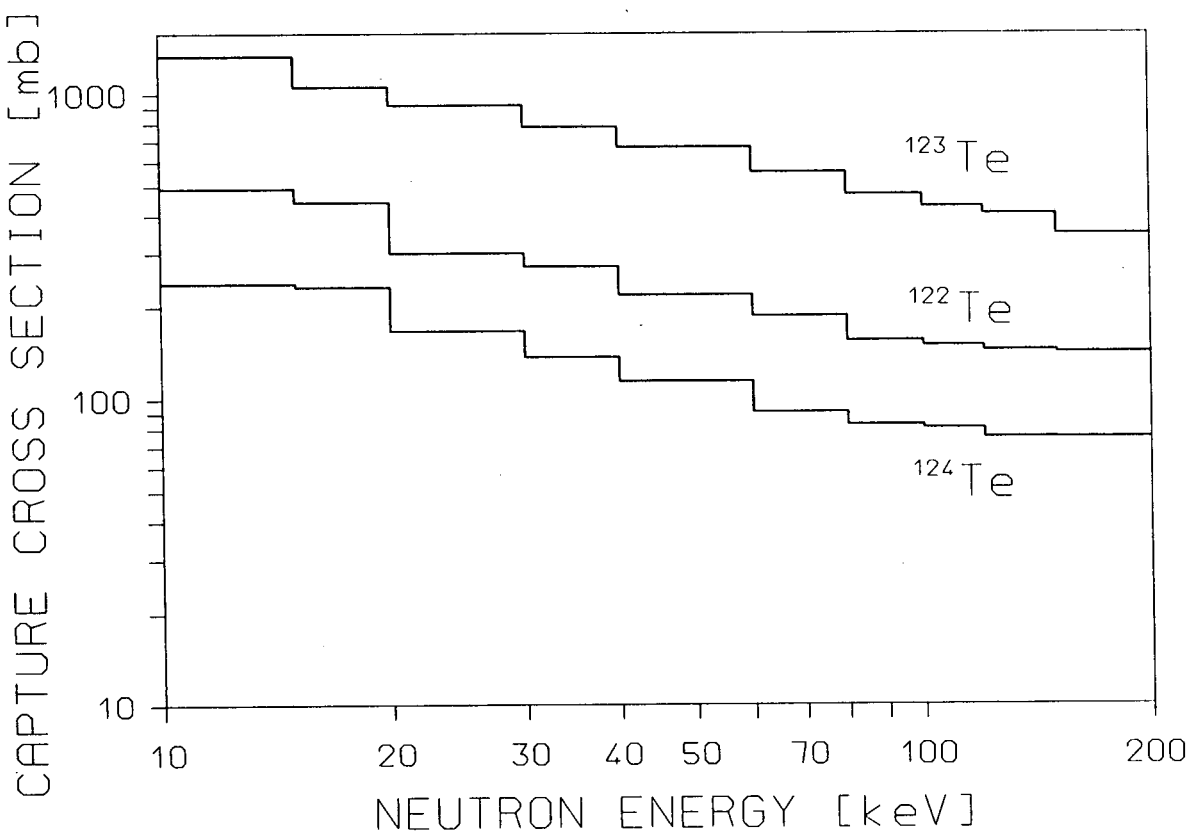

Fig.1 Preliminary results for the neutron capture cross section of $^{122,123,124}Te$ in the neutron energy range from 10 to 200 keV.

4. NEUTRON CAPTURE CROSS SECTIONS OF ^{122}Te, ^{123}Te, AND ^{124}Te AT LOW ENERGIES

Y. Xia, Th. W. Gerstenhöfer, S. Jaag, F. Käppeler, G. Reffo*, and K. Wisshak

The preceding contribution presents (n,γ) cross section measurements on 5 tellurium isotopes in the energy range from 10 to 200 keV. The experimental uncertainties of ≤1% for cross section ratios are essential for the discussion of *s*-process nucleosynthesis in the mass region between A = 120 and 130. Possible branchings in the neutron capture path at A = 121, 122 being excluded by these data would have important consequences for stellar models of Red Giant stars. The currently favored *s*-process model is helium shell burning in low mass stars of low metallicity, which was shown to reproduce the observed *s*-abundances fairly well (1, 2). Since this model describes a scenario, where most of the neutron exposure takes place at rather low temperatures of $\sim 1.5 \cdot 10^8$ K, corresponding to a thermal energy of kT = 12 keV, the range covered by the 4π BaF_2 detector needs to be extended to lower neutron energies.

For this purpose, we have used a setup of Moxon-Rae detectors (see contr. 5 and 7), which yields sufficient sensitivity down to energies of 1 keV. The measurements were carried out with a flight path of 20 mm under identical conditions as described there. In this way, the differential (n,γ) cross section were determined from 1 to 100 keV with statistical uncertainties smaller than 2%. Normalization to the results obtained with the 4π BaF_2 detector yields then a reliable extrapolation to 1 keV neutron energy.

In addition to the Moxon-Rae detectors, the setup includes a ^{6}Li glass detector under zero degree with respect to the proton beam, which is normally used as a neutron monitor. With that detector it was possible to determine the total neutron cross sections for these isotopes in the present experiment as well. These data are important for the analysis of the results obtained with the 4π BaF_2 detector, since they are required for evaluating the respective neutron scattering corrections (3). Up to now, sufficiently complete total cross sections for the tellurium isotopes were not available in literature. The present results exhibit uncertainties of typically 5%.

*E.N.E.A. Bologna, I-40138 Bologna, Italy

(1) R. Gallino 1989, *The Evolution of Peculiar Red Giants*, IAU Symposium No. 106, eds. H. Johnson and B. Zuckerman (Cambridge, Cambridge University Press) p. 176.
(2) F. Käppeler, R. Gallino, M. Busso, G. Picchio, C. M. Raiteri, Ap. J. 345, 630 (1990).
(3) K. Wisshak, F. Voß, F. Käppeler, and G. Reffo, report KfK 4674, Kernforschungszentrum Karlsruhe (1990); Phys. Rev. C 42, 1731 (1990).

5. ^{147}Pm - An EXPERIMENTAL STELLAR CROSS SECTION FOR A SHORT-LIVED *s*-PROCESS BRANCHING POINT

Th. W. Gerstenhöfer, F. Käppeler, K. Wisshak, and G. Reffo

Radioactive nuclei with $t_{1/2} < 10$ yr hold a key position in the synthesis of the heavy elements. In the *s*-process, neutron captures occur at rates of ~1 yr and are, therefore, comparable to the beta decay rates of some of the involved isotopes, such as ^{147}Pm ($t_{1/2} = 2.6$ yr). The resulting branching of the neutron capture flow yields a characteristic abundance pattern for the neighboring isotopes that can be analyzed in terms of the physical conditions during the *s*-process. In case of ^{147}Pm, these studies yield an estimate for the stellar neutron density (1). For the quantitative discussion of this scenario, the neutron capture cross section of ^{147}Pm was measured for the first time in the keV range via two independent methods: (i) direct detection of the prompt capture gamma-rays by means of Moxon-Rae detectors, using the TOF technique at a neutron flight path of only 2 cm, and (ii) activation in a quasi-stellar neutron spectrum and detection of the induced ^{148}Pm activity.

The measurements were carried out at the Karlsruhe 3.75 MV Van de Graaff accelerator. Neutrons were produced by means of the ^{7}Li(p,n)^{7}Be reaction. For proton energies of 1912 keV this reaction is known to yield a quasi-stellar neutron spectrum for a thermal energy of kT = 25 keV, very close to the conditions during the *s*-process (2, 3). The ^{197}Au(n,γ) reaction was used as a cross section standard (4, 5).

A ^{147}Pm sample was prepared such that it could be used in both measurements. Freshly separated Pm_2O_3 powder with a total activity of about $1.5 \cdot 10^{11}$ Bq was sandwiched between two lead foils, and then pressed to a compact disk. The foils (10 mm in diameter and 0.1 mm thick) were of enriched ^{208}Pb (99.8 %) in order to minimize backgrounds in the TOF measurement.

Activation Measurement: The ^{147}Pm sample was irradiated between two gold foils in a flux of about 10^9 neutrons per second for 47.9 h. The induced ^{148}Pm activity was then counted by means of a HPGe detector. From the decay scheme, gamma-ray lines associated with the decay of the short-lived ground state ($t_{1/2} = 5.4$ d) are expected at 611 and 1465 keV. The decay of the isomer ($t_{1/2} = 41.3$ d) yields lines at 630, 726, and 1014 keV, whereas the 550 and 915 keV transitions are common to both decay modes. The relative gamma-ray intensities of the ^{148}Pm transitions were taken from (5). The gold activity was determined via the well-known intensity of the 412 keV transition (6).

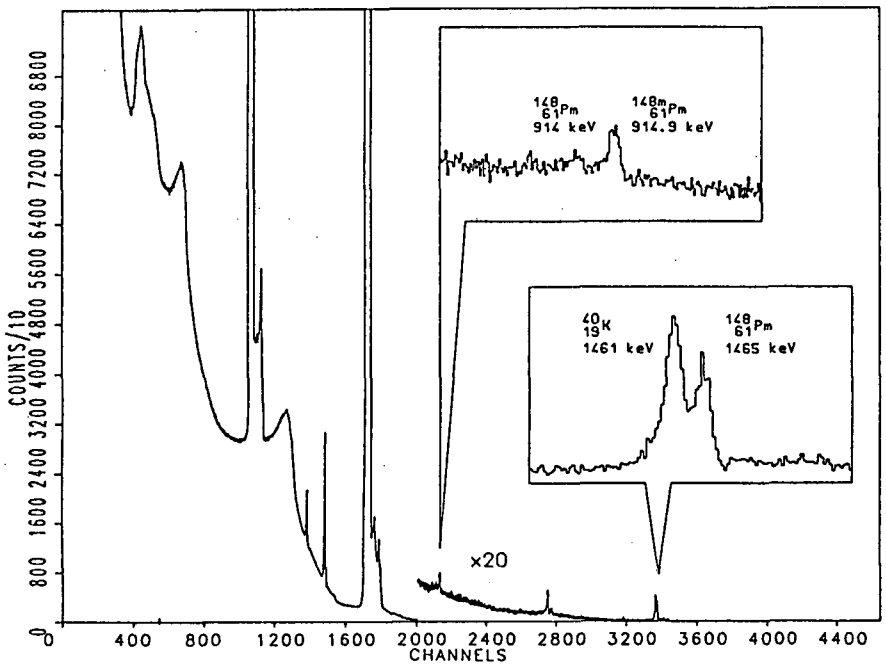

Fig. 1 The gamma-ray spectrum of the activated promethium sample. The relevant transitions for the cross section determination are presented in the insets.

Among the observed lines, those at high energies were most useful for the activity determination, because the low enery part of the spectrum was dominated by gamma-rays from a ^{146}Pm impurity and from sample-induced backgrounds. Fig. 1 shows the measured gamma-ray spectrum of the activated Pm sample, and the insets illustrate the relevant lines in detail. Note, that the isomer decay appears fainter due to its longer half-life.

Time-of-flight experiment: Three Moxon-Rae detectors with different converter materials (7) were used to detect the prompt gamma-rays from the ^{147}Pm(n,γ)^{148}Pm reaction. The overall time resolution of the setup of $\leq$1 ns allowed the separation of the capture events from the prompt gamma-ray peak in the TOF spectrum even at a flight path of only 2 cm. Hence, the sample could be exposed to a high neutron flux of $\sim 10^8$ s^{-1}, resulting in a significant signal-to-background ratio. Though data analysis is still under way, it can be stated that this technique is well suited for investigating even small amounts of radioactive samples.

1. R. R. Winters, F. Käppeler, K. Wisshak, A. Mengoni, G. Reffo: Ap. J. 300, 41 (1986)
2. H. Beer and F. Käppeler: Phys. Rev. C 21, 534 (1980)
3. W. Ratynski and F. Käppeler: Phys. Rev. C 37, 595

4. R. L. Macklin: private communication
5. C. M. Lederer and V. S. Shirley: *Table of Isotopes* (New York: Wiley 1978)
6. R. L. Auble: Nucl. Data Sheets 36, 411 (1983)
7. S. Jaag: Diplom thesis University of Karlsruhe (1990) and contribution 7.

6. THE STELLAR (n,γ) CROSS SECTION OF ^{192}Pt - A NEW CONSTRAINT FOR THE s-PROCESS

M. Tepe and F. Käppeler

The stellar (n,γ) cross section of the *s*-only isotope ^{192}Pt has been measured for the first time via the activation technique. This cross section is important for analyzing the *s*-process branchings at ^{191}Os and ^{192}Ir, which are expected to yield an independent estimate for the mean neutron density during the *s*-process. Together with similar information from other branchings, this can be used to constrain the conditions at the stellar *s*-process site, i.e. during helium shell burning in Red Giant stars.

Isotopically enriched samples of 1.7 and 3.5 mg/cm^2 thickness were prepared by electrodeposition on thin carbon backings. The samples were irradiated in a quasi-stellar neutron spectrum for kT = 25 keV that is obtained from the ^{7}Li(p,n)^{7}Be reaction by bombarding a lithium target with protons of 1912 keV (1,2). The measurements were performed relative to the gold cross section as a standard. Variation of the experimental conditions in different activations and the use of different samples allowed to determine corrections and to evaluate systematic uncertainties.

The ^{193}Pt produced during the activations decays by electron capture with a half-life of 50 yr, which causes two major difficulties:

(i) The ^{193}Pt activity was rather low despite of the long irradiation periods of several weeks. Therefore, considerable efforts were required for reducing the low energy background in the 4π Si(Li) spectrometer for X-ray counting.

(ii) The only accessible radiation emitted in that decay are the iridium LX-rays in the energy range from 8 to 13 keV. Apart from the fact that one has to correct for sizable absorption losses, it turned out that the relative decay intensities as well as the half-life of ^{193}Pt represent the limiting uncertainties of the present measurement. Both quantities are only known to ±20%.

The X-ray spectrum measured in one of the activations is shown in Fig. 1. The cross section that was eventually obtained is almost a factor of two smaller than previously calculated (3, 4). In terms of the astrophysical interpretation of the *s*-process branching,

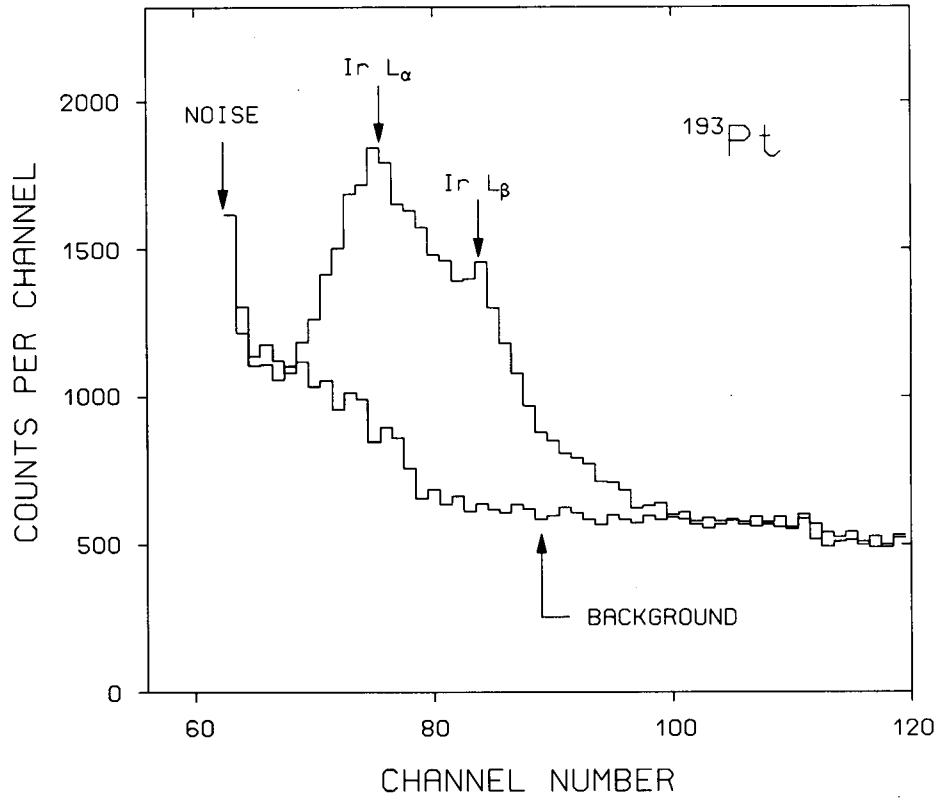

Fig. 1. The X-ray spectrum of an activated ^{192}Pt sample.

this yields a mean neutron density of $n_n = (4.3 \pm {}^{3.4}_{2.5}) \cdot 10^8$ cm^{-3}, in very good agreement with the respective results obtained for the branchings at A = 147, 148 (5) and at A = 185, 186 (6).

(1) H. Beer and F. Käppeler, Phys. Rev. C 21, 534 (1980).
(2) W. Ratynski and F. Käppeler, Phys. Rev. C 37, 595 (1988).
(3) M. J. Harris, Ap. Space Sci. 77, 357 (1981).
(4) J. A. Holmes, S. E. Woosley, W. A. Fowler, and B. A. Zimmerman, Atomic Data and Nuclear Data Tables 18, 305 (1976).
(5) F. Käppeler, R. Gallino, M. Busso, G. Picchio, and C. M. Raiteri, Ap. J. 345, 630 (1990).
(6) F. Käppeler, Z. Y. Bao, S. Jaag, and G. Reffo, Ap. J. 366, 605 (1991).

7. THE STELLAR CROSS SECTION OF ^{209}Bi: IMPLICATIONS FOR THE *s*-PROCESS

S. JAAG and F. KÄPPELER

The abundances of the neutron magic nuclei ^{208}Pb and ^{209}Bi at the termination of the *s*-process path are difficult to reproduce by the classical *s*-process approach (1,2). A major part of this problem is to determine the very small (n,γ) cross sections of these isotopes with sufficient accuracy; this has been a challenge for experimentalists since many years. For ^{208}Pb, this problem could be solved by using the activation technique (3), but for ^{209}Bi only the partial cross section to the short-lived ground state could be determined in this way.

Up to now, the only experimental approach avoiding the problem with backscattered neutrons in a direct measurement was to use a setup with very short primary flight paths (4). Capture events were registered by a set of Moxon-Rae detectors located at a larger distance. In this way, prompt capture gamma-rays and scattered neutrons could be discriminated by their different TOF. This setup was modified in order to obtain the required sensitivity for measuring the very small cross sections of neutron magic isotopes. In particular, the energy and time resolution of the Moxon-Rae detectors were improved by reducing the overall dimensions and by using smaller photomultipliers.

The measurements were carried out at the Karlsruhe Van de Graaff accelerator, using the ^{7}Li(p,n)^{7}Be reaction for neutron production (5,6). The neutrons are collimated due to the reaction kinematics. This keeps neutron induced backgrounds at a minimum, since all massive parts of the setup are located outside of the neutron beam. A primary flight path of only 20 mm between neutron target and sample was sufficient to distinguish true capture events from the intense TOF peak due to gamma-rays created by the interaction of the proton beam pulse with the lithium and the target backing. The comparably high neutron flux at the sample position allows for cross section measurements down to ~1 mbarn.

The new stellar cross section for kT = 30 keV, $\langle\sigma\rangle$ = 1.70 ± 0.18 mbarn, is about six times smaller than the existing differential measurement (7). Even the partial cross section to the short-lived ground state in ^{210}Bi of 2.54 mbarns, which was determined at kT = 25 keV via activation (3) is larger than the present result. In view of these discrepancies, the reliability of the present technique was checked by including a ^{181}Ta sample in one of the two experimental runs. The resulting cross section of ^{181}Ta was found to agree within 4 % with a recent precision measurement (8), thus confirming the 10 % accuracy claimed for the present ^{209}Bi cross section.

The astrophysical implications of the smaller (n,γ) cross sections of ^{208}Pb (3) and of the present value for ^{209}Bi have been investigated for the classical *s*-process approach as well as for the successful *s*-process model for helium shell burning in low mass stars of low metallicity (9, 10).

(1) H. Beer and R. L. Macklin, Phys. Rev. C 32, 738 (1985).
(2) F. Käppeler, H. Beer, and K. Wisshak, Rep. Prog. Phys. 52, 945 (1989).
(3) U. Ratzel, thesis, University of Karlsuhe (1988).
(4) K. Wisshak and F. Käppeler, Nucl. Sci. Eng. 77, 58 (1981).
(5) H. Beer and F. Käppeler, Phys. Rev. C 21, 534 (1980).
(6) W. Ratynski and F. Käppeler, Phys. Rev. C 37, 595 (1988).
(7) R. L. Macklin and J. Halperin, Phys. Rev. C 14, 1389 (1976).
(8) K. Wisshak, F. Voß, F. Käppeler, and G. Reffo, report KfK 4674, Kernforschungszentrum Karlsruhe (1990); Phys. Rev. C 42, 1731 (1990).
(9) R. Gallino, M. Busso, G. Picchio, C. M. Raiteri, and A. Renzini, Ap. J. (*Letters*), *334*, L45 (1988).
(10) R. Gallino, private communications (1990).

KERNFORSCHUNGSZENTRUM KARLSRUHE
INSTITUT FÜR MATERIALFORSCHUNG

1. Nuclear Data Needs for Fusion Materials Research and Low-Activation Materials Development

S. Cierjacks, K. Anderko, K. Ehrlich

Presently, there are two major goals in fusion materials research which ought to be achieved simultaneously: (1) The development of materials which are resistant to large fluences of fusion neutrons, and (2) the development of so-called "low-activation" (LA) materials for the first wall and other structural components which cause minimum activity during and after a fusion reactor operation period. Thus, in addition to a large variety of engineering property specifications, a number of radiological requirements need to be fulfilled, not all of which may be satisfied simultaneously in an optimum manner. The significance of nuclear data for fusion materials research and the nuclear data requirements for materials optimization as low-activation versions have been surveyed [1-4]. For materials programs aiming at the development of more-radiation-resistant materials, it is mainly the quantification of "standard" irradiation parameters such as displacement rates and gaseous or solid foreign element transmutation rates

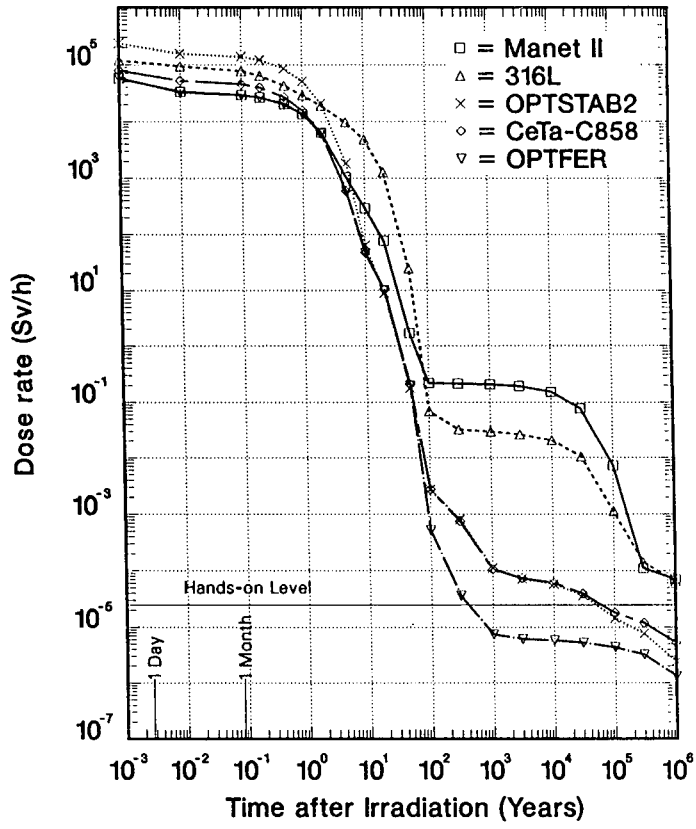

Fig. 1. Comparison of calculated surface γ-dose rates of three LA Fe-basis alloys with two non-optimized stainless steels. The calculations refer to irradiations in the first wall of a DEMO fusion reactor. A first-wall 14-MeV neutron load of 12.5 MW yr m^{-2} was assumed.

which lead to the important nuclear data needs. Since present programs of materials testing do not only involve neutrons, but also light- and heavy-ion beams, neutron as well as charged-parcticle data are needed. Two other tasks which are related to additional nuclear data requirements are neutron dosimetry in various test environments and current comparative studies of candidate high-intensity neutron sources for end-of-life fusion materials testing. Concerning low-activation materials development, another large amount of nuclear data is required; primarily energy-dependent neutron activation cross sections and nuclear decay data for a large number of stable and radioactive nuclides. In addition, other nuclear and atomic data such as Bremsstrahlung data (for the estimate of dose rates and decay heats), neutron-induced charged-particle emission cross sections, charge-particle-induced reaction cross sections, and charged-particle stopping powers (for the treatment of sequential (x,n) reactions) or CEDE factors (for the prediction of biological hazards) are necessary. The present status of existing data libraries has been screened, and lacking or unsufficiently known data were identified. Low-activation materials are presently seen as an important means for improving the safety and environmental characteristics of future fusion reactors. This is illustrated in Fig. 1 which was taken from our contemporary activation calculations, and compares some LA-optimized with some non-optimized Fe-basis alloys. It can be seen that the surface γ-dose rates at long cooling times are up to 3 orders of magnitude lower for the LA-optimized alloys (OPTSTAB2, CeTa-C858) than those for the non-optimized stainless steels (MANET II, 316L). For the presently proposed improved version of CeTa-C858, OPTFER, a further reduction in dose rate by another order of magnitude can be achieved by reducing typical tramp-impurity elements such as Ag, Tb, Ho to concentrations of $\lesssim 10^{-3}$ ppm.

2. Investigation of Element Activation by Sequential (x,n) Reactions

S. Cierjacks, Y. Hino [1], P. Obložinský [2], S. Kelzenberg

The previous investigations of the effects of so-called "sequential (x,n) reactions" (SxRs) on fusion materials activation have been continued. In a broader sense, SxRs are processes in which charged particles x , produced in first-step neutron-induced A(n,yx) reactions, lead to a subsequent nuclear interaction $\overline{A}$ (x,n)C with the nucleus $\overline{A}$ producing the residual nucleus C (note that $\overline{A}$ is not necessarily identical with A). Since the nucleus C is not produced by any of the primary neutron-induced reactions, SxRs give rise to additional radioactivities, if either this nucleus itself or any subsequent build-up product of C is unstable. Such contributions to the induced radioactivity have been neglected in all investigations heretofore. While it had been shown for several selected examples [5-8] that SxRs can contribute substantially to the total radioactive inventory, additional work has been carried out to investigate the influence of these reactions more systematically. This required the production of new data libraries not hitherto available (compare Topic 3.). In the reporting period our investigations have been extended to all (p,n), (d,n) and (α,n) reactions on all stable and radioactive nuclides with $T_{1/2} \geq 1$ day in the mass range $9 \leq A \leq 100$. The calculated quantities included the induced radioactivities as well as the related radiological properties such as surface γ-dose rates, decay heats, and biological hazards. From these studies it was found that SxRs are important for ~30% of the elements from B to Mo [9]. In these cases SxRs dominate all or some of the integral radiological quantities in major portions of the cooling time from 10^{-3} to 10^{6} years. A new extreme example identified in our extended studies is given in

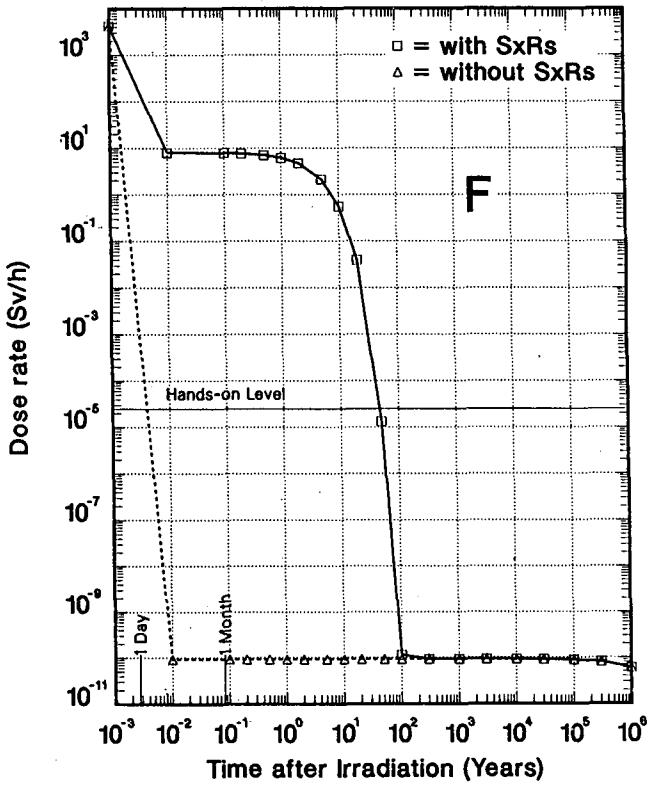

Fig. 2. Calculated dose rate versus cooling time for F. The results refer to neutron irradiation in the first wall of a DEMO fusion reactor. A first-wall 14-MeV neutron load of 12.5 MW yr m^{-2} was assumed.

Fig. 2. This figure shows the integral surface γ dose-rate of F versus time after irradiation. The difference of the two curves is a measure of the contribution from the sequential $^{19}F(\alpha,n)^{22}Na$ reaction. It can be seen that this contribution is large in the time range from 10^{-3} to 10^{2} years, where the upper curve is dominated by the ^{22}Na activity ($T_{1/2}$ = 2.6 yr). Over a large fraction of the affected time range, the inclusion of the sequential (α,n) reaction alters the dose rate by 11 orders of magnitude. Important effects between 1 and 9 orders of magnitude have also been found for all or some of the integral radiological quantities of various other elements. The broad range of new results also indicated that SxRs cannot be restricted to light and medium weight nuclei and the most pronounced (p,n), (d,n) and (α,n) reactions only. Furthermore, it is desirable to treat also those SxRs which are presently still rejected in FISPACT inventory calculations due to the lack of input specifications for some additional product nuclei and their decay data specific to SxRs only.

3. Production of New Nuclear Data Libraries for an Extended Treatment of Sequential (x,n) Reactions in Fusion Materials Activation Calculations

P. Obložinský [2)], S. Cierjacks, B. Rzehorz, Y. Hino [1)]

From previous selected examples investigated in our laboratory it has been shown that sequential (x,n) reactions (SxRs) play an important role in fusion materials activation [5-8], and thus can not be neglec-

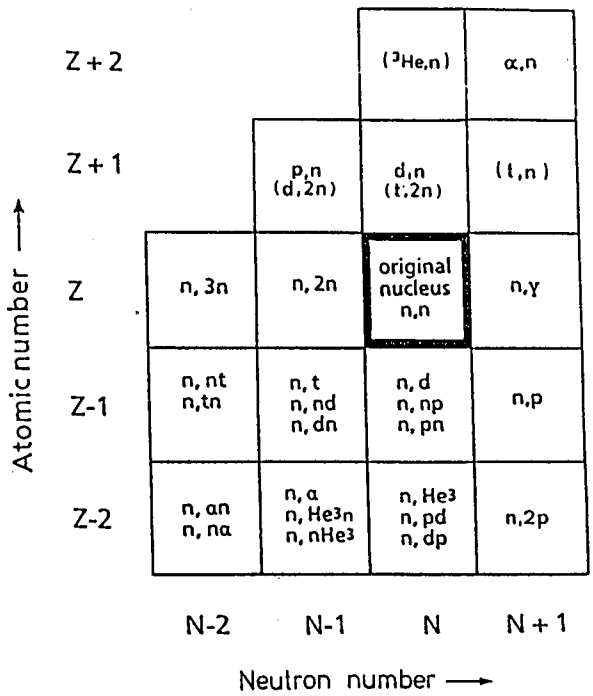

Fig. 3. Kinematically allowed neutron-induced and sequential (x,n) reactions for neutron energies ≤ 15 MeV. Given in parentheses are sequential reactions to be considered in our future work.

ted as experienced heretofore. A more systematic study of SxRs, however, required large new libraries for the following three types of nuclear and atomic data not hitherto available: (1) Neutron-induced charged particle emission cross sections as a function of both the incident neutron and the emitted charged-particle energy. (2) Charged-particle-induced neutron emission cross sections. (3) Differential particle ranges for all light ions produced in first-step neutron-induced reactions. In the report period, adequate new libraries for a more systematic treatment of SxRs have been produced [9,10]. Production cross sections for the first-step (n,x) reactions were taken from the evaluated European Activation File, EAF-1. For the corresponding normalized charged-particle spectra a new library, KFKSPEC, fully based on nuclear-reaction model calculations was created. This contains now 12.300 spectra with about 300.000 data points. The same approach was adopted to produce a starter library, KFKXN, for cross sections of charged particles x = p, d, α that now contains 1.025 reactions with 24.600 data points. A complete set of differential charged-particle ranges was generated by using the Ziegler formalism. The corresponding library, KFKSTOP, is complete for p, d, t, ^{3}He and α-particles and their ranges in all elements from H to U. The existing data libraries allowed the treatment of all SxRs involving the charge particles x = p, d, α on all stable and radioactive nuclides with $T_{1/2} \gtrsim 1$ day in the mass range $1 \leq A \leq 100$. Systematic studies of SxRs with the new libraries showed that sequential (p,n), (d,n) (α,n) reactions are important for many of the elements from B to Mo. Since the treatment of SxRs cannot be restricted to cases treated up to now (see Topic 2.), additional work has been started to extend the present libraries to the whole mass range from A = 1 - 209 and all other kinematically possible SxRs. The kinematically possible neutron-induced and sequential (x,n) reactions on an individual nucleus for neutron energies $E_n \leq 15$ MeV are shown in Fig. 3. SxRs to be considered in our future work are given in parentheses.

4. Program Development for a Unique Treatment of (n,x) and Sequential (x,n) Reactions in Global Activation Calculations

S. Ravndal, P. Obložinský [2], S. Cierjacks, S. Kelzenberg

Present inventory codes for the calculation of fusion materials activation are well established and designed to handle all kinematically possible (n,x) reactions and long chains of these processes. Especially the European reference code, FISPACT, is presently most advanced. The arising of transmuted nuclides and their associated activities, dose rates, decay heats and biological hazards are calculated in a most complete manner, but also FISPACT is, a priori, not designed for the treatment of SxRs. Therefore, we considered for this code the possibility of treating SxRs in addition to (n,x) reactions without changing the inherent code structure. On this basis, the KfK group developed an algorithm that allows to handle these reactions within the given framework of the code. This was possible by introducing socalled "pseudo" cross sections for the two-step SxRs. These are then used together with the "effective" (n,x) cross sections as a generalized input for the inventory code, where all pathways are traced that can contribute to the production of any possible product nucleus. An essential feature of the combined use of our new program system PCROSS with FISPACT is that charged particles x act on the isotope $\overline{A}$, and the density $N_{\overline{A}}$ is automatically updated by FISPACT. This means in turn that the present formalism can handle long chains of (n,x)- and sequential (x,n) reactions with no change of the structure of the FISPACT code. A complete coverage of all possible sequential (x,n) reactions requires, however, an adequate extension of the input parameter space for more reactions and decay data specific for several particular SxRs.

5. Benchmark Data Testing of Important Activation Cross Sections

S. Kelzenberg, S. Cierjacks, P. Obložinský [2], A. Möslang,
J. Möllenbeck [3], G. Peters [3].

Presently, the majority of the nuclear data used in fusion materials activation calculations are based on simple model predictions. This often implies large cross section uncertainties, and thus correspondingly large ambiguities in the resulting activation estimates. Since fusion materials programs typically require 10-15 years of development, more precise predictions are needed well in advance of the start-up of the corresponding research programs. Even though, in general, a tremendous number of activation cross sections is involved, only the most important ones need urgent nuclear data testing. The most important reactions have been identified by sensitivity studies, e.g. by means of a special sensitivity option of the European Reference Code, FISPACT. For benchmark data testing of important activation cross sections, a new test stand has been set up at the Karlsruhe Isochronous Cyclotron (KIZ). This facility involves a 50-MeV deuteron beam bombarding a thick beryllium target. Utilization of a continuous ~30-50 μA beam, provides a total neutron intensity of up to 4×10^{14} n/s and a 'white' neutron spectrum with an average energy of ~15 MeV. For benchmark data testing the total spectral yield in a forward cone of $\pm 15°$ is employed. The neutron-induced radioactivity is currently measured with a calibrated Ge(Li) detector device. Individual product radionuclides are identified by characteristic γ-lines, γ-ray multiplicities and half-lifes. First measurements have been performed for several (n,x) reactions on V and for the important sequential two-step process $^{19}F(n,\alpha) + {}^{19}F(n,y\alpha) \rightarrow {}^{19}F(\alpha,n)^{22}Na$. The evalu-

ation of these data is in progress. The test stand requires some further improvements to fulfill other important fusion needs. For instance, a calibrated Si(Li) detector device ought to be added, to allow also for weak X-ray measurements from radionuclides decaying by electron capture only.

6. Study of High-Intensity, High-Energy Neutron Sources for End-of-Life Fusion Materials Testing

S. Cierjacks, Y. Hino [1], M. Drosg [4], K. Ehrlich

The previous studies of an intense t-H source have been continued. Recently, the KfK proposal for a high-intensity 14-MeV cutoff neutron source based on the $^{1}H(t,n)^{3}He$ reaction [12-14] has been selected as one of four candidates for a worldwide Intense Fusion Materials Irradiation Facility (IFMIF) to be further developed by an IEA IFMIF Working Group. An initial task of this Group was related to the comparison of available test volumes and space-dependent flux spectra, in order to judge the resulting quantities such as pka spectra, displacement cross sections, and transmutation cross sections

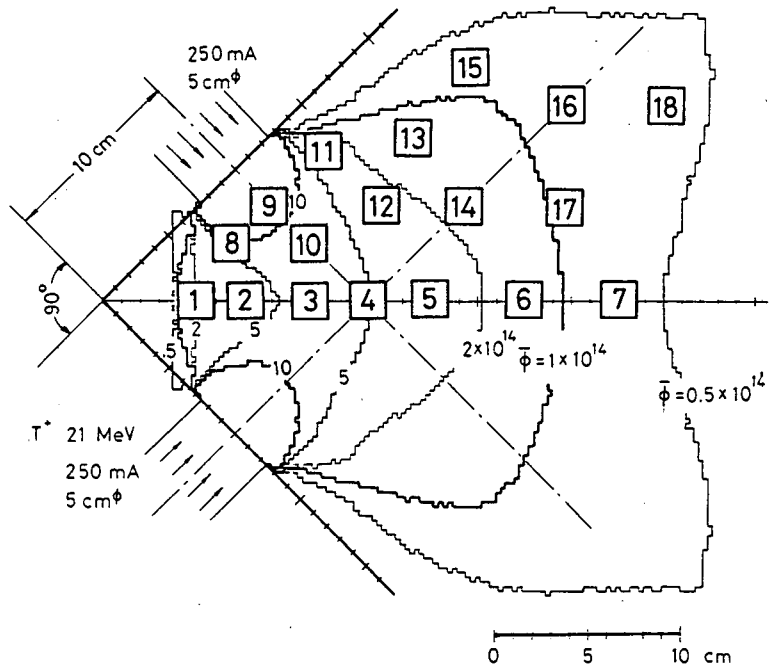

Fig. 4. Neutron flux contours and positions at which differential neutron spectra have been calculated for a special reference configuration of a two-beam, two-target $^{1}H(t,n)^{3}He$ neutron source. The diagram refers to the horizontal plane of the test cell. The square-marked numbered regions indicate the size and locations involved in recent spectrum calculations.

for critical gases and solid foreign elements. In this context, extensive differential flux and spectrum calculations have been performed for some special reference-design configurations of the t-H source [14,15]. These configurations all involve two or more 250-mA triton beams bombarding thick water-jet targets. A typical result from this work is given in Fig. 4. The diagram shows the integral flux contours in the horizontal plane of a test cell irradiated by two targets in facing geometry. The square-marked

numbered regions indicate test cell positions for which differential neutron spectra have been calculated in volumes of 2x2x2 cm^3 [15]. When a relative orientation angle of 90°, triton beam diameters of 5 cm, and distances of 10 cm from the common vertex are chosen, an average neutron flux of $\geq 1x10^{19}$ m^{-2} s^{-1} is achieved in a volume 160 cm^3; for a flux level of $\geq 1x10^{18}$ m^{-2} s^{-1} the corresponding value is 4.2 dm^3. In addition to the special $^1H(t,n)^3He$-source study, some surveys on the present status and the future potential of neutron sources for neutron physics, nuclear data measurements, fusion technology and fusion materials research have been coordinated and finalized [16-18].

---

1) Present address: Electrotechnical Laboratory, 1-1-4 Umezono, Ibaraki, Japan
2) On leave from the Institute of Physics, SAS, 842 28 Bratislava, Czechoslovakia
3) Kernforschungszentrum Karlsruhe, Hauptabteilung Zyklotron
4) Institut für Experimentalphysik, University of Vienna, Austria

References

[1] S. Cierjacks; Nuclear data needs for low-activation fusion materials development; Fusion Engrg. Des. 13, 229 (1990).

[2] S. Cierjacks; Invited paper; Low-activation fusion materials development and related nuclear data needs; IAEA Advisory Group Meeting on the Status and Requirements of Nuclear Data for Radiation Damage and Related Safety Aspects, Vienna, September 19-22, 1989, IAEA-TECDOC-572, p. 53, 1990.

[3] K. Anderko; Niedrig-aktivierende Werkstoffe - eine wichtige Aufgabe der Fusionsreaktorforschung; Paper presented at the IWR-Colloquium in the Research Center Jülich, Jülich, FRG, January 24, 1991.

[4] S. Cierjacks, K. Ehrlich; Invited paper on "Nuclear data for fusion materials research"; prepared for presentation at the Int. Conf. on Nuclear Data for Science and Technology, to be held in Jülich, FRG, May 13-17, 1991.

[5] S. Cierjacks, Y. Hino; The Role of sequential (x,n) reactions on element activation of fusion reactor materials and related nuclear data needs; Proc. NEANDC Specialists Meeting on Neutron Activation Cross Sections for Fission and Fusion Energy, Argonne, September, 13-15, 1989, Eds. M. Wagner, H. Vonach, NEA Paris, p. 19, 1990.

[6] S. Cierjacks, Y. Hino; The influence of sequential (x,n) reactions on total element activities; J. Nucl. Mater. 170, 134 (1990).

[7] S. Cierjacks, Y. Hino; Sequential (x,n) reactions: An important reaction mechanism for element activation of fusion reactor materials; Session 7-D3, 4th Int. Conf. on Fusion Reactor Materials, Kyoto, Japan, December 4-8, 1989.

[8] S. Cierjacks, Y. Hino; Status report on KfK work related to the European Activation Libraries and contemporary activation calculations; in 'Low Activation Materials', Proc. of a European

Workshop on Low Activation Materials, Sect. II, Contr. 2, Ispra, Italy, October 1-3, 1990, Commission of the European Communities, EUR/XII/457, January 1991.

[9] S. Cierjacks, P. Obložinský, B. Rzehorz, Nuclear data libraries for the treatment of sequential (x,n) reactions in activation calculation; Contribution to the IEA Workshop on Low Activation Materials, Culham, UK, April 7-12, 1991, Proceedings to be published.

[10] S. Cierjacks, P. Obložinský, B. Rzehorz; Nuclear Data Libraries for the Treatment of Sequential (x,n) Reactions in Fusion materials Activation Calculations; Preprint, Kernforschungszentrum Karlsruhe Report, KfK-4867, March 1991.

[11] S. Cierjacks; High-energy neutron production by the $^{1}H(t,n)^{3}He$ source reaction; Proc. Int. Fusion Materials Irradiation Facility (IFMIF) Workshop for the International Energy Agency, San Diego, February 14-17, 1989; Ed. R. Verbeek, Commission of the European Communities, Directorate XII, Brussels, Belgium, p. 329, 1990.

[12] S. Cierjacks: High-intensity 14-MeV cutoff neutron production by the $^{1}H(t,n)^{3}He$ source reaction: J. Fusion Energy 8, 193 (1990).

[13] S. Cierjacks, Y. Hino, M. Drosg; Proposal for a high-intensity 14-MeV cutoff neutron source based on the $^{1}H(t,n)^{3}He$ source reaction; Nucl. Sci. Eng. 106, 183 (1990).

[14] S. Cierjacks, Y. Hino; Differential flux and spectrum calculations for a novel high-intensity 14-MeV cutoff neutron source based on the $^{1}H(t,n)^{3}He$ source reaction; Acta Physica Hungarica, in press.

[15] S. Cierjacks, Y. Hino; Additional studies related to the proposal for a novel high-intensity 14-MeV cutoff neutron source based on the $^{1}H(t,n)^{3}He$ source reaction; Proc. Internat. Panel on 14-MeV IntenseNeutron Sources Based on Accelerators for Fusion Materials Study; Eds. A. Miyahara, F.W. Wiffen; Tokyo, Japan, January 14-16, 1991, Nagoya National Institute for Fusion Science Report, NIFS-WS-2, p. 147, 1991.

[16] S. Cierjacks, K. Ehrlich, E.T. Cheng, H. Conrads, H. Ullmaier; High-intensity fast neutron sources and neutron fields for fusion technology and fusion materials research; Nucl. Sci. Eng. 106, 99 (1990).

[17] S. Cierjacks, Guest Editor; Special Issues of NS&E devoted to high-intensity fast neutron sources and calibrated neutron fields for fusion technology and fusion materials research; October and November 1990 Issues, Nucl. Sci. Eng. 106, Nos. 2 and 3, (1990).

[18] S. Cierjacks, Editor; Summary Report of the NEANDC Working Group on Intense Neutron Sources for Neutron Physics and Nuclear Data Measurements; NEANDC Report, NEANDC-274-U, September 1990.

KERNFORSCHUNGSZENTRUM KARLSRUHE
INSTITUT FÜR NEUTRONENPHYSIK UND REAKTORTECHNIK

Nuclear Data Evaluation

1. Evaluation of Neutron Cross Sections for ^{238}U in the Unresolved Resonance Region: JEF-2 Data Tests

F.H. Fröhner

The evaluation of the ^{238}U cross sections from 10 to 300 keV reported two years ago [1] has been adopted for the nuclear data libraries JEF-2 and ENDF/B-VI up to 200 and 149 keV, respectively. A number of tests have been performed in the meantime during the JEF-2 test phase, especially on the capture cross section which is of prime importance in fission reactor technology, and on the resonance structure implied by the average resonance parameters given in JEF-2 which is important for the calculation of safety-related phenomena such as self-shielding and temperature-dependent resonance absorption.

A recent absolute measurement of the capture cross section [2] gave

$$\langle \sigma_\gamma \rangle = 494 \pm 11 \text{ mb} \qquad \text{at} \quad E = 23 \text{ keV} ,$$

in excellent agreement with the JEF-2 value of 500 mb at the same energy. This confirms rather directly the normalisation of the recommended capture cross section.

The resonance-averaged transmission of a sample with areal density n (at./b),

$$\langle e^{-n\sigma} \rangle = e^{-n\langle\sigma\rangle} \left(1 + \frac{n^2}{2} \operatorname{var} \sigma - + \ldots \right) ,$$

is sensitive to the average total cross section $\langle\sigma\rangle$ but also, especially for thick samples, to the variance and higher moments of the total cross section distribution. The resonance structure implied by the average parameters in JEF-2 (average partial widths, mean level spacing, effective nuclear radii) can therefore be tested by comparing calculated thick-sample transmission values with measured ones. The Monte Carlo code SESH [3] was used to sample resonances, to calculate Doppler-broadened cross sections, the corresponding transmissions and finally their averages. Table 1 and Fig. 1 show that the computed values agree very well with recent data [4]. The resonance structure of the total cross section is evidently well represented by the average resonance parameters given in JEF-2.

Self-indication measurements differ from transmission experiments only insofar as the flux detector measuring the transmitted part of the beam consists of a thin "indicator" sample (or "radiator") made of the same material as the filter sample, viewed by gamma ray detectors. From "filter in" and "filter out" runs one obtains the ratio

$$\frac{\langle e^{-n\sigma}\sigma_\gamma\rangle}{\langle\sigma_\gamma\rangle} = e^{-n\langle\sigma\rangle}\left(1 - n\,\frac{\mathrm{cov}(\sigma,\sigma_\gamma)}{\langle\sigma_\gamma\rangle} + - \ldots\right).$$

In practice indicator samples are not ideally thin so that the capture cross section σ_γ ought to be replaced by the capture yield y_γ that includes self-shielding and multiple-collision capture. The self-indication ratio depends on the average total and capture cross section and on their correlated resonance structure, transmission dips coinciding with capture peaks. Self-indication ratios computed with the SESH code from JEF-2 (with full account of self-shielding and multiple scattering) were compared with recently measured data. Fig. 2 and Table 2 show that agreement with the data [4] is again very good. This indicates that also the capture resonance structure is well represented by the average resonance parameters in JEF-2.

Similar agreement with other recent capture, transmission and self-indication ratio measurements indicates that finally, after five decades of effort, the ^{238}U average capture cross section (the group cross section for infinite dilution) in the resolved and unresolved resonance range is now known to about the accuracy requested for technological applications: 1 to 2 % . Self-shielding (Bondarenko) factors, which depend on the relative resonance structure but not on absolute capture cross sections,

$$f_\gamma = \frac{\langle\sigma_\gamma/(\sigma+\sigma_d)\rangle}{\langle\sigma_\gamma\rangle\,\langle 1/(\sigma+\sigma_d)\rangle} = \frac{\int_0^\infty dn\, e^{-n\sigma_d}\,\langle e^{-n\sigma}\sigma_\gamma\rangle/\langle\sigma_\gamma\rangle}{\int_0^\infty dn\, e^{-n\sigma_d}\,\langle e^{-n\sigma}\rangle},$$

where σ_d is the usual (constant) dilution cross section of group constant sets, appear to be obtainable now with an accuracy approaching 1 % .

[1] F.H. Fröhner, Nucl. Sci. Eng. 52 (1989) 119

[2] E. Quang and G. Knoll, Prog. Rept BNL-NCS-44362 (1990) 112

[3] F.H. Fröhner, Report GA-8380 (1968)

[4] M.V. Bokhovko, V.N. Kononov, G.N. Manturov, E.D. Poletaev, V.V. Sinitsa, A.A. Voevodskiy, Yad. Konst. 3 (1988) 11; Engl. transl. INDC(CCP)-322 (1990) 5

Table 1. Thick-sample transmissions and uncertainties of Bokhovko et al. (1988) compared with Monte Carlo results based on JEF-2, as plotted in Fig. 1.

E (keV)	Sample Thicknesses (at./b) 0.0091 (2 mm)	0.0237 (5 mm)	0.0474 (10 mm)	0.0707 (15 mm)	0.0943 (20 mm)	0.19 (40 mm)
10-14	0.884±0.006	0.718±0.005	0.525±0.009	0.398±0.008	0.299±0.005	0.104±0.005
	0.875	0.717	0.526	0.396	0.296	0.100
18-22	0.880±0.004	0.719±0.004	0.531±0.006	0.400±0.005	0.288±0.002	0.093±0.003
	0.880	0.723	0.535	0.399	0.296	0.098
26-30	0.881±0.004	0.722±0.003	0.527±0.006	0.398±0.004	0.292±0.002	0.093±0.002
	0.883	0.728	0.537	0.403	0.296	0.097
40-50	0.887±0.004	0.739±0.003	0.540±0.004	0.417±0.004	0.304±0.002	0.099±0.002
	0.888	0.736	0.546	0.410	0.305	0.099
60-70	0.893±0.004	0.748±0.003	0.554±0.004	0.425±0.004	0.316±0.002	0.103±0.002
	0.891	0.743	0.556	0.420	0.314	0.103
80-90	0.896±0.004	0.751±0.003	0.563±0.004	0.435±0.004	0.324±0.002	0.108±0.002
	0.894	0.749	0.564	0.429	0.322	0.108
100-120	0.904±0.004	0.760±0.003	0.573±0.003	0.447±0.003	0.337±0.002	0.114±0.002
	0.898	0.756	0.574	0.439	0.333	0.114

Table 2. Self-indication ratios and uncertainties of Bokhovko et al. (1988) compared with Monte Carlo results based on JEF-2, as plotted in Fig. 2.

E (keV)	Sample Thicknesses (at./b) 0.0237 (5 mm)	0.0474 (10 mm)	0.0707 (15 mm)	0.0943 (20 mm)	0.19 (40 mm)
10-14	0.641±0.069	0.438±0.060	0.329±0.060	0.221±0.049	0.084±0.030
	0.654	0.455	0.317	0.229	0.065
18-22	0.683±0.025	0.477±0.021	0.363±0.024	0.254±0.025	0.085±0.017
	0.682	0.478	0.342	0.245	0.070
26-30	0.698±0.016	0.488±0.014	0.365±0.015	0.261±0.012	0.083±0.012
	0.696	0.495	0.357	0.260	0.076
40-50	0.726±0.014	0.511±0.012	0.390±0.011	0.279±0.010	0.084±0.010
	0.716	0.519	0.381	0.280	0.084
60-70	0.738±0.011	0.541±0.012	0.412±0.011	0.301±0.008	0.093±0.007
	0.728	0.538	0.400	0.295	0.092
80-90	0.745±0.010	0.544±0.009	0.422±0.009	0.316±0.008	0.094±0.006
	0.736	0.549	0.415	0.309	0.098
100-120	0.753±0.008	0.562±0.007	0.443±0.008	0.327±0.007	0.109±0.006
	0.751	0.565	0.431	0.324	0.102

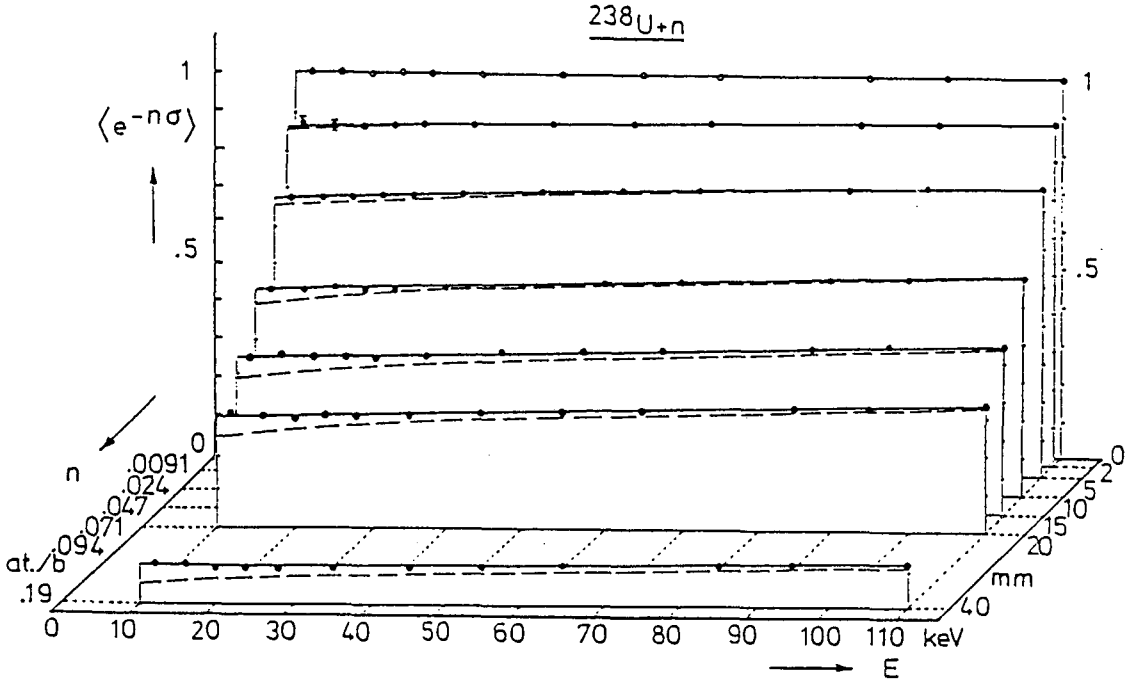

Fig. 1. Thick-sample transmission data of Bokhovko et al. (1988) (solid circles) and curves generated with Monte Carlo techniques from JEF-2 average resonance parameters (solid lines). Also shown are the transmission curves obtained without due account of resonance self-shielding (broken lines). Most error bars are slightly smaller than the point symbols.

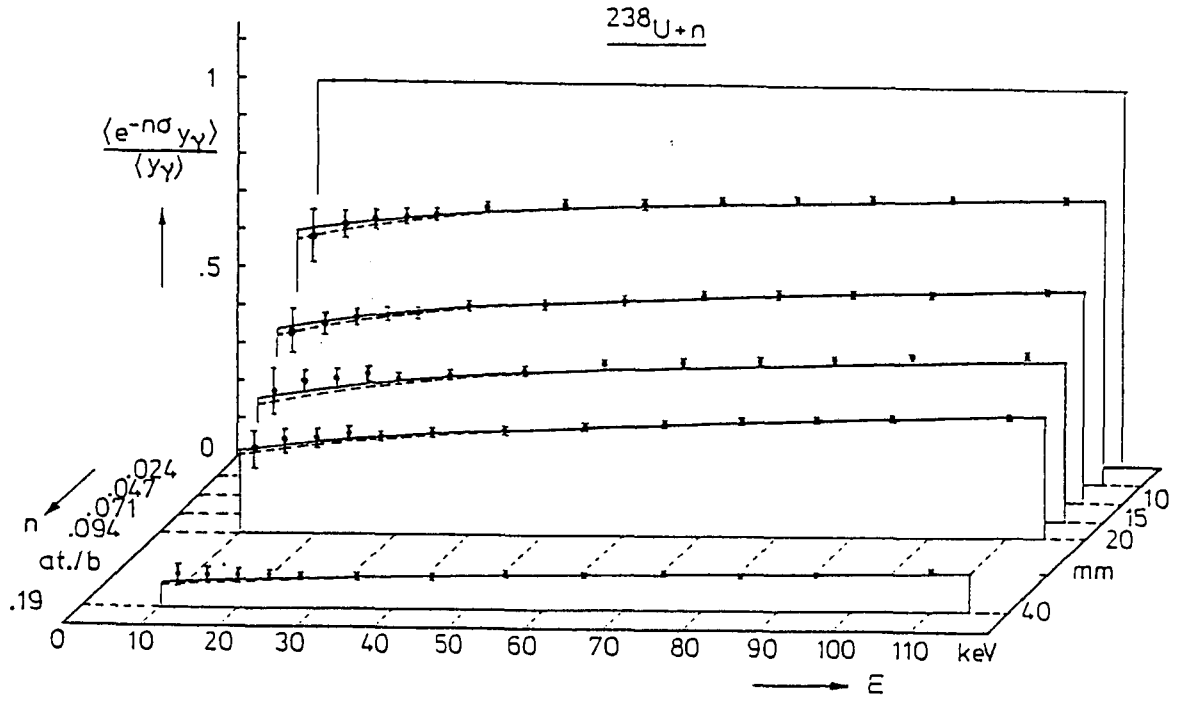

Fig. 2. Self-indication ratios measured by Bokhovko et al. (1988) (solid circles) and curves generated with Monte Carlo techniques from JEF-2 average resonance parameters (solid lines). Also shown are the results obtained without account for resonance self-shielding and multiple-collision capture, i. e. for vanishing radiator sample thickness (broken lines). The actual radiator sample thickness was 0.00646 at./b.

INSTITUT FÜR CHEMIE (1): NUKLEARCHEMIE FORSCHUNGSZENTRUM JÜLICH

1. Studies of Complex Particle Emission Reactions

B. Scholten, S.M. Qaim, G. Stöcklin

In continuation of our fundamental studies on nuclear reactions involving complex particle emission the excitation function of the $^{139}La(n,^{3}He)^{137}Cs$ reaction was determined radiochemically in the energy range of 16 to 20 MeV. Hauser-Feshbach calculations show that the contribution of statistical processes to ^{3}He-particle emission is negligibly small (for details cf. [1]).

As reported in the last Progress Report the emission of ^{7}Be was investigated further both in proton and neutron induced reactions. The results for $(p,^{7}Be)$ reactions are shown in Fig. 1. The cross sections for V, Nb and Au show only a

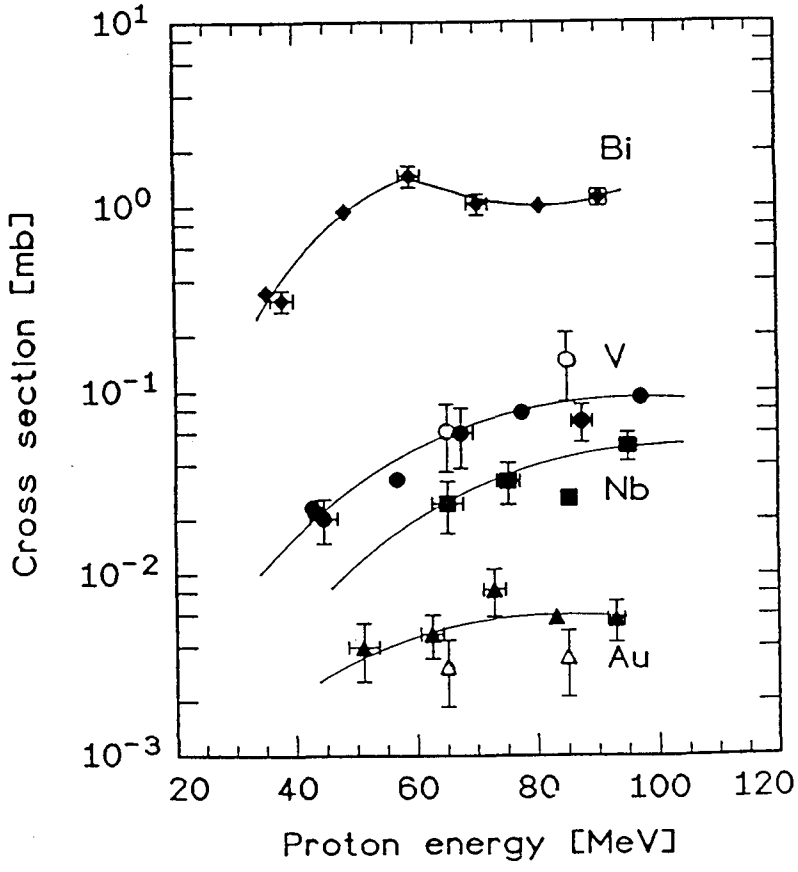

Fig. 1 $(p,^{7}Be)$ cross sections for V, Nb, Au and Bi as a function of proton energy [cf. 2].

slight increase with the incident proton energy. The data for Bi, however, show a strong increase at lower energy, forming a plateau at 60 to 90 MeV. The unusually high cross section for Bi may be due to a different reaction mechanism.

The (n,^{7}Be) cross sections with 53 MeV d(Be) breakup neutrons were found to lie between 0.3 and 5 μb and are more than three orders of magnitude lower than the corresponding (n,t) and (n,^{3}He) cross sections. The (n,^{7}Be) cross section decreases with increasing proton number of the target nucleus (for details cf. [2]).

2. Isomeric Cross Section Ratios

I. Birn, F. Cserpák, S. Sudár, S.M. Qaim

Continuing our studies on isomeric cross-section ratios [3,4] we investigated the ^{58}Ni(n,p)^{58m,g}Co, ^{60}Ni(n,p)^{60m,g}Co, ^{63}Cu(n,α)^{60m,g}Co, ^{65}Cu(n,α)^{62m,g}Co and ^{75}As(n,p)^{75m,g}Ge processes in the energy range of 5 to 10.5 MeV. Cross sections for the formation of all the metastable states have been measured for the first time. Statistical model calculations taking into account precompound effects are underway in collaboration with the Technical University Dresden and Kossuth University, Debrecen, Hungary.

3. Cross Section Measurements for Fusion Reactor Technology

F. Cserpák, S. Sudár, S.M. Qaim, G. Stöcklin
(Relevant to request identification numbers: 742127R, 812002F, 812003F, 861175F, 872030R, 873007R)

Measurements on the excitation functions of ^{nat}Ti(n,x)^{46,47,48}Sc, ^{48}Ti(n,α)^{45}Ca and ^{50}Ti(n,α)^{47}Ca processes up to E_n = 20 MeV, described in the last Progress Report, were completed [cf. 5,6]. From the isotopic data and systematics, cross sections for the emission of helium gas from ^{nat}Ti were deduced [6].

Cross sections were measured for the neutron dosimetry reaction ^{60}Ni(n,p)^{60}Co from threshold up to 12 MeV in cooperation with the Kossuth University, Debrecen, Hungary [7]. The existing discrepancy in the region of 9 to 12 MeV was solved.

Excitation function of the ^{65}Cu(n,α)^{62}Co reaction was measured from 5 to 11 MeV.

Studies on the nuclear reactions ^{151}Eu(n,2n)$^{150m/}$Eu and ^{159}Tb(n,2n)^{158}Tb in the energy range of 8 to 10.5 MeV were completed under an IAEA-research agreement. These reactions lead to the formation of long-lived activation products. Investigations on the ^{63}Cu(n,p)^{63}Ni process are underway.

4. Excitation Functions Relevant to Radioisotope Production

Z. Kovács, F. Tárkányi, H. Piel, S.M. Qaim, G. Stöcklin

Continuing our studies [cf. 8-11] on the production of medically important short-lived radioisotopes we measured for the first time excitation functions for the formation of β^+ emitting radioisotopes ^{38}K, ^{62}Cu and ^{82m}Rb at a small-sized cyclotron.

Investigations on the $^{38}Ar(p,n)^{38}K$ and $^{82}Kr(p,n)^{82m}Rb$ reactions were carried out in cooperation with ATOMKI Debrecen, Hungary using highly enriched gases as target materials. The results for the formation of ^{38}K are shown in Fig. 2. The optimum energy range for the production of ^{38}K is $E_p = 16 \rightarrow 12$ MeV. A somewhat similar energy range ($E_p = 15 \rightarrow 10$ MeV) was found suitable for the production of ^{82m}Rb [cf. 12]. Calculations of thick target yields showed that both ^{38}K and ^{82m}Rb can be produced at a small-sized cyclotron in quantities sufficient for PET applications. Both the radioisotopes are useful or potentially useful myocardial blood flow agents.

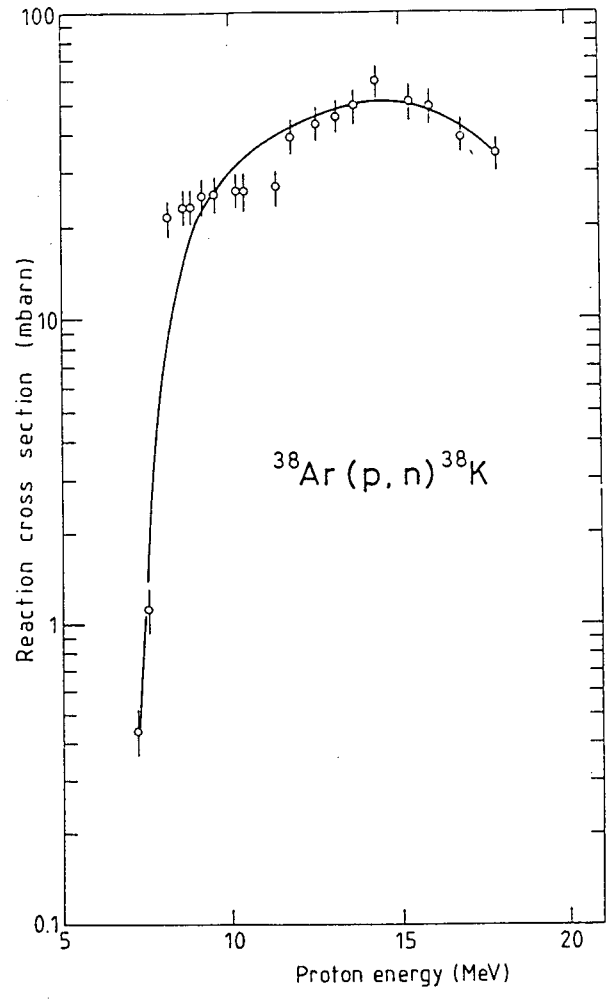

Fig. 2 Excitation function of $^{38}Ar(p,n)^{38}K$ reaction measured using highly enriched ^{38}Ar gas.

The excitation function of the $^{62}Ni(p,n)^{62}Cu$ reaction was measured using the stacked-foil technique. For this purpose an electrolytic method was developed to obtain thin films of highly enriched ^{62}Ni on Au-backing. Results show that the optimum energy range for the production of ^{62}Cu is $E_p = 14 \rightarrow 10$ MeV and yields of about 200 mCi/μAh are expected.

References

[1] S.M. Qaim, R. Wölfle: Excitation function of $^{139}La(n,^3He)^{137}Cs$ reaction near its threshold, Acta Physica Hungarica, in press

[2] B. Scholten, S.M. Qaim, G. Stöcklin: ^7Be emission in proton and neutron induced reactions, Proc. Int. Conf. on Nuclear Data for Science and Technology, Jülich, May 1991, in press

[3] S.M. Qaim, M. Ibn Majah, R. Wölfle, B. Strohmaier: Excitation functions and isomeric cross-section ratios for the $^{90}Zr(n,p)^{90m,g}Y$ and $^{91}Zr(n,p)^{91m,g}Y$ processes, Phys. Rev. C42 (1990) 363

[4] N.I. Molla, S.M. Qaim, M. Uhl: Activation cross section and isomeric cross section ratio for the $^{46}Ti(n,p)^{46m,g}Sc$ process, Phys. Rev. C42 (1990) 1540

[5] N.I. Molla, S.M. Qaim, H. Liskien, R. Widera: Excitation functions of $^{nat}Ti(n,x)^{46,47,48}Sc$ processes in the energy range of 12.5 - 19.6 MeV, Appl. Radiat. Isotopes 42 (1991) 337

[6] S.M. Qaim, N.I. Molla, R. Wölfle, G. Stöcklin: Differential and integral cross section measurements of some (n, charged particle) reactions on titanium, Proc. Int. Conf. on Nuclear Data for Science and Technology, Jülich, May 1991, in press

[7] S. Sudár, J. Csikai, S.M. Qaim, G. Stöcklin: Neutron activation cross sections for $^{60}Ni(n,p)^{60m}Co$, $^{60}Ni(n,p)^{60m+g}Co$ and $^{58}Ni(n,p)^{58m}Co$ reactions in the 5 to 12 MeV energy range, Proc. Int. Conf. on Nuclear Data for Science and Technology, Jülich, May 1991, in press

[8] F. Tárkányi, S.M. Qaim, G. Stöcklin, M. Sajjad, R.M. Lambrecht, H. Schweickert: Excitation functions of (p,2n) and (p,pn) reactions and differential and integral yields of ^{123}I in proton induced nuclear reactions on highly enriched ^{124}Xe, Appl. Radiat. Isotopes 42 (1991) 221

[9] F. Tárkányi, S.M. Qaim, G. Stöcklin, M. Sajjad, R.M. Lambrecht: Nuclear reaction cross sections relevant to the production of the $^{122}Xe \rightarrow ^{122}I$ generator system using highly enriched ^{124}Xe and a medium-sized cyclotron, Appl. Radiat. Isotopes 42 (1991) 229

[10] Z. Kovács, F. Tárkányi, S.M. Qaim, G. Stöcklin: Excitation functions for the formation of some radioisotopes of rubidium in proton induced nuclear reactions on ^{nat}Kr, ^{82}Kr and ^{83}Kr with special reference to the production of $^{81}Rb(^{81m}Kr)$ generator radionuclide, Appl. Radiat. Isotopes 42 (1991) 329

[11] Z. Kovács, F. Tárkányi, S.M. Qaim, G. Stöcklin: Production of 6.5 h ^{82m}Rb via the $^{82}Kr(p,n)$-process at a low-energy cyclotron: a potential substitute for ^{82}Rb, Appl. Radiat. Isotopes, in press

[12] Z. Kovács, F. Tárkányi, S.M. Qaim, G. Stöcklin: Cross sections of proton induced nuclear reactions on Kr gas relevant to the production of medically important radioisotopes ^{81}Rb and ^{82m}Rb, Proc. Int. Conf. on Nuclear Data for Science and Technology, Jülich, May 1991, in press

INSTITUT FÜR KERNPHYSIK
ARBEITSGRUPPE STRAHLUNGSTRANSPORT
FORSCHUNGSZENTRUM JÜLICH

1. Neutron Spectra Measurements and Monte Carlo Simulations of (p,xn) Reactions at 597 MeV and 800 MeV

W. Amian, P. Cloth, P. Dragovitsch*, V. Drüke, D. Filges, M.M. Meier**

Double differential neutron production cross sections were measured at the LAMPF-WNR facility at Los Alamos between 100 MeV and 800 MeV incident proton energy using time-of-flight techniques. Virtually systematic results were gained by a large number of different angles, energy points and target materials from low to high atomic masses. The measured spectra were compared to detailed Monte Carlo simulations using the KFA version of the intra-nuclear cascade code HETC. The results are also compared with earlier measurements and those of other authors. Here we present the latest series of these measurements, which were performed at 597 MeV and 800 MeV incident proton energy.

The experiments were performed by the LANL-KFA collaboration in the period from 1981 to 1990. Single measurements in this series and in one case comparison with Monte Carlo simulations have been published earlier [1]. In Table 1 an overview about the recent measurements is given.

Table 1. Thin Target (p,xn) Measurements

Energy (MeV)	Target Materials	Angle (degree)
597	Be,B,C,N,O,Al,Fe,Pb,U	30,60,120,150
800	Be,B,C,N,O,Al,Cd,Fe,W,Pb,U	30,60,120,150
800	C,Al,Ni,Ta,W,Pb,U	7.5,30

The intranuclear cascade evaporation model (INCE), as implemented in the high energy radiation transport code HETC of the HERMES system [2,3], is used in the calculation of double differential cross sections of proton induced neutron production [1].

To achieve optimum comparison, identical energy intervals as used in the experimental analysis were provided in the HETC calculations. Depending on target material, emission angle and incident proton energy, the number of spallation events varied from 2.5×10^5 to 6.0×10^5 to achieve reasonable statistics in the calculations.

Some examples out of this recent series of measurements together with the respective Monte Carlo simulations are presented in the following figures. With these and the earlier measurements proton induced neutron production cross sections are available now for a wide range of target masses, incident energies and neutron emission angles. Discrepancies observed between earlier measurements and INCE simulations, become considerably smaller with the latest measurements. A first outline is given in Ref. [4].

*SCRI, Florida State University, Tallahassee, USA
**Los Alamos National Laboratory, NM 87545, USA

References:

[1] P. Cloth et al., KFA-Report Jül-2295 (1989)

[2] P. Cloth et al., KFA-Report Jül-2203 (1988)

[3] T.W. Armstrong, K.C. Chandler, Nucl. Sci. Eng. 49, 110 (1972)

[4] W. Amian et al., to be published in the proceedings of the International Conference on Nuclear Data in Science and Technology May 13-17, 1991, Jülich Germany

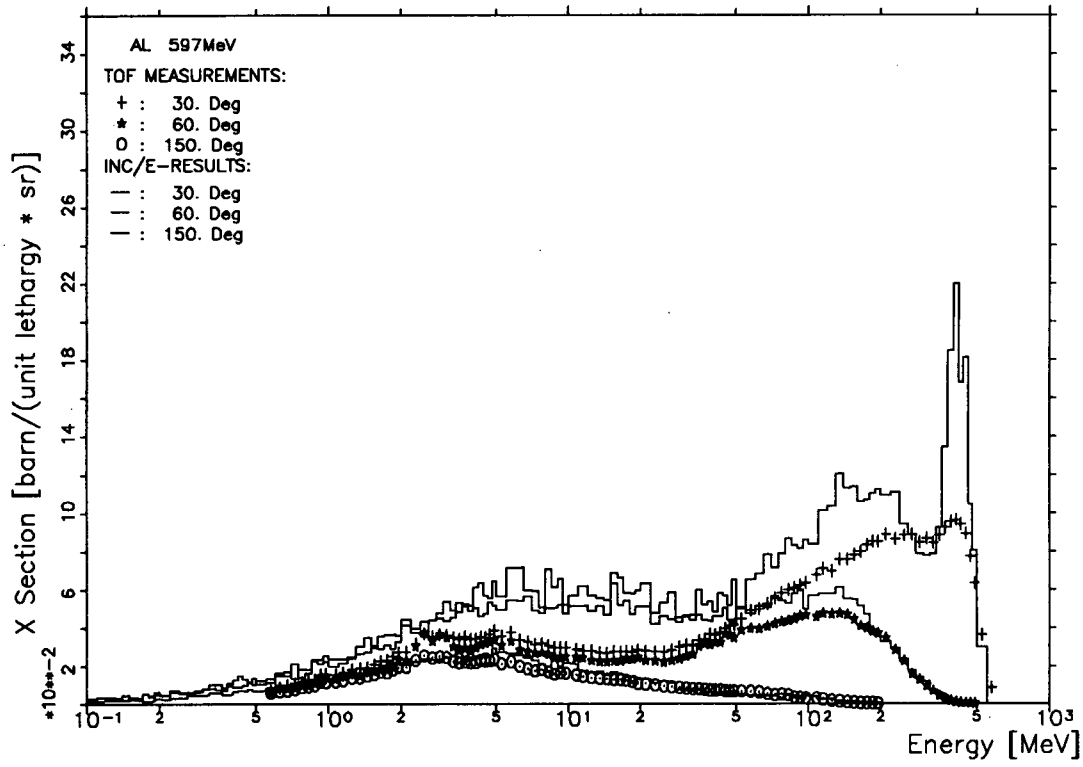

Fig. 1. Neutrons from 597 MeV protons on aluminum

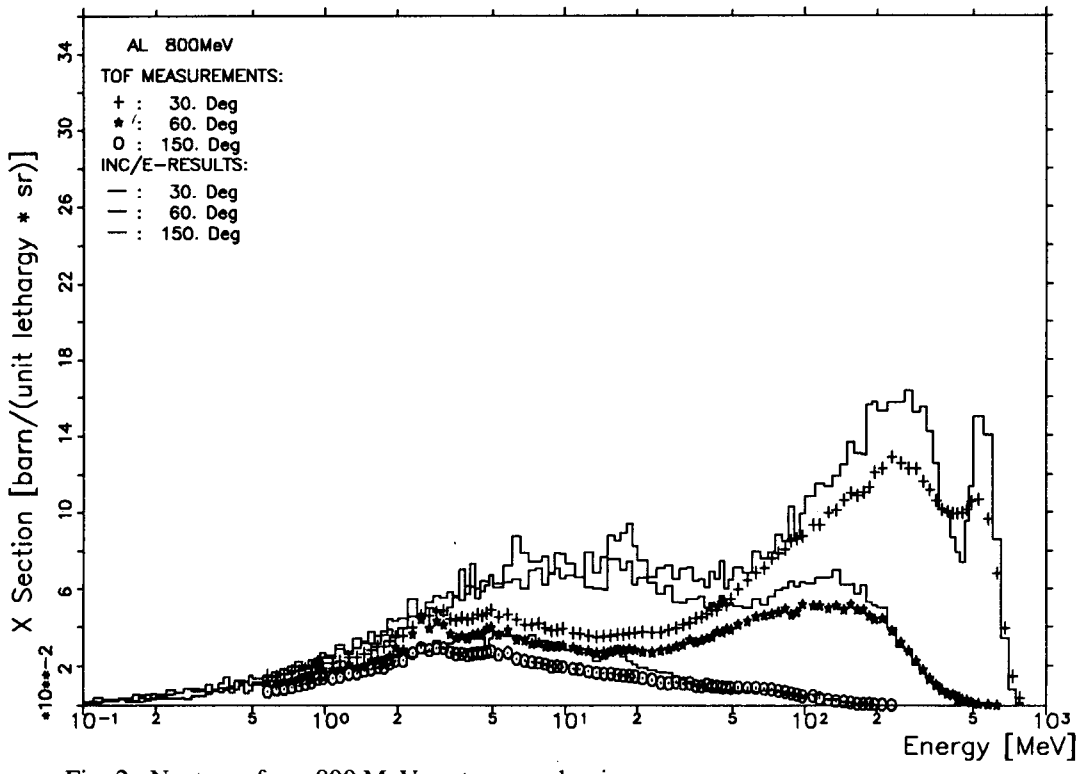

Fig. 2. Neutrons from 800 MeV protons on aluminum

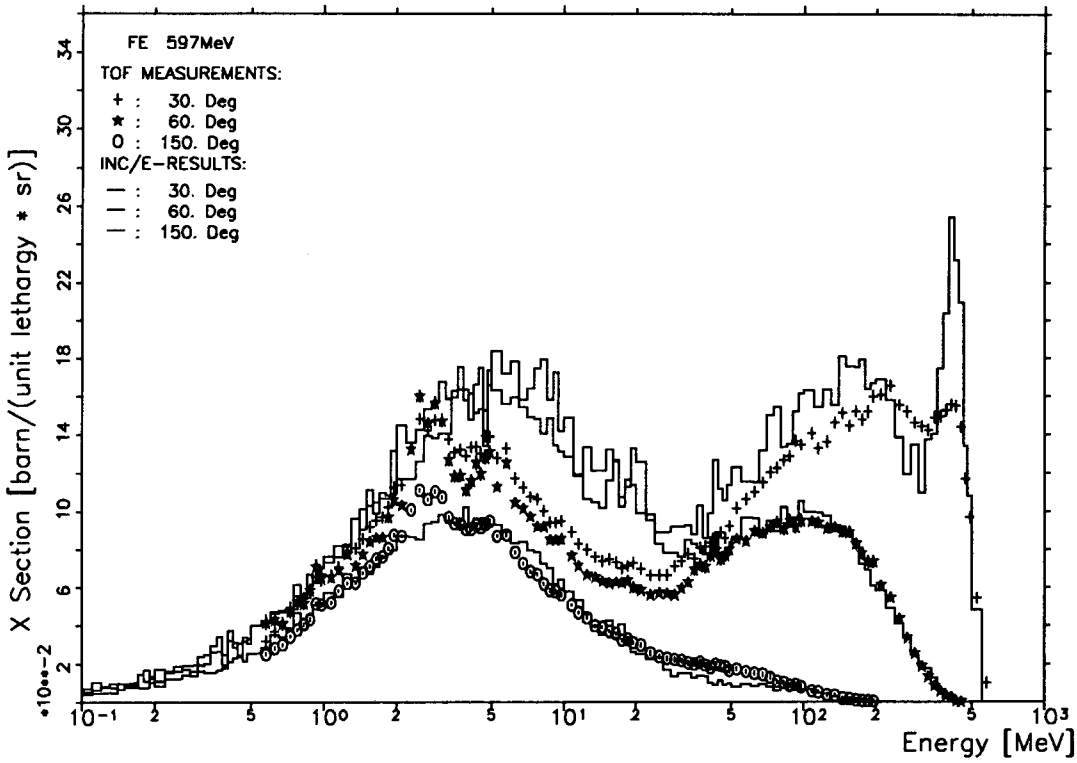

Fig. 3. Neutrons from 597 MeV protons on iron

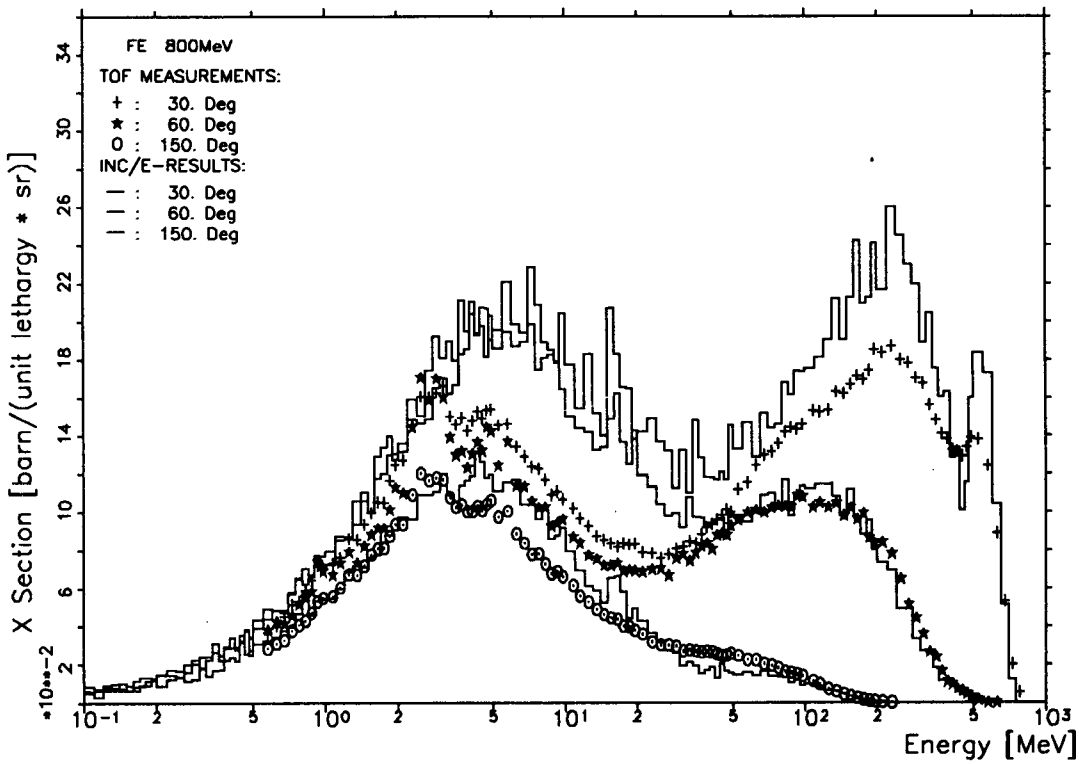

Fig. 4. Neutrons from 800 MeV protons on iron

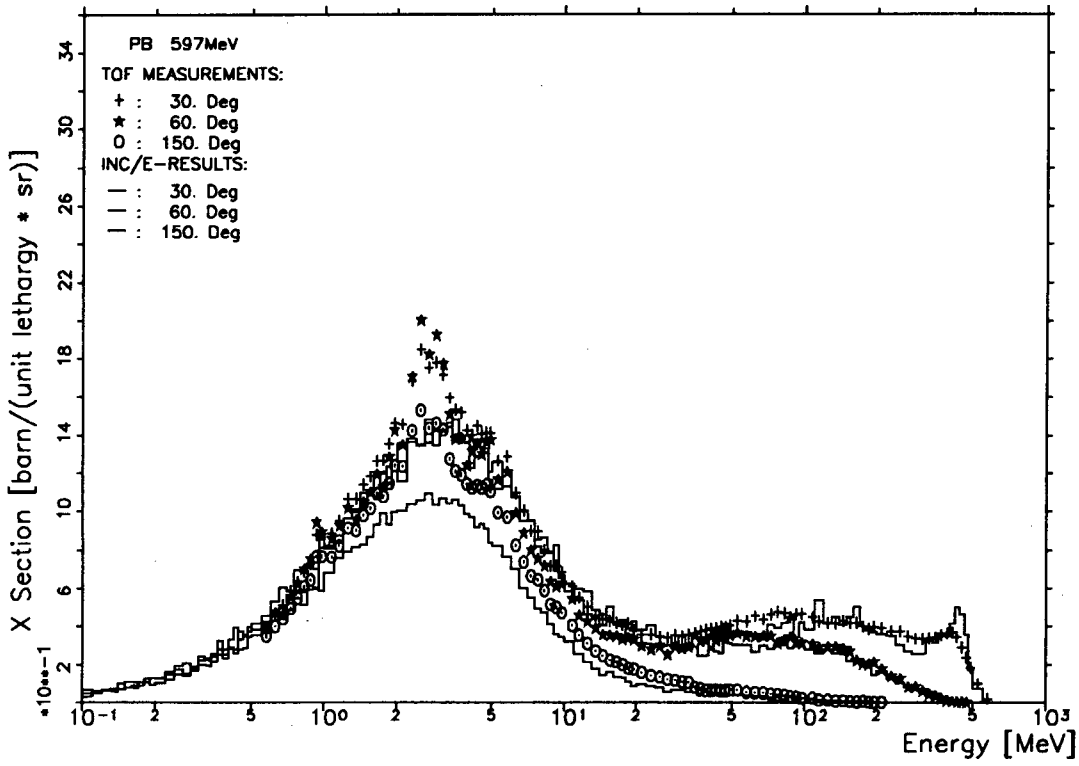

Fig. 5. Neutrons from 597 MeV protons on lead

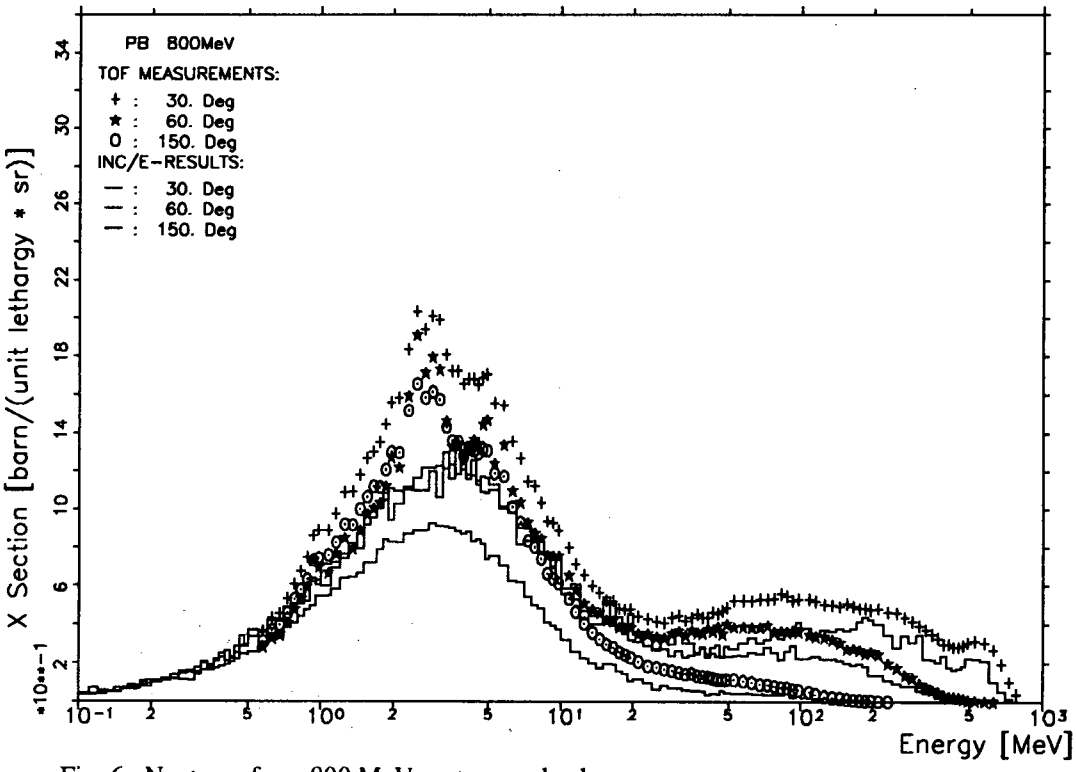

Fig. 6. Neutrons from 800 MeV protons on lead

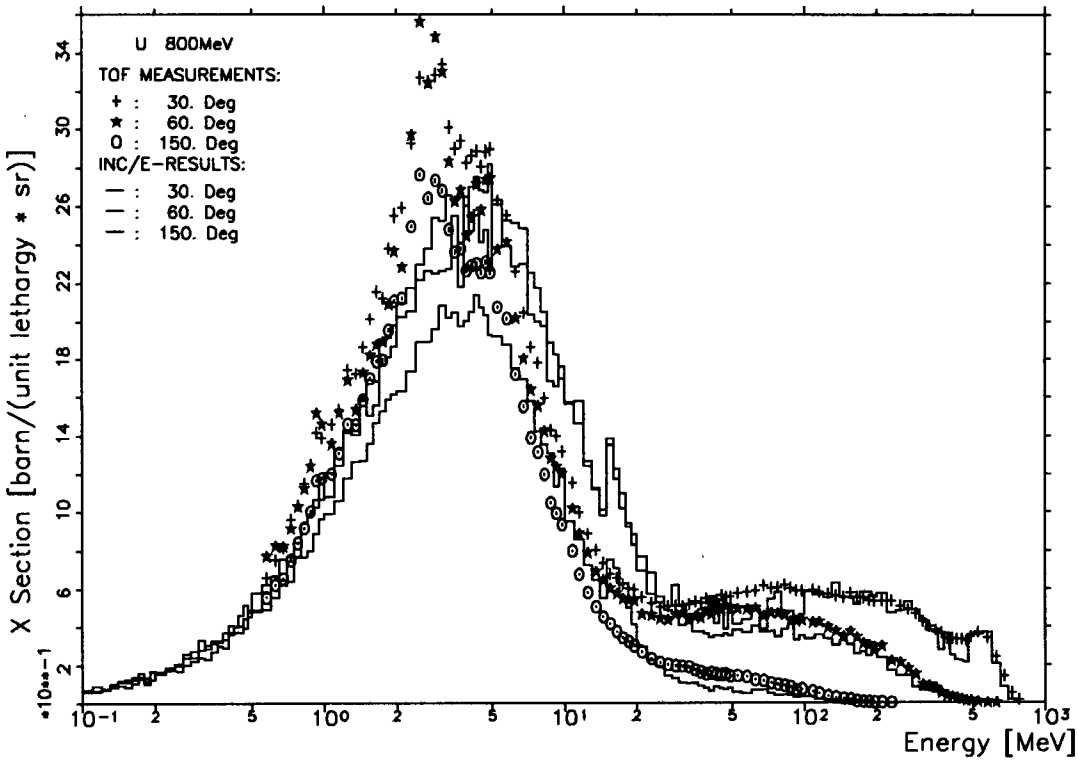

Fig. 7. Neutrons from 800 MeV protons on uranium

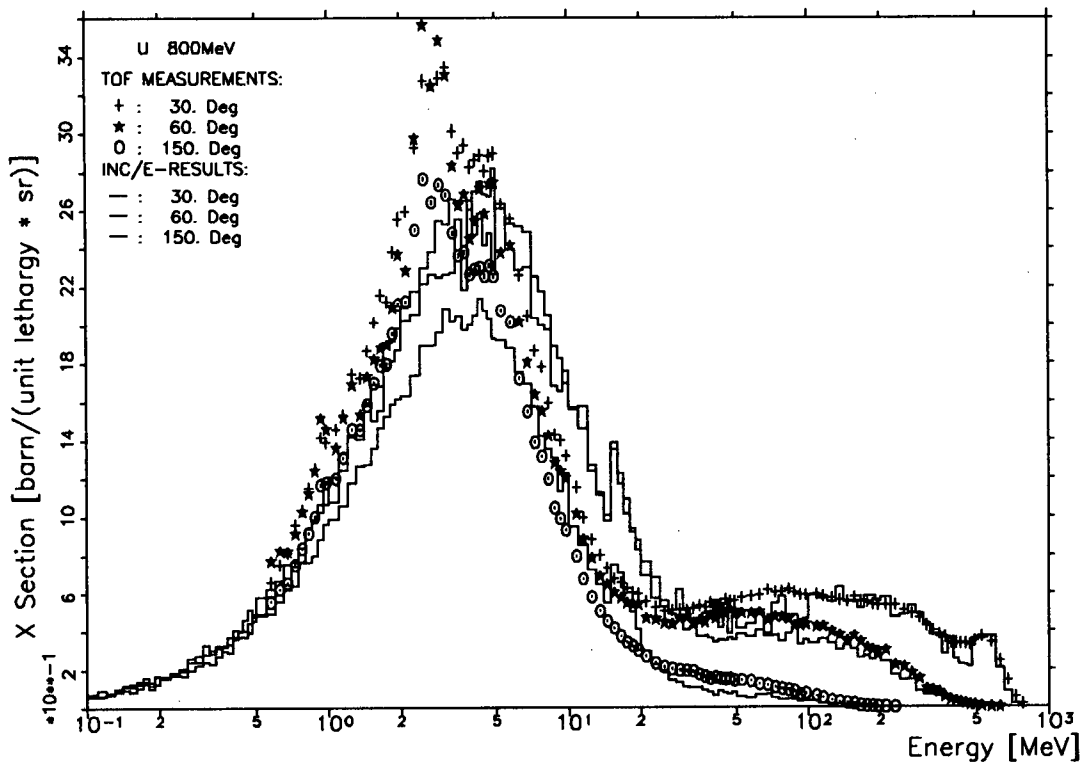

Fig. 8. Neutrons from 800 MeV protons on uranium

BEREICH REAKTORPHYSIK
ZENTRALINSTITUT FÜR KERNFORSCHUNG ROSSENDORF

1. Integral Test of Neutron Data by Reactivity Measurement in Critical Assemblies with Predetermined Adjoint Flux

K.Dietze, G.Hüttel, H.Kumpf, E.Lehmann*

Laboratory: Zentralinstitut für Kernforschung Rossendorf
Postfach 19, O-8051 Dresden, F.R.Germany

*now Paul Scherrer Institut, CH-5232 Villigen PSI

Names: K.Dietze, G.Hüttel, H.Kumpf, E.Lehmann*

Facilities: Rossendorf Annular Zone Reactor (RRR) with Fast Insertion Lattices (SEG)

SEG-4 and SEG-5:
Both configurations are characterized by an energy-independent adjoint flux, differences are in the admixtures of Cd and B-10, respectively.

SEG-6: Monotonous rising adjoint spectrum, hard neutron spectrum

SEG-7: Extremely soft neutron spectrum and a nearly energy-independent adjoint spectrum, k_∞ near 1

Experiment: Integral test of neutron data by C/E-ratios
Separation of reactivity effects by especially designed adjoint function

1. Integral test of neutron absorption data of structural materials and FP-nuclides in SEG-4 and SEG-5

2. Test of scattering data, especially of inelastic cross-sections, for structural materials and U-238 in SEG-6

3. Investigation of the U-235/B-10 -discrepancy and check of the neutron absorption data (f_c-factors!) of interesting materials in the resonance region in SEG-7

Method: Sample reactivity measurement by means of pile oscillation technique
Measurement of the mass dependence to check different self-shielding data
Extrapolation to infinitely small mass values
Determination of CRW's and/or effective absorption cross-sections, relative to the standards B-10, U-235 or C-12 (SEG-6), to check cross-sections of different data sets
Generation of ABBN-group data
Comparison of different data

Samples: Structural and reactor materials Fe,Cr,Ni,Mo,Mn, Zr,Ti,Cu,W,V,Al,Co,Nb,Ta,Cd,Pb,Be,Bi,U-238,H,Na

FP-nuclides Mo-95,97,98,100,Rh-103,Pd-105,Ag-109, Cs-133,Nd-143,145,Sm-149,Eu-153

Standards B-10,U-235,Au,C

Accuracy: $\Delta k/k \approx 10^{-8}$
5...15% in C/E-ratios
$\Delta\rho \approx$ +- 0,3 mCent

Completion: SEG-4,5,6: completed
SEG-7: work in progress

Discrepancies to other reported data have been stated for different materials and data sets, e.g. Sm-149, W, Cd and stainless steel components

A great number of discrepancies exist for f_c-factors

In all our SEG-configurations the U-235/B-10 -discrepancy of their C/E-ratios, stated also by other authors, amounts to +5...20%

Publications:

SEG-4,-5: K.Dietze et al., Kernenergie 29 (1986) 401
K.Dietze et al., Kerntechnik 53/2 (1988) 143
E.Lehmann et al., ZfK-656 (1988)
K.Dietze, H.Kumpf, Kernenergie 34 (1991) 1
SEG-6: E.Lehmann et al., Kernenergie 34 (1991) 9
E.Lehmann et al., ZfK-729 (1990)
SEG-4..7: K.Dietze et al., Proc.Int.Conf.on Nuclear Data for Sci.and Techn., Mai 1991, Jülich/FRG (in print)

Contact: K.Dietze

ABTEILUNG NUKLEARE ANALYTIK
ZENTRALINSTITUT
FÜR ISOTOPEN- UND STRAHLENFORSCHUNG LEIPZIG

New Decay Data for neutron-deficient Hafnium, Tantalum and Tungsten Isotopes

H. Bruchertseifer, F. Riedel, B. Eichler [1]
J. Estevec [2], V.B. Zlokazov [2]

New short-lived Isotopes of Hafnium, Tantalum and Tungsten were produced by fusion-evaporation nuclear reactions of ^{20}Ne and ^{22}Ne-ions with different targets at the U-400 and U-300 Cyclotrons of the Joint Institute for Nuclear Research Dubna.
A fast experimental approach to continuous radiochemical isolation of elements with Z = 72-74 was developed [1].
The multistep procedure is based on

- transportation of the radioactive nuclides from the cyclotron target to laboratory by an aerosol stream (N_2 + KCl),
- separation and dissolution of the aerosol particulates,
- isolation of the elements of interest by ion exchange or extraction techniques,
- measurement by X-ray and γ-spectrometry.

The most intensive γ-lines have been assigned (computer code ACTIV) and the isotope identification was based on the half-live analysis of generic related mother-daughter-nuclides. Computer code (DECAN) for parameter estimation of the complex exponential distribution of the decay of generic related nuclides were applied.

^{144}Sm (^{22}Ne,xn) $^{166\text{-}xn}$Hf (x = 3,4,5)
^{147}Sm (^{20}Ne,xn) $^{167\text{-}xn}$Hf (x = 3,4,5,6)
^{147}Sm (^{22}Ne,xn) $^{169\text{-}xn}$Hf (x = 4,5,6)
^{151}Eu (^{20}Ne,xn) $^{171\text{-}xn}$Ta (x = 6,7,8)
^{154}Gd (^{20}Ne,xn) $^{174\text{-}xn}$W (x = 4,5,6,7)
^{154}Gd (^{22}Ne,xn) $^{176\text{-}xn}$W (x = 4,5,6,7)
^{155}Gd (^{20}Ne,xn) $^{175\text{-}xn}$W (x = 6,7)

Tab. 1 Survey of the different nuclear reactions used for production of Hf, Ta and W-Isotopes

The measured half-live $T_{1/2}$ = 2,5 min of the isotope ^{171}W is in good agreement with other recent published determinations [3]. The decay curves of Tungsten-171 displays two components, the 2,5(2) min one and a 10,7(7) min one [2].

The continuous radiochemical separation techniques allows a very clean and efficient separation of refractory elements.
Decay studies of Tungsten isotopes with mass less then 166 are now in progress.

References

[1] Bruchertseifer H.; Eichler B.; Estevez J.; Zvara I.: Radiochimica Acta 47,41-46(1989)
[2] Bruchertseifer H.; Riedel F.; Eichler B.; Estevez J.; Zlokazov V.B.: ZfI-Mitteilungen 161 ,71 (1990)
[3] Meissner F.; Schmidt-Ott W.-D.; Freystein V.; Hild T.; Runte E.; Salewski H.: Z. Phys. A - Atomic Nuclei 337,45-56 (1990)

[1] Zentralinstitut für Kernforschung Rossendorf
[2] Joint Institute for Nuclear Research Dubna, USSR

HAFNIUM - ISOTOPES

^{161}Hf	$T_{1/2}$: 20 ± 3 s	E_γ(keV): 135,6; 180,0
^{162}Hf	$T_{1/2}$: 41± 6 s	E_γ(keV): 173,7; 195,9
^{163}Hf	$T_{1/2}$: 44± 6 s	E_γ(keV): 71,0; 62,1
^{164}Hf	$T_{1/2}$:2,8 ± 0,2 min	E_γ(keV): 122,1; 153,5
^{165}Hf	$T_{1/2}$:1,7 ± 0,1 min	E_γ(keV): 179,9

TANTALUM - ISOTOPES

^{163}Ta	$T_{1/2}$: 8 ± 4 s	E_γ(keV): 71,0
^{164}Ta	$T_{1/2}$: 20 ± 7 s	E_γ(keV): 210,6
^{165}Ta	$T_{1/2}$: 35 ±10 s	E_γ(keV): 94,1; 162,8

TUNGSTEN - ISOTOPES

^{167}W	$T_{1/2}$: 19 ± 7 s	E_γ(keV): 141,6
^{168}W	$T_{1/2}$: 49 ± 7 s	E_γ(keV): 178,2
^{169}W	$T_{1/2}$: 55 ±10 s	E_γ(keV): 96,9; 136,0; 169,5
^{170}W	$T_{1/2}$: 2,4±0,1 min	E_γ(keV): 42,3; 124,7;144,0; 316,4
^{171A}W	$T_{1/2}$: 2,5±0,2 min	E_γ(keV): 52,0; 53,5; 128,3; 129,6; 131,1; 132,1; 139,2; 171,4; 174,4; 184,5; 204,8; 294,7; 300,6; 479,2
^{171B}W	$T_{1/2}$: 10,7±0,7 min	$E_{\gamma(keV)}$: 39,3; 89,9; 113,3; 114,9

Tab. 2 New assigned half-lifes and γ -radiation energies of Hafnium, Tantalum and Tungsten isotopes

INSTITUT FÜR KERN- UND ATOMPHYSIK TECHNISCHE UNIVERSITÄT DRESDEN

1. Tritium Breeding Rate of a LiAl Blanket Assembly

T. Elfruth, D. Hebert [1], J. Klose, D. Markovskij [2], M. Toepfer, D. Seeliger, K. Seidel, G. Shatalov [2], W. Stolz [1], S. Unholzer

A hybrid-reactor blanket-model is investigated experimentally, as well as by calculating tritium production rates. The assembly consists of homogeneous slabs (100 cm * 100 cm) of the following materials:

- steel (2 cm thickness) — simulating First Wall,
- uranium depleted in ^{235}U (10 cm),
- LiAl (three slabs, each of 4 cm thickness),
- CH_2 (sheets of 2 cm which separate LiAl) — acting as moderator,
- steel (11 cm) — simulating a shield.

The assembly was irradiated by a point-like d-T neutron source located at the z-axis (crossing the centres of the slabs) at a distance of 19 cm from the first slab. The number of 14 MeV source neutrons generated was determined by counting the associated α-particles.

The tritium production was measured in the three LiAl-slabs along the z-axis and perpendicular to it with a spatial resolution of $\leq$ 1 mm and with a density of the measuring positions allowing volume integration. Two independent methods were used:

- the ^3H induced in Li_2CO_3 probes is determined by β-counting in a liquid scintillator,
- LiF–thermoluminescense probes are excited and the glow-curve maxima are recorded.

The measured tritium production per one 14 MeV source neutron and their spatial distributions have been compared with calculated values obtained with the three-dimensional Monte-Carlo codes BLANK, MORSE, and MCNP using data of the ENDF/B-IV– as well as ENDL-library for the neutron transport and of the ENDF/B-V–dosimetry file for the tritium producing reactions of ^6Li and ^7Li. An example for such a comparison is show in the figure.

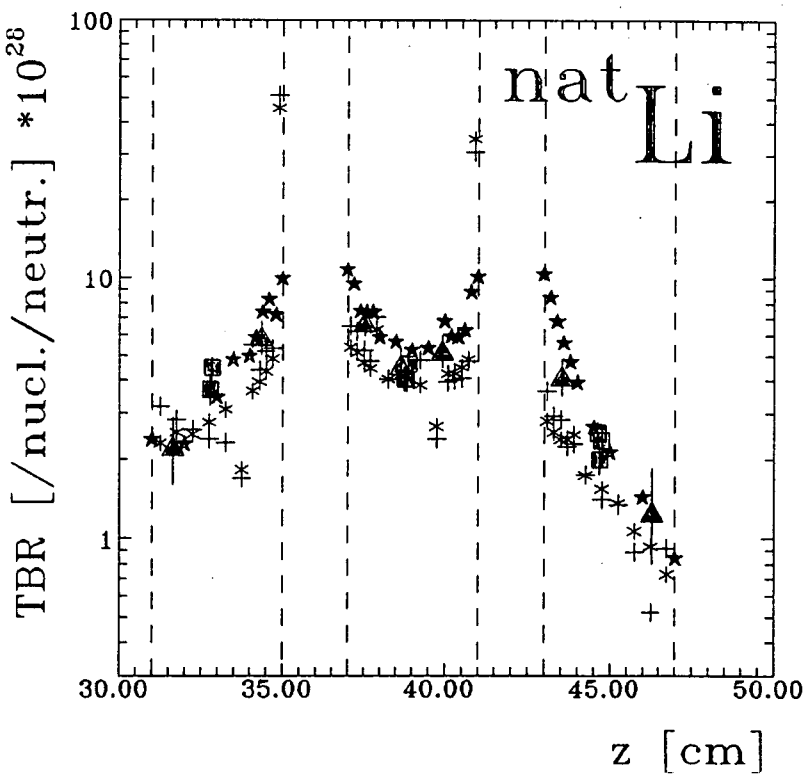

Fig. 1: z-dependence of the tritium production rate in the LiAl-slabs. The experimental results for Li_2CO_3– [△] and LiF–probes [□] are compared with BLANK(ENDL)– [∗, +] and MORSE(ENDF/B-IV)–calculation results [stars].

Further neutron transport calculations on the base of the recent ENDF/B–, ENDL–, and EFF–libraries to investigate the status of these libraries for tritium production calcutions in hybrid blanket mock-ups are in progress.

1) Bergakademie Freiberg, Freiberg, Germany
2) Kurchatov Institute of Atomic Energy, Moscow, USSR

2. Neutron Leakage TOF Measurement and Transport Calculations for a Hybrid-Reactor Blanket Module

T. Elfruth, T. Hehl [1], D. Markovskij [2], M. Toepfer, D. Seeliger K. Seidel, G. Shatalov [2], S. Unholzer

The transport of neutrons through a hybrid-reactor blanket-module bombarded with 14 MeV neutrons is investigated experimentally by means of time-of-flight technique and theoretically using Monte-Carlo methods.

The main components of the blanket-module built up in slab geometry are an uranium section for neutron and energy multiplication, a tritium breeding section consisting of LiAl and polyethylene and an iron section simulating a shield. Time distributions

of leaking neutrons per one 14 MeV source neutron have been measured for three configurations:

- the uranium section only,
- the blanket-module without the iron shield,
- the complete arrangement.

Neutron transport calculations (time and energy distributions of the neutrons) on the base of ENDF/B-IV- and ENDL-78-data libraries for these three configurations have been carried out using the three-dimensional codes BLANK, MORSE, and MCNP. An example for calculation results is shown in the figure. Obviously are the deviations in the spectral shape arising from different data libraries.

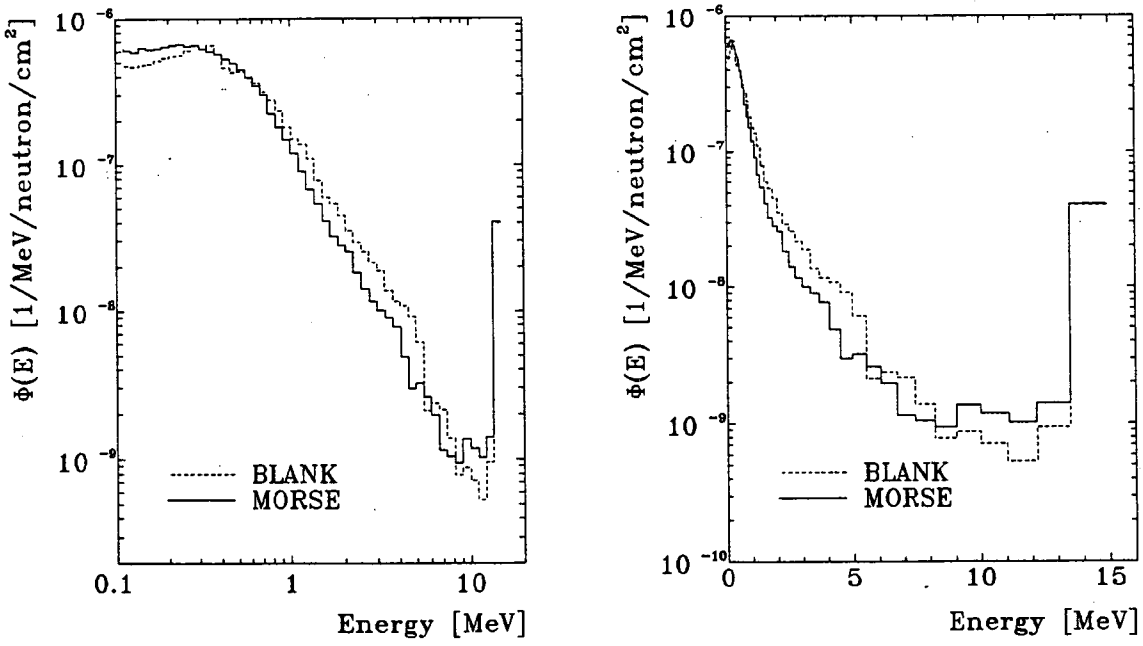

Fig. 1: Comparison of MORSE(ENDF/B-IV)- and BLANK(ENDL-78)-calculation results for the neutron fluence at detector position (2.50 m behind the blanket-module; uranium section only).

First comparisons with the measured time-of-flight spectra including an estimation of the experimental background tend to a good agreement between experimental data and ENDF/B-IV-calculations.

Further neutron transport calculations on the base of the recent ENDF/B-, ENDL-, and EFF-libraries and a detailed calculation of the experimental background are in progress.

1) Present address: Universität Tübingen, Tübingen, Germany
2) Kurchatov Institute of Atomic Energy, Moscow, USSR

3. Nuclear Data from Statistical Multistep Theory between 1 and 100 MeV

H. Kalka, M. Toepfer, E. Schubert, S. Eckstein, D. Seeliger

A unique description of (a,xb) emission spectra where a, b = n, p, α and γ (neutron, proton, alpha, and γ-ray) as well as excitation functions (activation cross sections) is proposed within a pure statistical multistep approach. This analytical model [1-3] is based on random matrix physics and Green's function formalism. In this approach the total emission spectrum is divided in three main parts,

$$\frac{d\sigma_{a,xb}(E_a)}{dE_b} = \frac{d\sigma_{a,b}^{SMD}(E_a)}{dE_b} + \frac{d\sigma_{a,b}^{SMC}(E_a)}{dE_b} + \frac{d\sigma_{a,xb}^{MPE}(E_a)}{dE_b}$$

The first term denotes the statistical multistep direct (SMD) part which contains up to five-step contributions. Here, besides non-collective particle-hole excitations also collective (vibrational) excitations are considered. The second term symbolizes the statistical multistep compound (SMC) emission based on a master equation. Both terms together (SMD plus SMC) represent the so-called *first*-chance emission process. All *higher*-chance emission processes are included in the last term. So far, MPE

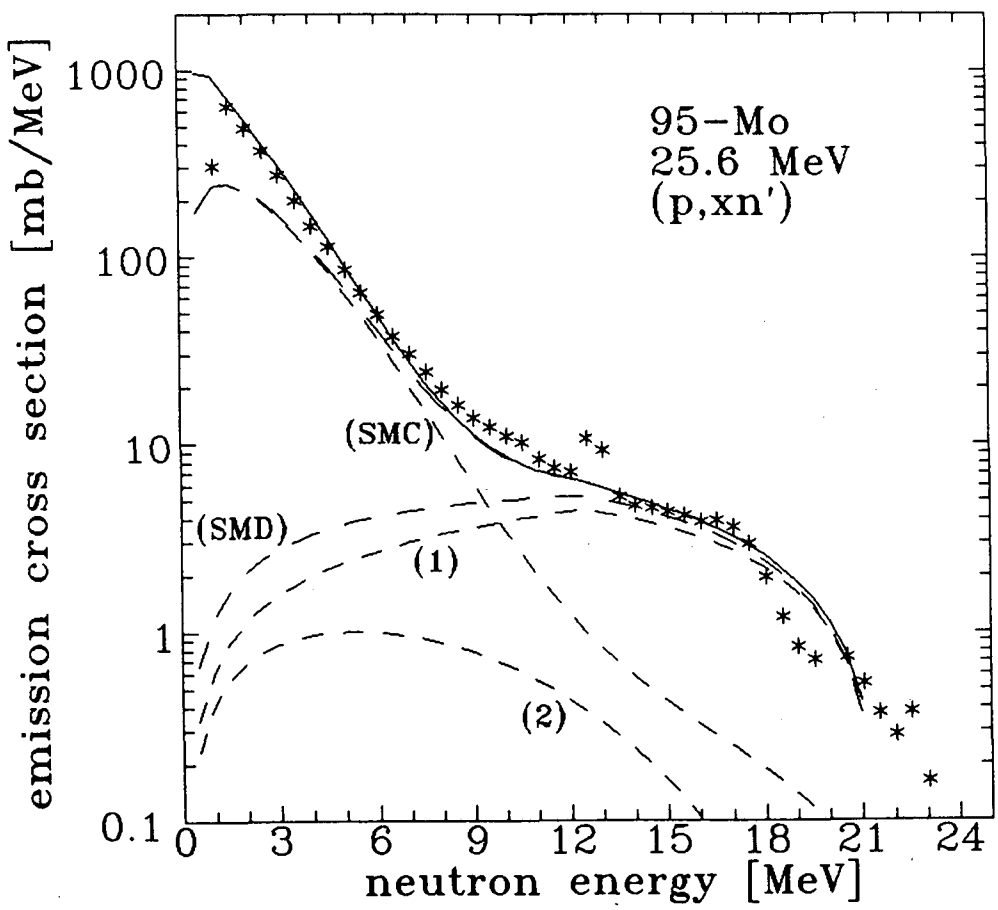

are considered up to three decays of the compound system. Angular distributions are calculated from the above cross section by simple parametrizations (see [4] and references therein).

Calculations for about 120 nuclei ($A > 20$) are performed with code EXIFON [5] using the same global parametr set: strength of residual interaction F_0, radius parameter r_0, Fermi energy E_F, and real potential depth V_0. Single-particle state densities g are calculated directly from r_0 and E_F. The only adjustable parameter is the pairing shift Δ (default $\Delta = 12.8\ A^{-1/2}$ MeV). Binding energies and the β-parameters of the 2 low-lying phonon states are taken from nuclear tables.

All cross sections and emission spectra produced by the above statistical multistep model (code EXIFON) are transformed into a restricted ENDF-6 format. This is realized by the nuclear data file generation code MAKE6 [6].

For example, the calculated (p,xn)-spectra for ^{95}Mo at 25 MeV incident energy is compared with experimental data [7] in the figure.

References

[1] Kalka,H., Torjman,M., and Seeliger,D.: Phys. Rev. **C40**, 1619, 1989

[2] Kalka,H., Torjman,M., Lien,H.N., Lopez,R., Seeliger,D.: Z. Phys. **A335**, 163, 1990

[3] Kalka,H.: submitted to Z. Phys. **A**

[4] Kumabe, I. et. al.: Nucl. Sc. Eng. **104**, 280, 1990

[5] Kalka, H.: code EXIFON (version 2.0), 1991

[6] Toepfer, M. and Schubert, E.: code MAKE6, 1991

[7] Mordhorst, E. et al.: Phys. Rev. **C34**, 103, 1986

4. Fission Neutron Data Systematics

I. Düring, H. Märten, A. Ruben, D. Seeliger

Based on recent theoretical approaches [1,2], systematic calculations of fission neutron data were performed for actinides in the Th-Cf region. The data obtained cover the incident neutron energy (E_i) range from 0 (threshold) to 20 MeV, i.e. including multiple chance fission at $E_i > 6$ MeV, as well as spontaneous fission. The model calculations were based on *global* parameter sets adjusted in the case of well-known fission data (fragment distributions; neutron yield, energy, and angular distributions) as available for ^{252}Cf (sf) and ^{235}U (n_{th},f). The theoretical models used are:

(i) Scission point model including phenomenological, temperature- dependent shell energies for solving the energy partition problem as function of mass asymmetry

A_1/A_2, e.g. calculation of the distribution in excitation energy and kinetic energy of the fragments [1]

(ii) 5-Gaussian approach to fragment mass yield curves considering two asymmetric and one symmetric fission modes, whose parameters were obtained as function of E_i by fits to available experimental data (and use of interpolation routines in applying them to any fission reaction at any E_i)

(iii) Temperature-distribution model (code FINESSE) [2] to calculate yields $\overline{\nu}$, energy, and angular distributions N(E,Θ) of post-fission neutrons

(iv) Reaction theory including the fission channel to account for multiple chance fission and pre-fission neutron emission:

- Hauser-Feshbach theory (code STAPRE) [3]
- Statistical multistep theory (code EXIFON) [4]

FINESSE calculations reproduce ^{252}Cf (sf) data with high accuracy [2,5]. The spectral shapes of post-fission neutron distributions correspond neither to Maxwellian nor to Watt distributions. Fig. 1 shows an example of calculational results: the dependence of $\overline{E}$ on E_i, where at $E_i > 6$ MeV the effect of pre-fission neutron emission becomes obvious. The relation between $\overline{E}$ and the average number of neutrons $\overline{\nu}$ cannot be parameterized in a global form as done by Terrell [6]. For pure (n,f) reactions, we obtained ($X = Z^2/A$)

$$\overline{E} = (0.0698X - 0.8825) + (0.641 - 0.0133X)\ \overline{\nu}$$

whereas spontaneous-fission data can be represented by

$$\overline{E} = 0.1181X - 2.35907.$$

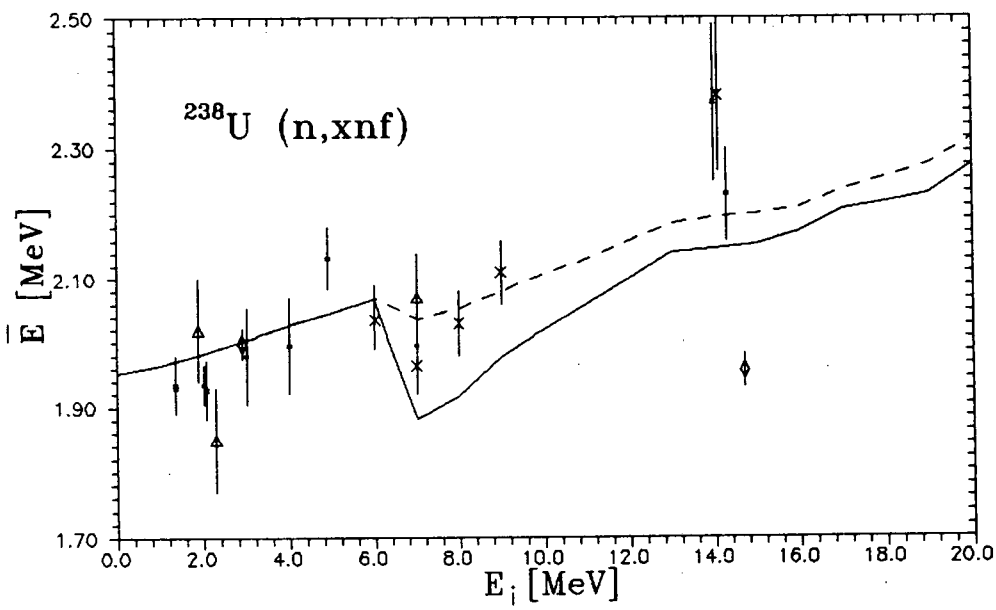

Fig. 1 Average emission energy of fission neutrons as function of neutron incidence energy for ^{238}U (dashed line - without pre-fission neutrons, experimental data - cf. CINDA)

References

[1] Ruben, A. et al., Z. Phys. A 338 (1991) 67

[2] Märten, H. et al., Proc. Int. Conf. on 50 YEARS WITH NUCLEAR FISSION, Gaithersburg, 1989, ed. by J. W. Behrens and A. D. Carlson, ANS(1989) Vol. II, p.743

[3] Uhl, M. and Strohmaier, B., Report IRK-76/01 (1976)

[4] Polster, D. and Kalka, H., submitted to Z. Phys.

[5] Arnold, K. et al., Nucl. Phys. A 502 (1989) 325c

[6] Terrell, J., Proc. IAEA Symp. on PHYSICS AND CHEMISTRY OF FISSION, Salzburg, 1965 (IAEA, Vienna, 1965) Vol. II, p. 3

5. Evaluation of Total Fission Characteristics for ^{235}U in the Neutron Resonance Region

U. Gohs [1)]

An energy conservation consistent evaluation of fission characteristics $\bar{X}_\lambda$ as total fragment kinetic energy $\overline{TKE}$, average number of neutrons $\bar{\nu}$, total number of γ-rays $\bar{N}_\gamma$, and average total energy of γ-rays $\bar{E}_\gamma$ was performed for $J^\pi = 4^-$ neutron resonances of ^{235}U numbered by λ (with total fission width $\Gamma_{f\lambda}$) on the basis of multimode model in a combined fission mode (d) / fission channel (k) representation [1,2]. If considering the contribution of (n,γf) processes with an average width $\bar{\Gamma}_{\gamma f}$ (without account for channel effects) the fission data of interest were evaluated on the basis of

$$\bar{X}_\lambda = \frac{\bar{\Gamma}_{\gamma f}}{\Gamma_{f\lambda}} \sum_d W_{d\lambda} \bar{X}_d^\gamma + (1 - \frac{\bar{\Gamma}_{\gamma f}}{\Gamma_{f\lambda}}) \sum_d \sum_k P_{k\lambda} W_d^k \bar{X}_d^k,$$

where $P_{k\lambda}$ is the relative contribution of fission channel k to a given resonance λ. W_d^k is the relative population of mode d for channel k, $W_{d\lambda}$ is the relative population of mode d for resonance λ. All the population probabilities were deduced from experimental data [3]. Experimental fission characteristics (fragment kinetic energy and neutron multiplicity) as function of fragment mass number for thermal-neutron induced fission were used to define the parameters of energy partition at scission point [4]. In the case of the (n,γf) process the excitation energy at scission point is reduced by the average γ-ray energy, whereas the total number of gamma-rays increases by 1. According to the present evaluation, the (n,γf) reaction for 4^- neutron resonances of ^{235}U is characterized by the following averages

- $\bar{\Gamma}_{\gamma f} \bar{N}_{\gamma f} = (0.33 \pm 0.13) meV \qquad \bar{\Gamma}_{\gamma f} \bar{E}_{\gamma f} = (300 \pm 120) eV^2$

The calculations based on the combined fission mode/fission channel model with account for the (n,γf)-process reproduce experimental data well. Fig. 1 represents an excample of calculational results. $\overline{TKE}$ data for several 4^- resonances of ^{235}U are shown in comparison with experimental data [3].

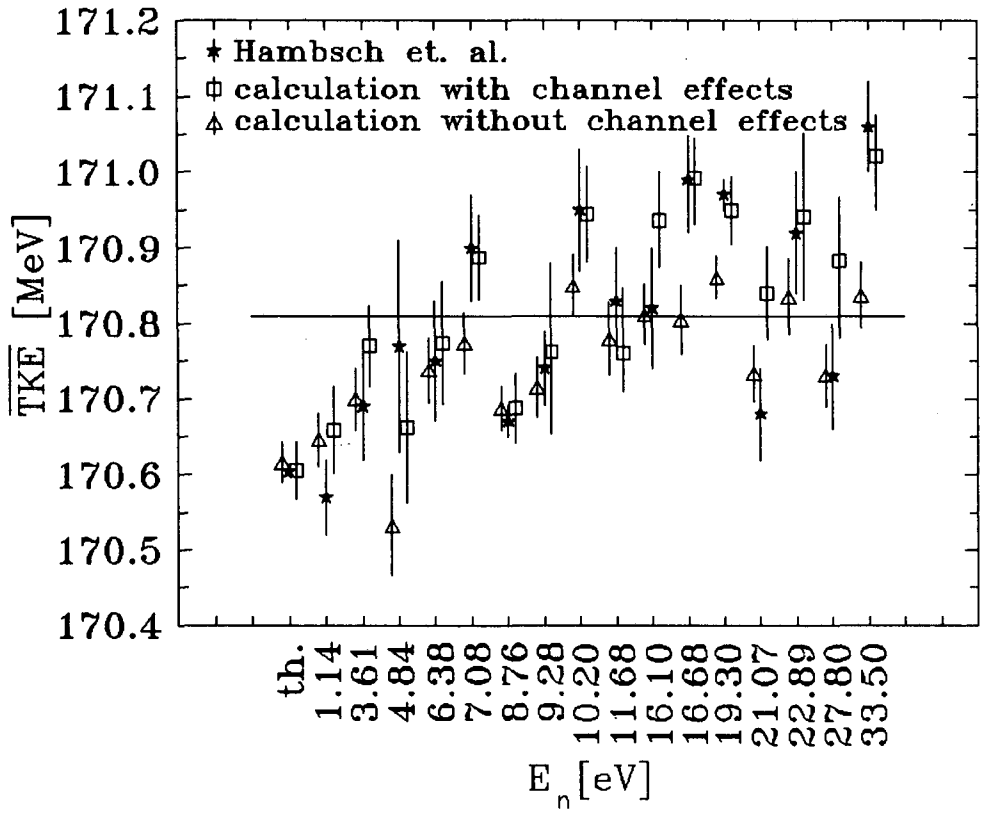

Fig. 1: $\overline{TKE}$ for several 4^- neutron resonances of ^{235}U

1) Present address: JINR Dubna, Laboratory on Neutron Physics, Dubna 1411980, USSR

References

[1] Brosa, U. et al., Z. Naturforschung 41a (1986) 1341

[2] Furman, V.I. and Kliman, J., Proc. Int. Symp. on Nucl. Physics, Gaussig, 1987, ZfK-646 (1988) 142

[3] Hambsch, F.J. et al., Nucl. Phys. A491 (1989) 56

[4] Ruben, A. et al., Z. Phys. A338 (1991) 67

6. Double-Differential Neutron Emission Cross Sections of ^{51}V, ^{181}Ta, ^{nat}W and ^{238}U at 14 MeV Neutron Incidence Energy

H. Al Obiesi, T. Elfruth, T. Hehl *), M. Toepfer, D. Seeliger, K. Seidel, S. Unholzer

In designs of fusion reactors Vanadium, Tantalum and Tungsten are structure and shielding materials. Uranium is used in hybrid reactor projects for neutron multiplication, energy enhancement by fission and plutonium breeding. The neutron emission induced by 14 MeV neutrons is of importance as much as the materials are arranged near the plasma. On the other hand, the 14 MeV data are a fixpoint for the evaluation of neutron emission cross sections at lower energies. Besides the energy-differential neutron emission data the angular distributions of the emitted neutrons have also to be taken into account in transport calculations. In library files of evaluated data for the four elements investigated high-energy neutron emission components are neglected, underestimated, or only artificially described. Angular distributions are assumed to be isotropic with the exception of the scattering from only a few low-lying levels.

In the frame of the IAEA Co-ordinated Research Programme on "Measurement and analysis of 14 MeV neutron-induced double-differential neutron emission cross sections needed for fission and fusion reactor technology" neutron emission cross sections have been measured using a pulsed d-T neutron generator and a time-of- flight spectrometer

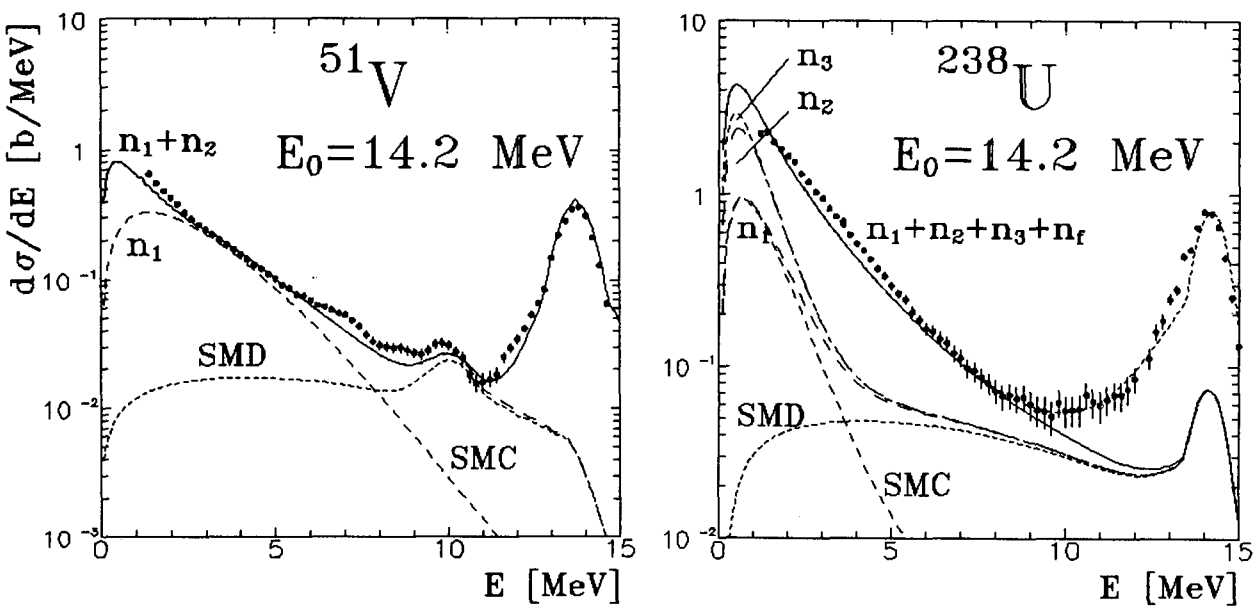

Fig. 1: Angle-integrated neutron emission spectra processed from the measured data in comparison with nuclear model calculations. SMD and SMC denote the multi-step direct and compound contributions of "first chance emission", respectively. The n_i represent the partial contributions from the nuclear cascade multiple chance emission and n_f the neutrons evaporated from the fission fragments.

particularly constructed to study angular distributions of the neutron emission [1].

The measured data have been compared with previous experimental results as well as evaluated library data. Calculations including direct collective and statistical single-particle excitations as well as multiple chance emissions from the compound nucleus cascade (n_i) and from the fission fragments (n_f) have been carried out using the SMD/SMC-model code EXIFON [2] and FINESSE [3], respectively.

Conclusions have been drawn for the improvement of the 14 MeV data status. An evaluation of the double-differential neutron emission spectra at 14 MeV for Vanadium and Uranium is in progress.

*) Present address: Universität Tübingen, Tübingen, Germany

References

[1] Al Obiesi, H. et al.: INDC(GDR)-58/L, IAEA, Vienna, 1990

[2] Kalka, H.: code EXIFON (version 2.0), 1991

[3] Märten, H.: Proc. Int.Conf. on *50 Years with Nuclear-Fission*, Gaithersburg, 25–28 April 1989, ed. by J. W. Behrens and A. D. Carlson, ANS(1989) Vol.II, p.743

7. Measurement and Calculation of Neutron Spectra from the Fission of ^{232}Th, ^{235}U, ^{237}Np and ^{239}Pu Induced by Fast Neutrons

I. Düring, H. Märten, A. Ruben, A.V. Polyakov *), G.N. Lovchikova *), B.V. Shuravlev *), S.E. Sukhikh *), V.A. Vinogradov *), A.M. Trufanov *)

Standard neutron time-of-flight spectroscopy was applied to measure fission neutron spectra for several actinide nuclei. In the following, the main characteristics of measurement and analysis are summarized:

- Neutron detection by the use of NE213 and stilbene scintillators combined with an efficient pulse shape discrimination,
- Fast fragment detection by multiplate ionization chambers with about 1 g actinide material on 40 electrodes with sectorwise readout [1],
- Incident neutron production at energies 1.5 and 7-10 MeV via the reactions T(p,n) and D(d,n) (gas targets), respectively, at the Tandem facilities in Obninsk and Rossendorf,
- Application of the sliding-bias method to minimize experimental uncertainties [2],

- Data correction for several systematic influences (resolution, fragment detection efficiency, etc.) [2],
- Measurement with reference to the ^{252}Cf spectrum (nuclear standard).

The code FINESSE [3] (cf. contribution to this annual report) reproduces the measured data in all cases without any parameter fit. An example is presented in Fig.1.

Tab. 1 Average emission energies of fission neutrons for the reactions measured. Th.1 and Th.2 indicate calculational results without and with consideration of pre-fission neutrons, respectively.

NUCLEUS	E_i [MeV]	$\overline{E}$ [MeV] (Exp.)	$\overline{E}$ [MeV] (Th.1)	$\overline{E}$ [MeV] (Th.2)
^{232}Th	1.5	1.88 ± 0.06	1.82	
	7.3	1.96 ± 0.08	1.88	1.64
^{235}U	1.5	1.94 ± 0.06	2.00	
^{237}Np	7.8	2.03 ± 0.08	2.17	2.08
^{239}Pu	1.5	2.14 ± 0.07	2.11	
	7.5	2.24 ± 0.10	2.23	2.14
	10.0	2.11 ± 0.10	2.29	2.22

In the case of neutron incident energies $E_i > 6$ MeV, multiple chance fission is adequately considered. Note that fission neutron anisotropies with reference to incident beam direction were also described by the complex statistical model calculations [4]. The experimental and calculational results are summarized in Tab.1.

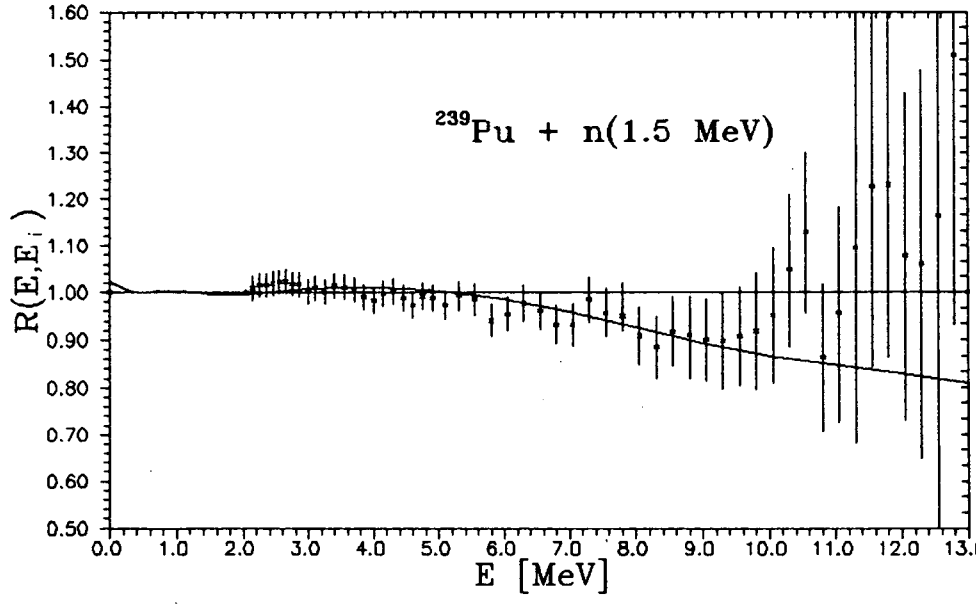

Fig. 1 Ratio of the measured neutron spectrum from the ^{239}Pu fission by E_i = 1.5 MeV neutrons to the ^{252}Cf standard spectrum (norm 1. in each case): FINESSE calculation (solid line) in comparison with measured data.

There is a remarkable dependence of the $\overline{E}$ data deduced from measured data on the energy range covered in the experiment (1.5 - 15 MeV in the present case). Considering this fact, the comparison between measured and calculated $\overline{E}$ data as listed in Tab.1 should be interpreted.

*) Institute for Physics and Power Engineering, Obninsk, USSR

References

[1] Sukhikh, S.E. et al., Report FEI-1927 (Obninsk, 1988)

[2] Märten, H. et al., Nucl. Sci. Eng. 106 (1990) 353

[3] Märten, H. et al., Proc. Int. Conf. on 50 YEARS WITH NUCLEAR FISSION, Gaithersburg, 1989, ed. by J. W. Behrens and A. D. Carlson, ANS(1989) Vol. II, p.743

[4] Sukhikh, S.E. et al., Atomnaya Energiya 69 (1990) 28

ABTEILUNG NUKLEARCHEMIE
UNIVERSITÄT ZU KÖLN
AND
ZENTRALEINRICHTUNG FÜR STRAHLENSCHUTZ
UNIVERSITÄT HANNOVER

1. Production of radionuclides from C, N, O, Mg, Al, and Si by alpha-induced reactions up to 170 MeV

B. Dittrich[1,3], U. Herpers[1], R. Rösel[1], H.-J. Lange[2], T. Hahn[2], R. Michel[2], H.J. Hofmann[3], W. Wölfli[3]

^{4}He-induced reactions significantly contribute to the production of cosmogenic nuclides in extraterrestrial materials such as the lunar surface, meteorites and cosmic dust, as well as in the earth's atmosphere. The knowledge of thin-target cross sections of the underlying nuclear reactions is a basic requirement for any interpretation of the observed abundances of cosmogenic nuclides.

Up to now, most of the required excitation functions of ^{4}He-induced reactions are poorly known, if at all. Therefore, we extended our earlier investigations of ^{4}He-induced reactions on Ti, V, Mn, Fe, Co, and Ni [1-3] with respect to the target element coverage. The target elements C, N, O, Mg, Al, and Si were investigated for ^{4}He-energies up to 170 MeV using the stacked-foil technique. Cross sections for the production of ^{7}Be, ^{10}Be, ^{22}Na, ^{24}Na, ^{28}Mg and ^{26}Al were determined.

Irradiation experiments with ^{4}He were performed at the sector cyclotron at PSI/Villigen (E = 119.7 MeV) and at the isochronous cyclotron JULIC at KFA Jülich (E = 170.5 MeV). C, Mg, Al, and Si were irradiated as pure element foils with thicknesses between 0.025 and 1 mm. For nitrogen and oxygen foils made of Si_3N_4 and SiO_2 with thicknesses of 1 mm were used. The contributions to the residual nuclide production from Si was later corrected for. For each target material investigated one stack was irradiated at PSI and at KFA.

1 Abteilung Nuklearchemie, Universität zu Köln, F.R.G.
2 Zentraleinrichtung für Strahlenschutz, Universität Hannover, F.R.G.
3 Inst. für Mittelenergiephysik, ETH-Hönggerberg, Zürich, Switzerland

The alpha-energies in the individual target foil were calculated according to the work of Williamson et al. [4]. The beam current was determined by Faraday cup measurements at the JULIC accelerator. At PSI the reaction $^{27}Al(^{4}He,4p5n)^{22}Na$ was used as monitor reaction adopting the recommended cross sections from the evaluation by Tobailem and de Lassus St. Genies [5] at 119.7 MeV. The excitation functions determined from the irradiations at the different accelerators overlap between 120 and 80 MeV. Here, the cross sections are in excellent agreement, demonstrating the consistency of the flux determinations used.

Gamma-spectrometry and experimental techniques for the AMS measurements were identical to those used earlier [1-3,6]. $^{10}Be/^{9}Be$ and $^{26}Al/^{27}Al$ ratios were measured at the PSI-ETH AMS-facility in Zürich [7]. For ^{10}Be the standard "S433" was used, which according to recent investigations [8] has a $^{10}Be/^{9}Be$ ratio of $(9.31 \pm 0.23) * 10^{-11}$. For ^{26}Al the standard "Al9" ($^{26}Al/^{27}Al = 1.19 * 10^{-9}$) was used, which was prepared at Cologne [9].

The new cross sections for the production of ^{7}Be, ^{10}Be, ^{22}Na, ^{24}Na, ^{28}Mg, and ^{26}Al by ^{4}He-induced reactions on C, N, O, Mg, Al, and Si are presented in tables 1 - 5.

References

[1] R. Michel, G. Brinkmann, Nucl. Phys. A 338 (1980) 167.

[2] R. Michel, R. Stueck, in: K.H.Boeckhoff, Ed., Proc. Int. Conf. Nucl. Data Sci. Techn., Sept.6-10, 1982, Antwerpen (1983) 599.

[3] R. Michel, G. Brinkmann, R. Stueck, Radiochim. Acta 32 (1983) 173.

[4] C.F. Williamson, J.P. Boyot, J. Picard, CEA-R3042 (1966).

[5] J. Tobailem, C.H. de Lassus St. Genies, CEA-N-1466(5) (1981).

[6] B. Dittrich, U. Herpers, H.J. Hofmann, W. Wölfli, M. Lüpke, R. Michel, P. Dragovitsch, D. Filges, Nucl. Instr. Meth. Phys. Res. B52 (1990) 588.

Tab. 1: Experimental cross sections for the production of ^{7}Be and ^{10}Be from carbon, nitrogen and oxygen by ^{4}He-induced reactions.

E ± dE [MeV]	σ ± dσ [mb]	E ± dE [MeV]	σ ± dσ [mb]
$C(^{4}He,4pXn)^{7}Be$		**$N(^{4}He,5pXn)^{7}Be$**	
78.7 ± 1.0	20.8 ± 1.5	44.2 ± 17.2	7.0 ± 0.5
83.6 ± 1.1	26.7 ± 1.9	71.9 ± 11.5	21.8 ± 2.1
89.7 ± 1.0	33.2 ± 2.4	92.0 ± 9.6	29.2 ± 2.2
92.3 ± 1.0	33.5 ± 2.4	108. ± 8.7	28.8 ± 2.2
96.6 ± 0.9	33.2 ± 2.4	109. ± 8.3	31.0 ± 2.3
98.9 ± 1.3	30.3 ± 3.2	124. ± 7.9	29.0 ± 2.4
98.9 ± 0.9	31.9 ± 2.3	138. ± 7.2	27.0 ± 2.0
103. ± 0.8	33.6 ± 2.4	151. ± 6.7	26.2 ± 2.2
105. ± 0.8	33.5 ± 2.4	163. ± 6.3	26.7 ± 2.1
107. ± 1.2	31.6 ± 3.3		
110. ± 0.8	32.5 ± 2.3	**$N(^{4}He,5pXn)^{10}Be$**	
113. ± 1.2	32.4 ± 5.5		
115. ± 0.7	32.6 ± 2.3	44.2 ± 17.2	0.17 ± 0.01
117. ± 0.7	28.9 ± 2.0	71.9 ± 11.5	1.23 ± 0.07
120. ± 1.1	31.8 ± 3.4	92.0 ± 9.6	2.93 ± 0.18
126. ± 1.0	32.1 ± 3.3	109. ± 8.3	3.18 ± 0.19
132. ± 1.0	33.8 ± 3.4		
137. ± 0.9	36.7 ± 3.5	**$O(^{4}He,6pXn)^{7}Be$**	
143. ± 0.9	34.0 ± 3.8		
149. ± 0.8	31.7 ± 3.5	53.8 ± 13.2	5.3 ± 0.4
155. ± 0.7	38.3 ± 3.7	76.1 ± 10.1	12.8 ± 1.4
159. ± 0.7	38.0 ± 3.5	81.1 ± 9.9	16.1 ± 1.6
165. ± 0.6	35.9 ± 3.7	94.0 ± 8.6	17.2 ± 1.3
		98.8 ± 9.0	18.5 ± 1.5
$C(^{4}He,4pXn)^{10}Be$		110. ± 7.7	18.4 ± 1.4
		115. ± 8.0	21.1 ± 1.7
78.7 ± 1.0	3.47 ± 0.32	128. ± 6.9	21.5 ± 1.6
80.9 ± 1.0	5.03 ± 0.46	141. ± 6.4	21.9 ± 1.6
96.6 ± 0.9	6.50 ± 0.60	153. ± 6.1	22.3 ± 1.6
98.9 ± 1.2	6.44 ± 0.56	164. ± 5.5	21.3 ± 1.7
103. ± 0.8	6.70 ± 0.61		
107. ± 1.2	7.14 ± 0.61	**$O(^{4}He,6pXn)^{10}Be$**	
110. ± 0.8	7.28 ± 0.67		
113. ± 1.2	7.56 ± 0.65	53.8 ± 13.2	0.12 ± 0.01
120. ± 1.1	7.33 ± 0.63	76.1 ± 10.1	1.16 ± 0.10
137. ± 0.9	8.68 ± 0.74	94.0 ± 8.6	2.14 ± 0.15
165. ± 0.6	9.38 ± 0.76	110. ± 7.7	2.47 ± 0.19

Tab. 2: Experimental cross sections for the production ^{7}Be, ^{22}Na, ^{24}Na and ^{28}Mg from magnesium by ^{4}He-induced reactions.

E ± dE [MeV]	σ ± dσ [mb]	σ ± dσ [mb]
	Mg(^{4}He,10pXn)^{7}Be	**Mg(^{4}He,3pXn)^{22}Na**
34.6 ± 2.3	0.076 ± 0.008	2.7 ± 0.2
44.3 ± 2.0	0.685 ± 0.054	74.3 ± 5.2
52.4 ± 1.9	1.79 ± 0.13	130. ± 9.
62.8 ± 1.6	3.39 ± 0.24	116. ± 8.
70.8 ± 1.3	4.58 ± 0.33	100. ± 7.
78.3 ± 1.4	5.42 ± 0.38	90.2 ± 6.0
86.7 ± 1.2	6.39 ± 0.46	91.9 ± 6.6
92.9 ± 1.6	7.55 ± 0.76	84.2 ± 5.9
94.4 ± 1.4	7.55 ± 0.76	79.5 ± 5.6
96.8 ± 1.2	7.94 ± 0.57	85.4 ± 6.0
105. ± 1.4	8.97 ± 0.90	78.3 ± 5.5
106. ± 1.0	8.61 ± 0.61	79.1 ± 5.6
107. ± 1.4	8.97 ± 0.90	78.5 ± 5.5
115. ± 0.7	8.37 ± 0.60	73.7 ± 5.2
117. ± 1.2	8.38 ± 0.84	74.6 ± 5.3
118. ± 1.3	8.38 ± 0.84	74.7 ± 5.2
130. ± 1.2	9.70 ± 0.97	71.4 ± 5.1
132. ± 1.2	9.70 ± 0.97	68.4 ± 4.8
143. ± 1.0	10.0 ± 1.0	70.4 ± 5.0
144. ± 1.0	10.0 ± 1.0	65.4 ± 4.6
152. ± 0.9	10.4 ± 1.0	68.1 ± 4.8
153. ± 0.9	10.4 ± 1.0	64.1 ± 4.5
163. ± 0.8	10.1 ± 1.0	64.8 ± 4.6
164. ± 0.7	10.1 ± 1.0	62.1 ± 4.4
	Mg(^{4}He,3pXn)^{24}Na	**Mg(^{4}He,2pXn)^{28}Mg**
92.9 ± 1.6	25.4 ± 1.8	0.191 ± 0.028
94.4 ± 1.4	25.8 ± 1.8	0.196 ± 0.033
105. ± 1.4	24.5 ± 1.8	0.145 ± 0.027
107. ± 1.4	25.8 ± 1.8	0.139 ± 0.029
117. ± 1.2	23.4 ± 1.7	0.113 ± 0.024
118. ± 1.3	24.9 ± 1.8	0.109 ± 0.023
130. ± 1.2	22.4 ± 1.6	0.087 ± 0.021
132. ± 1.2	24.0 ± 1.7	0.099 ± 0.021
143. ± 1.0	22.0 ± 1.6	0.066 ± 0.019
144. ± 1.0	23.4 ± 1.7	0.076 ± 0.020
152. ± 0.9	21.2 ± 1.5	0.055 ± 0.018
153. ± 0.9	22.5 ± 1.6	0.059 ± 0.019
163. ± 0.8	19.5 ± 1.4	0.046 ± 0.017
164. ± 0.7	21.4 ± 1.5	0.037 ± 0.013

Tab. 3: Experimental cross sections for the production ^{7}Be, ^{22}Na, ^{24}Na and ^{28}Mg from aluminum by ^{4}He-induced reactions.

E ± dE [MeV]	σ ± dσ [mb]	σ ± dσ [mb]
	$^{27}Al(^{4}He,11p13n)^{7}Be$	**$^{27}Al(^{4}He,4p5n)^{22}Na$**
24.6 ± 1.7		0.10 ± 0.01
32.3 ± 1.5		0.12 ± 0.01
37.3 ± 1.4	0.044 ± 0.007	0.84 ± 0.06
44.6 ± 1.2	0.217 ± 0.033	19.5 ± 1.4
49.8 ± 1.2	0.502 ± 0.057	39.3 ± 2.8
55.4 ± 2.2	0.883 ± 0.065	44.6 ± 3.1
61.7 ± 2.0	1.33 ± 0.10	37.5 ± 2.6
67.4 ± 1.9	1.80 ± 0.13	30.0 ± 2.1
72.8 ± 1.8	2.20 ± 0.16	25.9 ± 1.8
77.9 ± 1.7	2.64 ± 0.19	25.2 ± 1.8
82.7 ± 1.6	2.97 ± 0.21	28.6 ± 2.0
86.4 ± 1.9	3.16 ± 0.23	31.2 ± 2.2
87.4 ± 1.7	3.43 ± 0.24	33.2 ± 2.3
92.3 ± 1.6	3.85 ± 0.27	35.2 ± 2.5
97.0 ± 1.5	4.20 ± 0.30	35.6 ± 2.5
99.7 ± 1.7	3.93 ± 0.28	37.2 ± 2.6
104. ± 1.4	4.82 ± 0.35	37.7 ± 2.7
108. ± 1.3	5.00 ± 0.36	38.2 ± 2.7
112. ± 1.7	4.62 ± 0.34	40.2 ± 2.9
114. ± 1.2	5.37 ± 0.38	43.3 ± 3.1
116. ± 1.1	5.36 ± 0.39	42.6 ± 3.0
118. ± 0.4	4.44 ± 0.32	40.3 ± 2.9
118. ± 0.4	4.67 ± 0.33	39.9 ± 2.8
119. ± 0.4	4.94 ± 0.35	36.5 ± 2.6
125. ± 1.4	4.95 ± 0.35	41.2 ± 3.0
136. ± 1.3	5.12 ± 0.37	44.1 ± 3.1
148. ± 1.2	5.66 ± 0.41	42.8 ± 3.1
159. ± 1.1	5.80 ± 0.43	
170. ± 0.3	4.31 ± 0.32	41.6 ± 3.0
	$^{27}Al(^{4}He,4p3n)^{24}Na$	**$^{27}Al(^{4}He,3p)^{28}Mg$**
86.4 ± 1.9	35.9 ± 2.6	0.230 ± 0.029
99.7 ± 1.7	34.3 ± 2.5	0.197 ± 0.027
112. ± 1.7	32.5 ± 2.3	0.158 ± 0.024
125. ± 1.4	31.6 ± 2.3	0.121 ± 0.024
136. ± 1.3	31.7 ± 2.2	0.111 ± 0.022
148. ± 1.2	30.1 ± 2.1	0.100 ± 0.021
159. ± 1.1	28.9 ± 2.1	0.087 ± 0.019
170. ± 0.3	31.0 ± 2.2	0.080 ± 0.029

Tab. 4: Experimental cross sections for the production ^{7}Be, ^{22}Na, ^{24}Na and ^{28}Mg from silicon by ^{4}He-induced reactions.

E ± dE [MeV]	σ ± dσ [mb]	σ ± dσ [mb]
	Si(^{4}He,12pXn)^{7}Be	**Si(^{4}He,5pXn)^{22}Na**
45.9 ± 7.6	0.76 ± 0.05	0.70 ± 0.05
58.8 ± 6.4	1.95 ± 0.14	11.9 ± 0.8
69.8 ± 5.6	3.03 ± 0.21	35.5 ± 2.5
79.5 ± 5.1	3.96 ± 0.28	41.3 ± 2.9
80.6 ± 5.3	4.71 ± 0.34	42.6 ± 3.0
89.4 ± 4.9	5.95 ± 0.43	42.8 ± 3.0
90.8 ± 4.6	5.17 ± 0.36	37.6 ± 2.6
97.5 ± 4.6	6.71 ± 0.48	40.8 ± 3.0
98.9 ± 4.3	6.00 ± 0.42	39.6 ± 2.8
105. ± 4.4	6.97 ± 0.49	34.0 ± 2.4
107. ± 4.0	6.60 ± 0.47	41.3 ± 2.9
112. ± 4.2	7.49 ± 0.54	39.6 ± 2.8
114. ± 3.7	6.84 ± 0.48	42.4 ± 3.0
119. ± 4.0	7.80 ± 0.56	37.6 ± 2.7
126. ± 3.8	8.16 ± 0.58	34.5 ± 2.5
132. ± 3.6	8.50 ± 0.61	37.1 ± 2.6
138. ± 3.5	8.49 ± 0.60	33.9 ± 2.4
144. ± 3.4	8.41 ± 0.60	33.8 ± 2.4
150. ± 3.2	9.04 ± 0.64	37.5 ± 2.7
156. ± 3.1	8.66 ± 0.62	34.7 ± 2.5
161. ± 3.0		41.4 ± 3.1
	Si(^{4}He,5pXn)^{24}Na	**Si(^{4}He,4pXn)^{28}Mg**
80.6 ± 5.3	12.2 ± 0.9	0.150 ± 0.015
89.4 ± 4.9	15.1 ± 1.1	0.150 ± 0.016
97.5 ± 4.6	16.4 ± 1.2	0.160 ± 0.016
105. ± 4.4	14.4 ± 1.0	0.150 ± 0.016
112. ± 4.2	16.2 ± 1.1	0.158 ± 0.017
119. ± 4.0	15.9 ± 1.1	0.157 ± 0.016
126. ± 3.8	14.2 ± 1.0	0.158 ± 0.016
132. ± 3.6	15.0 ± 1.1	0.162 ± 0.017
138. ± 3.5	13.9 ± 1.0	0.162 ± 0.016
144. ± 3.4	13.9 ± 1.0	0.149 ± 0.015
150. ± 3.2	14.6 ± 1.0	0.163 ± 0.016
156. ± 3.1	14.2 ± 1.0	0.153 ± 0.016
161. ± 3.0	15.6 ± 1.1	0.168 ± 0.017
166. ± 2.8	13.9 ± 1.0	0.143 ± 0.015

Tab. 5: Experimental cross sections for the production of ^{10}Be and ^{26}Al from magnesium, aluminum and silicon by ^{4}He-induced reactions.

E ± dE [MeV]	σ ± dσ [mb]	σ ± dσ [mb]
	$Mg(^{4}He,10pXn)^{10}Be$	**$Mg(^{4}He,pXn)^{26}Al$**
27.5 ± 2.7	0.0044 ± 0.0008	213. ± 35.
34.6 ± 2.3	0.0045 ± 0.0010	255. ± 18.
41.2 ± 2.1	0.0140 ± 0.0015	135. ± 14.
62.8 ± 1.6	0.153 ± 0.012	44.5 ± 3.8
78.3 ± 1.4	0.353 ± 0.030	40.1 ± 2.9
92.1 ± 1.1	0.601 ± 0.053	21.8 ± 1.7
115. ± 0.7	0.998 ± 0.088	10.7 ± 0.8
	$^{27}Al(^{4}He,11p10n)^{10}Be$	**$^{27}Al(^{4}He,2p3n)^{26}Al$**
28.7 ± 1.6	0.0014 ± 0.0008	208. ± 16.
35.7 ± 1.4		223. ± 16.
40.4 ± 1.3		146. ± 11.
58.6 ± 2.1	0.100 ± 0.006	56.1 ± 4.9
70.1 ± 1.8	0.274 ± 0.009	70.2 ± 5.9
87.4 ± 1.7	0.462 ± 0.012	
116. ± 1.7	0.890 ± 0.027	
	$Si(^{4}He,12pXn)^{10}Be$	**$Si(^{4}He,3pXn)^{26}Al$**
58.8 ± 6.4	0.0147 ± 0.0012	156. ± 5.
79.5 ± 5.1	0.0909 ± 0.0080	78.7 ± 4.6
90.8 ± 4.5	0.140 ± 0.011	117. ± 5.
114. ± 3.8	0.315 ± 0.022	82.4 ± 4.6

[7] M. Suter, R. Balzer, G. Bonani, H.J. Hofmann, M. Morenzoni, M. Nessi, W. Wölfli, M. Andree, J. Beer, and H. Oeschger, Nucl. Instr. Meth. Phys. Res. B5 (1984) 117.

[8] H.J. Hofmann, J. Beer, G. Bonani, H.R. von Gunten, S. Raman, M. Suter, R.L. Walker, W. Wölfli and D. Zimmermann, Nucl. Instr. Meth. Phys. Res. B29 (1987) 32.

[9] R. Sarafin, Thesis, Universität zu Köln (1985) 132.

INSTITUT FÜR KERNCHEMIE
UNIVERSITÄT MAINZ

1. Mass Yields in the Chains with A = 69 to 87 in the Fission of ^{249}Cf by Thermal Neutrons

R. Hentzschel, H.O. Denschlag, H.R. Faust, J.E. Gindler, B. Wilkins

Mass yields in the fission of ^{249}Cf induced by thermal neutrons have been measured in the chains with mass numbers A = 69 to 87 using the mass separator LOHENGRIN at the Institut Laue-Langevin in Grenoble. As pointed out already in a preliminary note [1], a large discrepancy of more than a factor 100 exists for the lowest yields measured when compared to the predictions of the ENDF-V file [2]. In the following (Table 1), we are reporting the final yield values obtained in our work. Experimental details and the observation of odd-even effects increasing with increasing asymmetry of the fission process are discussed in [4].

References

[1] R. Hentzschel, H. O. Denschlag, H. R. Faust, J. E. Gindler, B. Wilkins in S. Cierjacks (Ed.) Progress Report on Nuclear Data Research in the Federal Republic of Germany, Report NE-ANDC(E)-312-U Vol.V, INDC(Ger)-35/LN+Special (1990)

[2] B.F. Rider, Compilation of Fission Product Yields, Vallecitos Nuclear Center, Report NEDO-12154-3(C), ENDF-322 (1981)

[3] M. Djebara, M. Asghar, J.P. Bocquet, R. Brissot, J. Crançon, Ch. Ristori, E. Aker, D. Engelhardt, J. Gindler, B.D. Wilkins, U. Quade, K. Rudolph, Nucl.Phys. A496, 346 (1986)

[4] R. Hentzschel, H. R. Faust, H. O. Denschlag, B. D. Wilkins, J. Gindler: Mass yields in the Very Asymmetric Fission of $^{249}Cf(n_{th},f)$, submitted to Proceedings of the International Conference on Nuclear Data for Science and Technology, Jülich, May 1991.

---

[1]Institut Laue-Langevin, Grenoble, France

[2]Argonne National Laboratory, Argonne, Illinois, USA

Mass	Mass Yield
88	$(5.20 \pm 0.12)\cdot 10^{-1}$
87	$(4.21 \pm 0.08)\cdot 10^{-1}$
86	$(3.43 \pm 0.19)\cdot 10^{-1}$
85	$(2.47 \pm 0.06)\cdot 10^{-1}$
84	$(1.89 \pm 0.04)\cdot 10^{-1}$
83	$(1.22 \pm 0.03)\cdot 10^{-1}$
82	$(7.37 \pm 0.16)\cdot 10^{-2}$
81	$(4.79 \pm 0.13)\cdot 10^{-2}$
80	$(3.01 \pm 0.15)\cdot 10^{-2}$
79	$(1,84 \pm 0.14)\cdot 10^{-2}$
78	$(8.15 \pm 0.23)\cdot 10^{-3}$
77	$(4.61 \pm 0.56)\cdot 10^{-3}$
76	$(1.86 \pm 0.15)\cdot 10^{-3}$
75	$(9.54 \pm 1.70)\cdot 10^{-4}$
74	$(5.32 \pm 0.89)\cdot 10^{-4}$
73	$(2.13 \pm 0.57)\cdot 10^{-4}$
72	$(1.09 \pm 0.24)\cdot 10^{-4}$
71	$(5.35 \pm 1.30)\cdot 10^{-5}$
70	$(3.02 \pm 0.76)\cdot 10^{-5}$
69	$(5.70 \pm 2.20)\cdot 10^{-6}$

Table 1: Mass yields as obtained in the present work. The yields are normalized relative to the yield of mass chain 88 as given by Djebara et al. [3].

2. Odd-even Effects in the Reaction ^{241}Am(2n,f)

P. Stumpf, U. Güttler, H.O. Denschlag, H.R. Faust

Up to now odd-even proton effects in fissioning systems with an odd number of protons were not considered possible, as, necessa-

---

[1]Institut Laue-Langevin, Grenoble, France

rily, in such a reaction a simultaneous formation of an even and an odd fragment takes place. We have observed an odd-even effect of a second kind, however, in the fission of the odd compound nucleus ^{243}Am (with Z = 95): fragments of the light mass range, are preferentially even (and those of the heavy mass range are correspondingly odd). The consequences of this effect on fission theory and on fission yield systematics are the same as for the conventional odd-even effect.

The measurements were performed at the recoil mass separator LOHENGRIN of the Institut Laue-Langevin in Grenoble (France) using targets of ^{241}Am that were converted to $^{242m+g}$Am in the target position of the mass separator. The identification of the atomic numbers of the fission products took place in the ionization chamber (BIC) [1].

The use of the method of Tracy et al. [2] to calculate local odd-even effects for protons (EOZ) and neutrons (EON), when applied to the experimental fission yields obtained in this work, results in the values indicated in Table 1 for the corresponding mean numbers of protons, <Z> and neutrons <N>.

<Z>	EOZ [%]	<N>	EON [%]
31.5	16.9±2.6	48.5	8.4±2.2
32.5	14.8±2.3	49.5	12.1±2.4

Table 1: Local odd-even effects for protons (EOZ) and for neutrons (EON) in the light mass region obtained in the present work using the method of Tracy et al. [2].

As the values of EON are affected by the prompt neutron emission, the following discussion will focus on EOZ.

The preferential formation of light fragments with even Z (and of heavy fragments with odd Z) may be due to two possible reasons:

1. The pairing term in the droplet model is δ/A ($\delta \approx 135$ MeV, A = mass number of atom). Consequently, the division of an odd nucleus into a light even fragment and a heavy odd fragment should be energetically more favorable (by about 1 MeV) than the division into a light odd fragment and a heavy even fragment.

2. The second argument is statistical. If we look at the americium nucleus (Z = 95) as a bag with 47 pairs of protons and one single proton and we imagine that we would take out either pairs of protons or the single proton indiscriminately to form a heavy and a light fragment we would have a larger statistical probability for the single proton to end up in the heavy fragment. This argument leads to a value of EOZ = 38 % for a light fragment with $Z \approx 30$. This value is an upper limit because it assumes that no proton pair is broken on the way to scission. If we assume one additional proton pair to break, a process which would give 3 unpaired protons, using a binomial distribution we can calculate a statistical EOZ of 1.04. A rough estimate of the situation of ^{243}Am brings us to the conclusion that in this case one additional proton pair is broken in every <u>second</u> fission reaction.

A more detailed presentation of this work will be found in Ref. [3].

<u>References</u>

[1] J. P. Bocquet, R. Brissot, H. R. Faust: A Large Ionization Chamber For Fission Fragment Nuclear Charge Identification at the LOHENGRIN Spectrometer; Nucl. Instr. Methods in Phys. Res. A267, 466-472 (1988)

[2] B. L. Tracy, J. Chaumont, R. Klapisch, J. M. Nitschke, A. M. Poskanzer, E. Roeckl, C. Thibault: Rb and Cs Isotopic Cross-Sections from 40-60 MeV Proton Fission of ^{238}U, ^{232}Th, and ^{235}U; Phys. Rev. C5, 222 (1972)

[3] P. Stumpf, U. Güttler, H. O. Denschlag, H. R. Faust: Odd-even Effects in the Reaction ^{241}Am(2n,f); submitted to Proceedings of the International Conference on Nuclear Data for Science and Technology, Jülich, May 1991

FRM-REAKTORSTATION GARCHING, FACHBEREICH PHYSIK TECHNISCHE UNIVERSITÄT MÜNCHEN

Coherent Neutron Scattering Lengths and Total Cross Sections

1. Neutron Scattering Lengths of Molten Metals Determined by Gravity Refractometry

G. Reiner, W. Waschkowski, L. Köster

Vary accurate values of the coherent neutron scattering lengths of the heavy elements Bi and Pb are important quantities for the investigation of the electric interactions of neutrons with atoms. We performed, therefore, a series of experiments to determine accurate scattering lengths by means of neutron gravity refractometry on liquid mirrors of molten metals. The possible perturbations of the necessary reflection measurements have been discussed in detail. After taking into account the uncertainties and corrections associated with observable perturbations we obtained the following values for bound atoms: b(Bi) = 8.532±0.002 fm, b(Pb) = 9.405±0.003 fm, b(Tl) = 8.776±0.005 fm, b(Sn) = 6.225±0.002 fm and B(Ga) = 7.288±0.002 fm. These data are corrected for the local field effect occuring in the refelection on liquids. The recently reported results for the neutron's electric polarizability and the neutron-electron scattering length are supported by the Bi- and Pb scattering length of this work.

Z. Phys. A- Atomic Nuclei 337, 221-228 (1990)

2. Cross Sections for Neutrons of 1970 eV and Contributions to Fundamental Neutron Interactions

L. Köster, W. Waschkowski, J. Meier

Neutrons of energies within a 50 eV interval at 1970 eV have been selected from reactor neutrons by means of neutron resonance scattering on a target of ^{63}Cu and subsequent scattering by the 1970 eV resonance of a ^{80}Se target, The insertion of stationary filters of Sc, Co and B and the technique of difference measurements with a resonance filter resulted in a high selectivity, which allowed the determination of cross sections for quasimonoenergetic neutrons. Values of total cross sections at 1970 eV are given for the elements H, C,

O, F, Na, Mg, Al, Si, P, Cl, K, Ca, Sc, Ti, V, Mn, Co, Ni, Cu, Ga, Pb and Bi in the attached table.

Substance	σ_{tot}(1970 eV) [b]	Substance	σ_{tot}(1970 eV) [b]
H	20.13 (3)	Ca	2.43 (5)
C	4.744 (5)	Sc	0.27 (2)
O	3.77 (3)	Ti	5.17 (2)
F	3.59 (1)	V	7.61 (2)
Na	12.77 (4)	Mn	125 (2)
Mg	3.35 (5)	Co	1.35 (2)
Al	1.350 (7)	Ni	15.04 (3)
Si	2.019(5)	Cu	29 (1)
P	3.23 (2)	Ga	8.41 (4)
Cl	1.60 (3)	Pb	11.198 (3)
K	1.58 (4)	Bi	8.292 (3)

The precision cross sections of Pb and H are of particular interest for the investigation of fundamental neutron interactions. In combination with cross sections at lower energies, the cross section $\sigma(\mathrm{Pb}) = 11.198 \pm 0.003$ b has been used to derive a value $\alpha_n = (0.7 \pm 1)\ 10^{-3}$ fm ^{3} for the electric polarizability of the neutron, by which the recently published values are confirmed. The neutron-proton cross section $\sigma(^1\mathrm{H}) = 20.13 \pm 0.03$ b and data at 143 keV, $<1.3>$ MeV, $<2.1>$ MeV and values for the literature allowed to establish a refined set of the neutron-proton scattering parameters for the shape-independent effective-range approximation of the neutron-proton interaction.

Z. Phys. A - Atomic Nuclei 337, 341-348 (1990)

3. Neutron ^{208}Pb Scattering and the Electric Polarizability of the Neutron

Yu. A. Alexandrov, L. Köster, G.S. Samosvat, W. Waschkowski

Neutron transmission cross sections of ^{208}Pb were measured for four energies. These data were the basis to eveluate the electric polarizability of the neutron a_n:

$\alpha_n = (0.4 \pm 1.5) \cdot 10^{-3}$ fm^3 for $a_{ne} = 1.32 \cdot 10^{-3}$ fm and
$\alpha_n = (-1.1 \pm 1.5) \cdot 10^{-3}$ fm^3 for $a_{ne} = 1.59 \cdot 10^{-3}$ fm

a_{ne} is the neutron electron interaction.

The investigation has been performed at the Laboratory of Neutron Physics, JINR, and in Garching FRM.

JINR Rapid Communications Nr. 6/45/48-50/ -90

4. Refined Interpretation of Christiansen-Filter Experiments and Neutron Scattering Lengths of the Lead Isotopes

L. Köster, K.Knopf

A refined interpretation of Christiansen filter experiments is described, which allows for the effects of inhomogeneities in the powder column of the filter. Using this procedure the evaluation of experiments on enriched samples of lead isotopes provided the neutron coherent scattering lengths (in fm) for the separated isotopes: $b(204) = 10.6 \pm 2.0$; $b(206) = 9.23 \pm 0.05$; $b(207) = 9.28 \pm 0.04$ and $b(208) = 9.50 \pm 0.06$. The corresponding potential scattering radius R' was obtained by taking account of resonance contributions as earlier used in the determination of the neutron's electric polarizability. The found $R' = 9.74 \pm 0.07$ fm is in good agreement with the literature. This confirms the correctness of the used resonance contributions.

INSTITUT FÜR KERNENERGETIK UND ENERGIESYSTEME UNIVERSITÄT STUTTGART

1. Calculation of Double-Differential Charged-Particle Induced Neutron Emission Cross Sections

A. Sohn, M. Mattes

To get information about nuclear cross sections where only a few data exists, we compared results of calculations using the pre-equilibrium model code ALICE [1] with measurements by proton and deuteron induced nuclear reactions at about 22 MeV. Therefore we have implemented the extended Kalbach systematics [2] in the code ALICE.
Fig. 1 shows the neutron emission cross sections. The experimental data were obtained from the double-differential cross sections [3] which are given together with the theoretical results in Fig. 2 and 3. Furthermore a comparison with the code EXIFON [4] was made for the reaction p + ^{181}Ta as an additional verification. The results of this calculation are indicated by the dotted curves in Fig. 1-3.

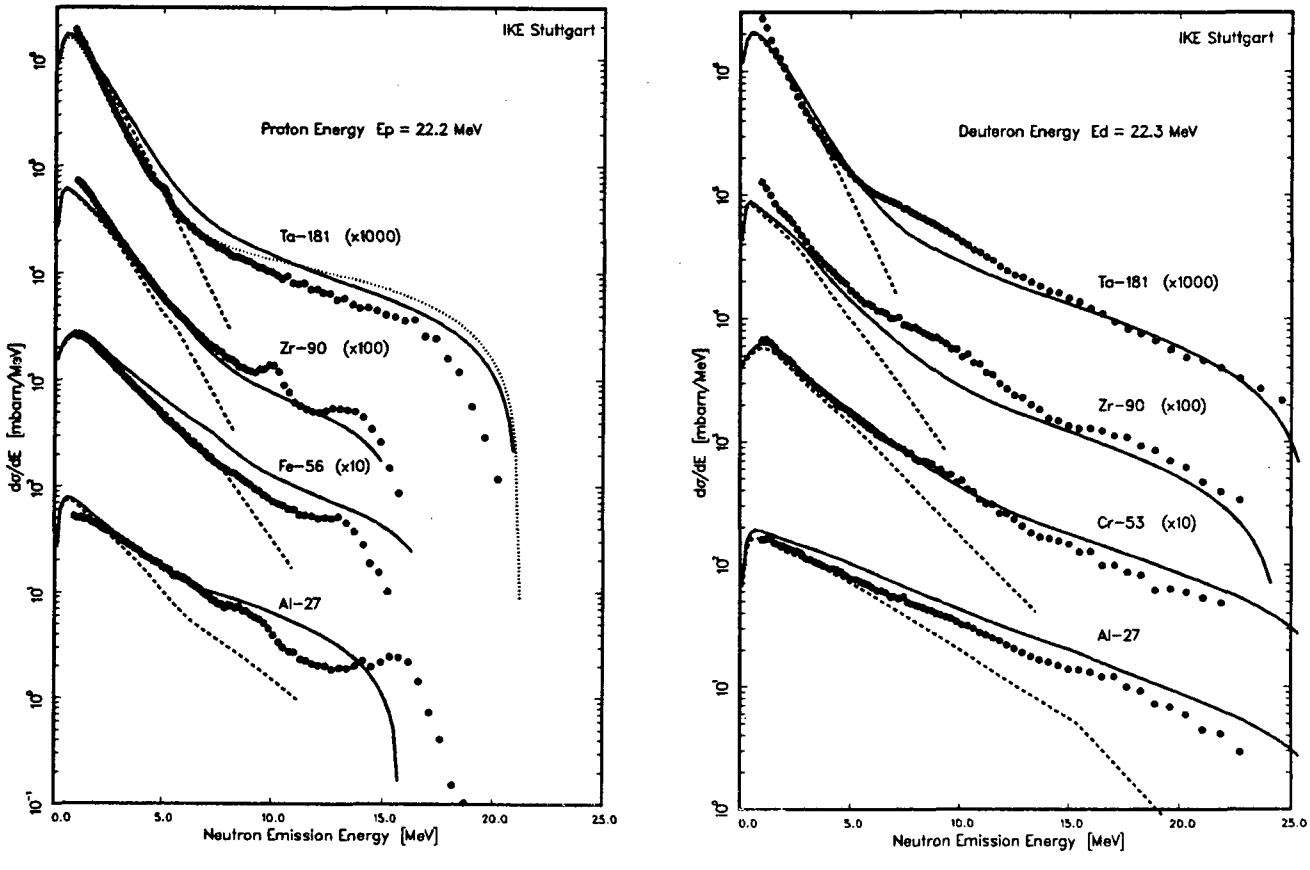

Fig. 1: Neutron emission cross section for 22.2 MeV incident protons (left) and 22.3 MeV incident deuterons (right) on several target nuclids. The dashed line shows the equilibrium part of the emission cross section.

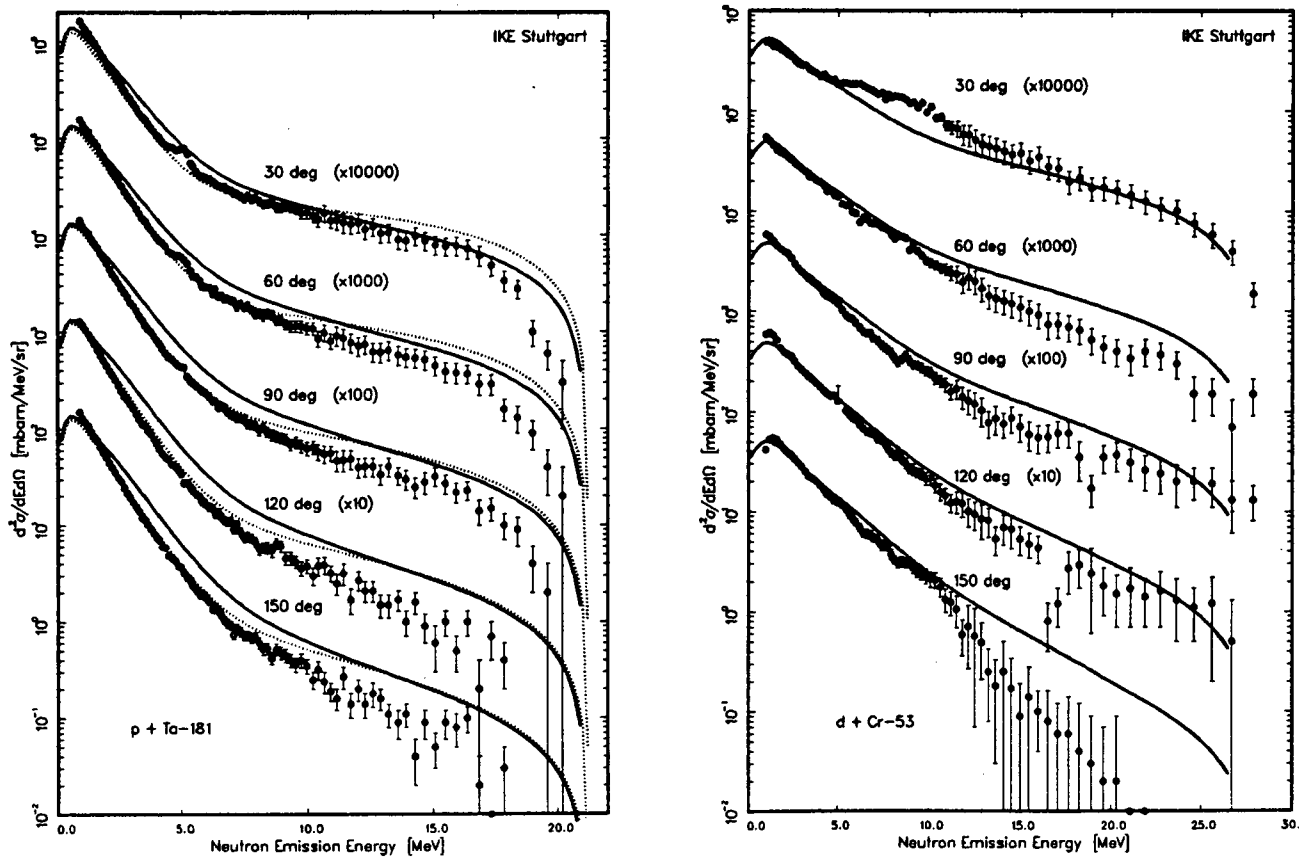

Fig. 2: Double differential cross section for incident protons of 22.2 MeV on ^{181}Ta (left) and for incident deuterons of 22.3 MeV on ^{53}Cr (right) for several neutron emission angles. The dotted line (left) shows the results of a calculation with the code EXIFON.

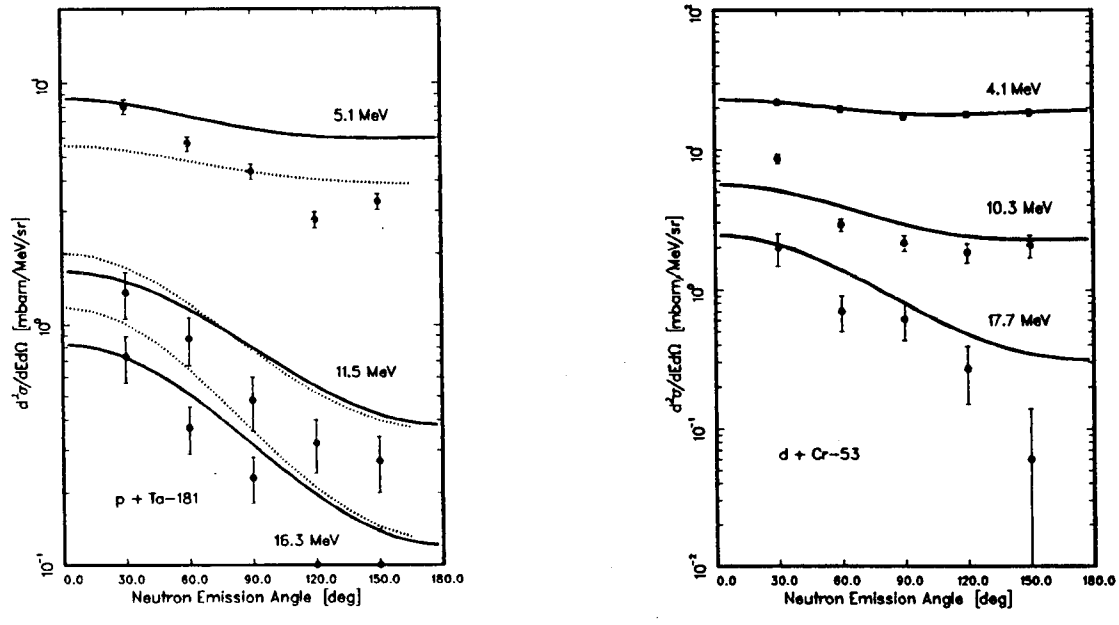

Fig. 3: Angular distribution for several secondary neutron energies for the same nuclear reactions as in Fig. 2.

References:

[1] Blann, M.; Bisplinghoff, J.: Code ALICE/Livermore 82. UCID-19614 (1982) and Update UCID-20169 (1985)

[2] Kalbach, C.: Systematics of continuum angular distributions. Extensions to higher energies. Phys. Rev. C37 (1988) 2350

[3] Birjukov, N.S.: (p,n)-Reactions at Proton Energy of 22.2 MeV. Data file EXFOR-50068. OECD/NEA Data Bank, Paris
Birjukov, N.S.: Neutron from (d,n)-Reaction on ^{27}Al, ^{53}Cr, ^{90,94}Zr, ^{122}Sn, ^{181}Ta. Data file EXFOR-A0302. OECD/NEA Data Bank, Paris

[4] Kalka, H.: A model for statistical multistep reactions (code EXIFON). INDC(GDR)-60/L (1990)

2. Neutron Cross-Sections for Beryllium and Bismuth at Low Temperatures[1]

S. Käfer, J. Keinert, M. Mattes

In superthermal neutron sources beryllium (T=2...25K) and bismuth (T=77K) are used as neutron filters and in addition Bi as γ-shielding material. For these temperatures adequate neutron cross-section data are not commonly available. Therefore neutron cross-sections for Be and Bi are generated for these temperatures. The data include incoherent scattering as well as coherent elastic scattering marked by the hexagonal (Be) and rhomboedric (Bi) lattice structures. For beryllium (hcp), the approved phonon spectrum of Koppel [1] is used for the incoherent scattering; the coherent scattering is calculated with NJOY. For bismuth the incoherent scattering is generated with a realistic frequency distribution derived from [2]. The coherent part is calculated by transforming the rhomboedric lattice structure to an equivalent hexagonal one and deriving the corresponding form function for use in the codes HEXSCAT or NJOY. In the following figures the calculated total neutron cross-sections for Be and Bi are compared with measured data.

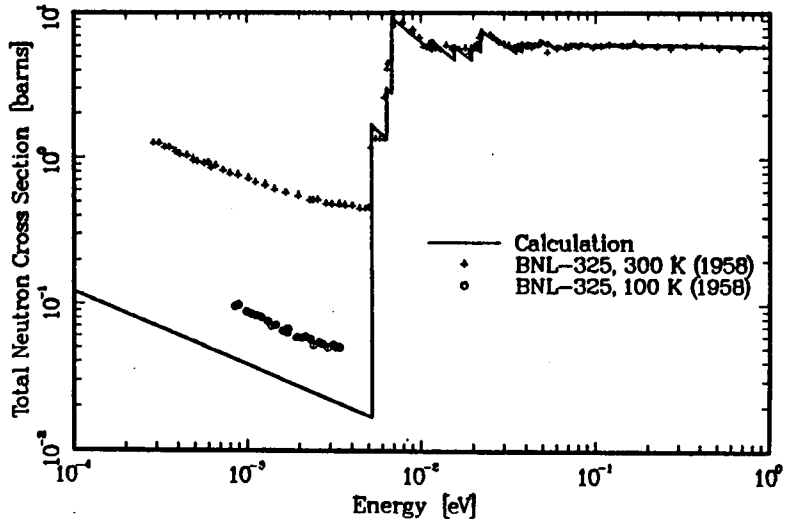

Fig. 1: Total Neutron Cross Section of Beryllium at T= 2.5 K

[1] funded by BMFT, Project 'Erforschung kondensierter Materie und Atomphysik'

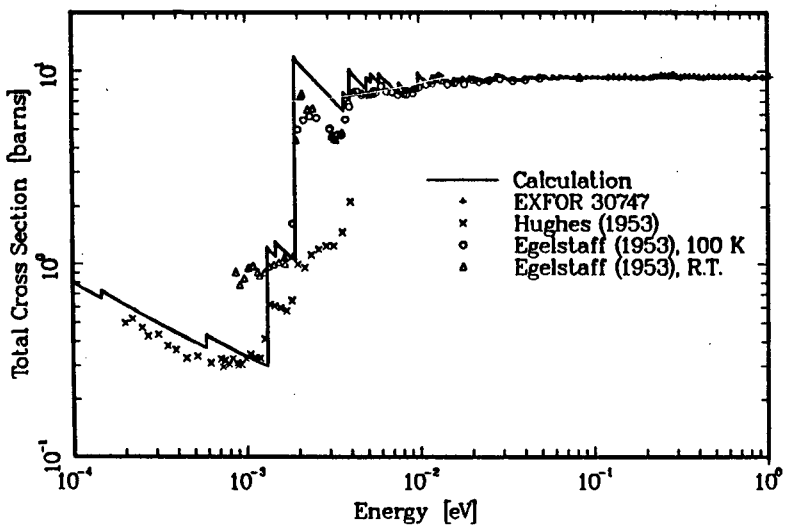

Fig. 2: Total Neutron Cross Section of Bismuth at T= 77 K

References:

[1] Koppel, J.U.; Houston, D.H.: Reference Manual for ENDF Thermal Neutron Scattering Data. GA - 8774 (ENDF-269) (1968)

[2] Kress, W.: Phonon Dispersion Curves, One-Phonon Densities of States and Impurity Vibrations of Metallic Systems. Physik Daten 26 – 1 (1987)

3. Neutron Cross-Sections for Liquid ^{4}He around T= 1 K [1]

J. Keinert, M. Predel

To generate ultracold neutrons, so-called superthermal neutron sources with a combination of zones with liquid H_2 at 20K and liquid ^{4}He at 1 K are discussed. In the past, we have derived improved cross-sections for liquid H_2 and D_2 [1]. For liquid ^{4}He at 1K, no adequate cross-section sets are available. So Scattering Law Data $S(\alpha,\beta)$ are generated in connecting data calculated in incoherent approximation for the monoatomic liquid with a realistic static structure factor according to the Sköld-approximation to account for the purely coherent contribution of the interatomic interaction. In the following figures our results are represented for the derived static structure factor and for the total neutron cross section compared with measurements.

[1]funded by BMFT, Project 'Erforschung kondensierter Materie und Atomphysik'

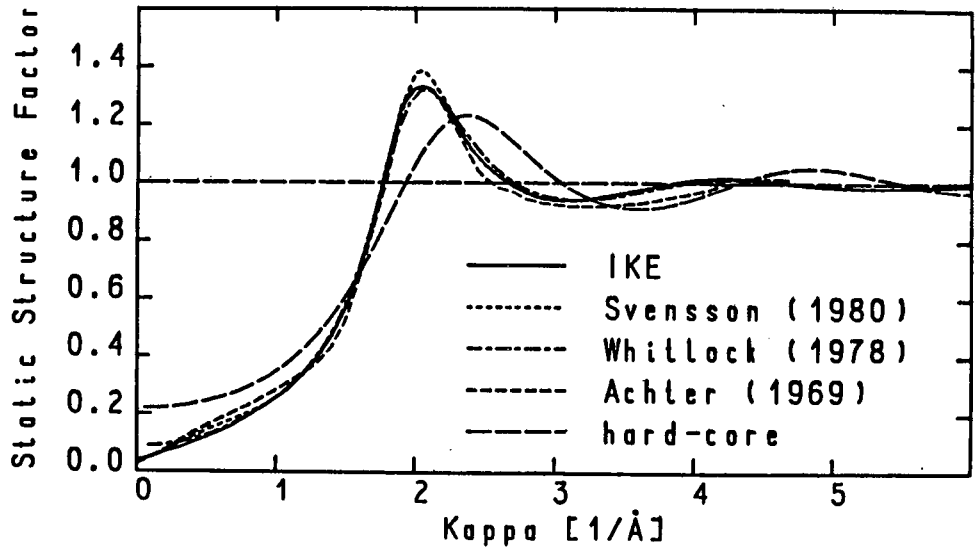

Fig. 1: Static structure factors of liquid ^{4}He around T=1 K

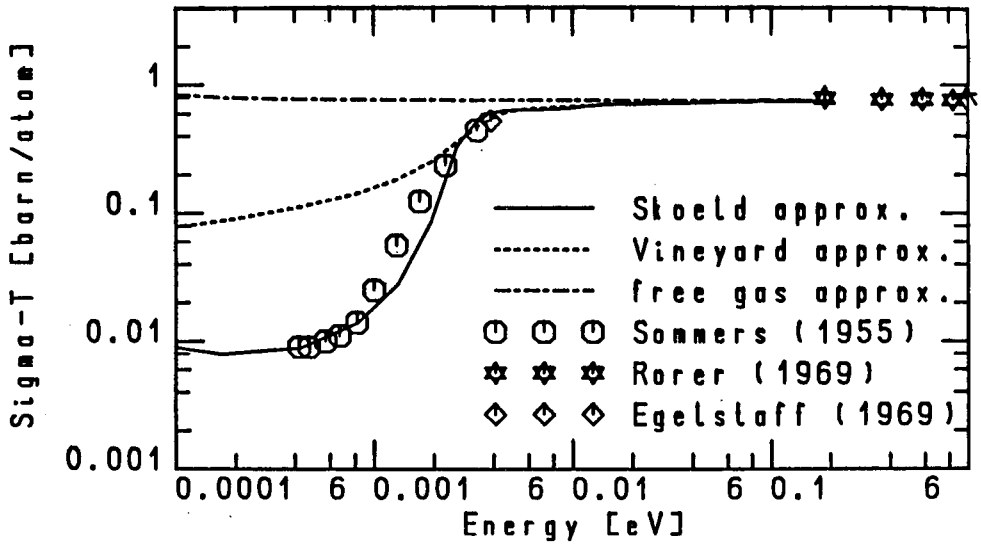

Fig. 2: Comparison of different approximations based on the IKE model for $S(\kappa)$ with experiments for the total neutron cross section of ^{4}He around T=1 K

References:

[1] Bernnat, W.; Emendörfer, D.; Keinert J.; Mattes M.: Flüssigkeitsmodelle für die Neutronenstreuung an Wasserstoff und Deuterium unter Berücksichtigung der innermolekularen und zwischenmolekularen Interferenz.
Stuttgart: IKE 6-175 (1989)

PHYSIKALISCH TECHNISCHE BUNDESANSTALT BRAUNSCHWEIG

1. Neutron Data

1.1 Measurement of the $^{12}C(n,\alpha)^{9}Be$ Cross Section via the Inverse Reaction $^{9}Be(\alpha,n)^{12}C$

D. Schmidt, R. Böttger, H. Klein, R. Nolte

Angular distributions of the reaction $^{9}Be(\alpha,n)^{12}C_{g.s.}$ are measured at laboratory angles between 0 deg. and 157 deg. and incident alpha energies E_α = 10.42 MeV and 12.61 MeV, respectively.

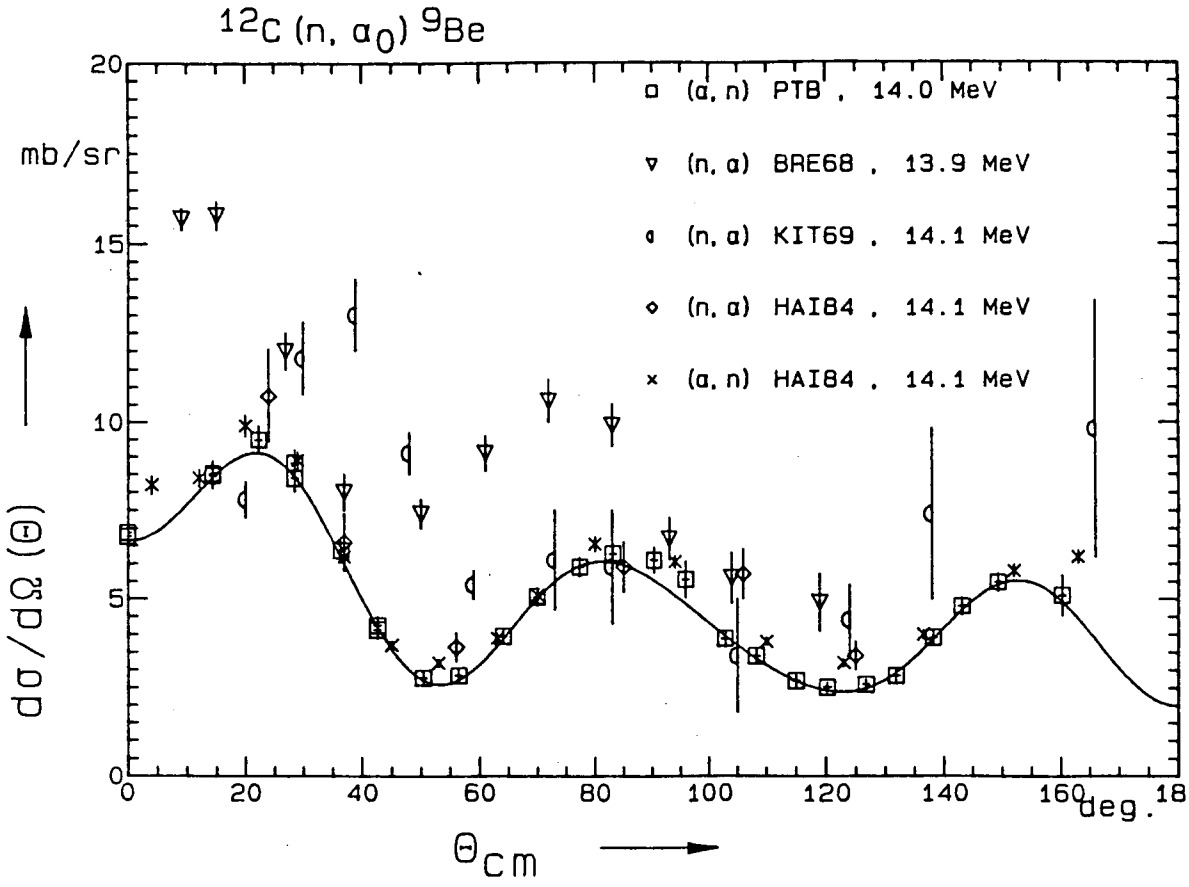

Fig. 1 Angular distribution of the $^{12}(C_n,\alpha)^{9}Be_{g.s.}$ reaction (PTB = this work). The curve is the Legendre expansion least-squares fit to our data; other data from Refs. [1] (BRE68), [2] (KIT69) and [3] (HAI84).

The aim of this work is to make a detailed analysis of error sources to obtain differential cross section uncertainties less than 5 %. In connection with a precise neutron energy threshold determination using a ^{252}Cf source, the efficiency calculated with the Monte Carlo code NEFF is known with an uncertainty of 2 %. The target mass was determined absolutely by weighting. Some measurements were carried out to check the homogeneity of the target layers as well as to test the target masses of the various targets in relation to each other. The target mass is therefore known with an uncertainty of 3 %.

For practical applications, the cross sections of the reaction $^{12}C(n,\alpha)^{9}Be_{g.s.}$ were derived using the detailed balance theorem. In this way accurate data at equivalent incident neutron energies E_n = 14.01 MeV and 15.65 MeV are available. As an example Fig. 1 shows the angular distribution measured in this work and data taken from the literature at neutron energies near 14 MeV.

1.2 Cross Sections for the $^{58}Ni(n,p)^{58}Co$ and $^{93}Nb(n,2n)^{92}Nb^{m}$ Reactions

W. Mannhart, D. Schmidt, R. Nolte

Within the framework of an international comparison of activation cross section measurements, the neutron cross sections for $^{58}Ni(n,p)^{58}Co$ and $^{93}Nb(n,2n)^{92}Nb^{m}$ were measured between 8.5 and 13.5 MeV. With a deuterium gas target, neutrons were generated with the $D(d,n)^{3}He$ reaction. The measurements were performed relative to the $^{238}U(n,f)$ fission cross section with a low-mass fission chamber acting as a neutron fluence monitor. The results together with those of the other participating laboratories were published in a recent paper [4]. A detailed documentation of the present experiment is in progress.

1.3 Cross Sections for $^{54}Fe(n,\alpha)^{51}Cr$, $^{54}Fe(n,p)^{54}Mn$ and $^{56}Fe(n,p)^{56}Mn$

W. Mannhart, G. Börker, G. Müller

Neutron cross sections for $^{54}Fe(n,\alpha)^{51}Cr$, $^{54}Fe(n,p)^{54}Mn$ and $^{56}Fe(n,p)^{56}Mn$ were determined between 9.1 and 14.6 MeV. Neutrons were produced via the $D(d,n)^{3}He$ reaction. The neutron fluence was monitored with the $^{27}Al(n,\alpha)^{24}Na$ reaction. The corrections for breakup neutrons from the D(d,np) reaction were carefully investigated and checked by a comparison with other data obtained at 14.7 MeV with the $T(d,n)^{4}He$ neutron-producing reaction. The data given in the present

work together with a supplementary experiment performed between 5.3 and 9.8 MeV at the Argonne National Laboratory were recently published [5]. A full docoumentation of the present data is being made.

1.4 ENDF/B-VI Evaluation of the Prompt Neutron Spectrum of Spontaneous Fission of ^{252}Cf

W. Mannhart

The previous evaluation of the ^{252}Cf fission neutron spectrum based on neutron time-of-flight experiments [6, 7] has been adopted for inclusion in the ENDF/B-VI library. The data will be given in the NSUB = 4 sublibrary of radioactive decay data. For this purpose the existing data were transformed to the ENDF/B-VI formats. The evaluation comprises the pointwise neutron spectrum between 0 and 20 MeV and an associated covariance matrix of the spectral data. The original data structures and the interpolation rules were slightly modified to fit the data into the required formats.

1.5 Dosimeter and Spectrometer Calibration by Iron-Filtered Neutrons: Investigation of the Total Cross-Section of Iron

W.G. Alberts, E. Dietz, K. Knauf, M. Matzke, A. Plewnia, G. Urbach, J. Wittstock

Filtered reactor neutrons produce neutron spectra with narrow, separated peaks. The peak energies and the shape of the spectra are determined by the total cross section of the filter material. Such spectra are used for calibrating neutron dosemeters and neutron spectrometers, in particular for the study of detector response functions. The spectra can be calculated by means of the transmission function of the filter provided that the incident neutron spectrum is known. The reliability of transmission calculations was previously checked by comparing transmission measurements with a filter consisting of 352 mm Fe + 230 mm Al + 75 mm S (the original PTB filter set-up [8]) using time-of-flight spectrometry at the GELINA accelerator [9] with calculations using JEF-1 cross section data [10]. These investigations showed good agreement between the measured and the calculated peak area integral at the main energy of the filter (24 keV) but revealed discrepancies at higher energies (e.g. up to 50 % at the 128 keV line). To explain the discrepancies the spectrum of iron-filtered neutrons was measured

between 10 keV and 1 MeV at the PTB reactor. It then was compared with calculations using the total cross section of iron given in the JEF-1 cross section library. Three iron cylinders (Armco) with lengths of L = 352 mm, L = 482 mm and L = 672 mm were investigated in succession. The measurements were carried out by means of proton recoil and ^{3}He proportional counters. Assuming that the neutron spectrum at the reactor-sided end of the filter is constant in the energy range of a peak, the transmission function and its integral over the peak area were calculated for 10 peaks and compared with the measurement results. Similar discrepancies as in the time-of-flight experiments were found. These differences between measurement and calculations can be removed by multiplying the total cross section of iron in the respective dips with a scaling factor K. Table 1 shows the results.

Table 1 Scaling factor K for the total cross section of iron for the energy ranges covered in the experiment

E_n in keV	18.5 - 29	53 - 89	114 - 151	155 - 198
K	1.07	1.08	1.09	1.06
E_n in keV	206 - 232	256 - 288	288 - 329	329 - 396
K	1.03	1.03	1.05	1.04
E_n in keV	680 - 720	893 - 1003		
K	1.05	1.00		

The uncertainties of the total cross section values in the JEF-1 library are expected to be in the range covered by the scaling factor K in Table 1. The relatively small increase in the cross sections leads to a considerable decrease in the transmission functions due to their exponential behaviour. The results of these investigations show that the position in energy of the peaks in the filtered spectrum can be well calculated, its amplitude, however, with good accuracy only for well-known total cross sections. It is intended to perform further calculations with the ENDF-B/VI cross section library.

2. Radionuclide Data

2.1 Half-lives

H. Schrader

Half-life values were obtained by following the radioactive decay with an ionization chamber [11]. New results will be reported for ^{90}Sr and $^{108}Ag^{m}$ at the Conference on Nuclear Data for Science and Technology [12].

2.2 Gamma- and X-ray Emission Probabilities

U. Schötzig, K. Debertin

Gamma and X-ray emission probabilities p per decay have been derived from emission rates measured with Ge and Si(Li) detectors, and activities measured with $4\pi\beta$-γ coincidence systems. Results of p will be reported for ^{56}Co, ^{57}Co (14.4 keV), ^{109}Cd, $^{123}Te^{m}$, ^{125}Sb and ^{125}I at the Conference mentioned above [12].

References

[1] M. Brendle, M. Mörike, G. Staudt, G. Steidle: Z. Naturforsch. 23a (1968) 1229
[2] H. Kitazawa, N. Yamamuro: J. Phys. Soc. Jpn. 26 (1969) 600
[3] R.C. Haight, S.M. Grimes, R.G. Johnson, H.H. Barschall: Nucl. Sci. Eng. 87 (1984) 41
[4] D.L. Smith, J.W. Meadows, H. Vonach, M. Wagner, R.C. Haight, W. Mannhart: Proc. Int. Conf. on Nuclear Data for Science and Technology, 13 - 17 May 1991, Jülich, FRG, paper O-18
[5] J.W. Meadows, D.L. Smith, L.R. Greenwood, L.P. Geraldo, W. Mannhart, G. Börker: Proc. Int. Conf. on Nuclear Data for Science and Technology, 13 - 17 May 1991, Jülich, FRG, paper O-19
[6] W. Mannhart: IAEA-TECDOC-410 (1987) 158
[7] W. Mannhart: INDC(NDS)-220/L (1989) 305
[8] W.G. Alberts, E. Dietz: Report PTB-FMRB-112, Braunschweig (1987)
[9] H.G. Priesmeyer, A. Brusegan, M. Matzke: (to be published)
[10] Index to the JEF-1 Nuclear Data Library, JEF-1 Report, NEA Data Bank, Paris (1985)
[11] H. Schrader, K.F. Walz: NEANDC(E)-292 U, Vol. V (1988) 58
[12] U. Schötzig, H. Schrader, K. Debertin: Proc. Int. Conf. on Nuclear Data for Science and Technology, 13 - 17 May 1991, Jülich, FRG, paper B-41

FACHINFORMATIONSZENTRUM KARLSRUHE

STATUS REPORT

H. Behrens, H.-W. Müller

1. Evaluated Nuclear Structure and Decay Data (ENSDF)

Nuclear Structure and Decay Data are evaluated by the International Network of Nuclear Structure and Decay Evaluators and published as the well-known Nuclear Data Sheets or in the Nuclear Physics journal. The computer readable version ENSDF contains 10,948 datasets, each representing a special type of experiment or ADOPTED LEVELS, GAMMAS properties. In total the file comprises 958,606 records of 80 bytes length.

As a contribution of the Fachinformationszentrum, the following mass chains have been evaluated and included in the ENSDF file:

Nuclear Data Sheets for A = 85
H. Sievers
Nuclear Data Sheets 62, 271 (1991)

Nuclear Data Sheets for A = 87
H. Sievers
Nuclear Data Sheets 62, 327 (1991)

Nuclear Data Sheets Update for A = 91
H.-W. Müller
Nuclear Data Sheets 60, 835 (1990)

With these mass chains the Fachinformationszentrum completed its active contribution to nuclear structure and decay data evaluations.

2. Catalog of Gamma Rays and Alpha Particles from Radioactive Decay (GAMCAT)

GAMCAT is a database system for personal computers, based on a compilation of gamma and alpha rays originating from radioactive decay. It is designed for the use of scientists and technicians engaged in quantitative assay of radionuclides, such as activation analysis, cross-section measurements, environmental pollution control, or waste composition control by means of gamma or alpha spectrometry. GAMCAT is also a helpful tool in nuclear spectrometry where it can be used, for example, to identify gamma or alpha rays emitted from daughter nuclei or source impurities. The content is as follows:

Nuclide file	2,587 nuclides
Gamma ray file	46,950 gammas
Alpha file	1,904 alpha lines

GAMCAT is available on two HD floppy disks from the Fachinformationszentrum. The system runs on an AT-compatible computer with hard disk and 640 K of memory, operating under DOS 2.11 or later. 2 Mbyte of storage are needed on the hard disk.

3. Data Compilations

A further issue with nuclear data appeared in our series PHYSICS DATA:

Evaluation of cross sections for 14 important neutron-dosimetry reactions
M. Wagner, H. Vonach, A. Pavlik, B. Strohmaier, S. Tagesen, J. Martinez-Rico
PHYSIK DATEN/PHYSICS DATA 13-5 (1990)

APPENDIX

Addresses of Contributing Laboratories

Institut für Kernphysik III
Director: Prof. Dr. G. Schatz
Senior reporter: Dr. F. Käppeler
Kernforschungszentrum Karlsruhe
Postfach 3640
W-7500 Karlsruhe

Institut für Materialforschung I
Director: Prof. Dr. Zum Gahr
Senior reporter: Dr. S. Cierjacks
Kernforschungszentrum Karlsruhe
Postfach 3640
W-7500 Karlsruhe

Institut für Neutronenphysik und Reaktortechnik
Director: Prof. Dr. G. Kessler
Senior reporter: Dr. F. Fröhner
Kernforschungszentrum Karlsruhe
Postfach 3640
W-7500 Karlsruhe

Institut für Chemie (1): Nuklearchemie
Director: Prof. Dr. G. Stöcklin
Senior reporter: Dr. S.M. Qaim
Forschungszentrum Jülich
Postfach 1913
W-5170 Jülich

Institut für Kernphysik,
Arbeitsgruppe Strahlungstransport
Head and senior reporter: Dr. D. Filges
Forschungszentrum Jülich
Postfach 1913
W-5170 Jülich

Bereich Reaktorphysik
Head and senior reporter: Dr. K. Dietze
Zentralinstitut für Kernforschung Rossendorf
Bautzner Landstraße
O-8101 Rossendorf b. Dresden

Abteilung Nukleare Analytik
Head and senior reporter: Prof. Dr. H. Bruchertseifer
Zentralinstitut für Isotopen- und Strahlenforschung
Permoserstr. 15
O-7050 Leipzig

Institut für Kern- und Atomphysik
Director: Prof. Dr. D. Seeliger
Senior Reporter: Dr. H. Märten
Technische Universität Dresden
Mommsenstr. 13
O-8027 Dresden

Zentraleinrichtung für Strahlenschutz
Head and senior reporter: Prof. Dr. H. Michel
Universität Hannover
Am Kleinen Felde 30
W-3000 Hannover 1

Abteilung Nuklearchemie
Director: Prof. Dr. G. Stöcklin
Senior reporter: Dr. U. Herpers
Universität zu Köln
Zülpicher Str. 47
W-5000 Köln 1

Institut für Kernchemie
Director: Prof. Dr. G. Herrmann
Senior reporter: Prof. Dr. H.O. Denschlag
Universität Mainz
Fritz-Strassmann-Weg 2
W-6500 Mainz

Fachbereich Physik der
Technischen Universität München
Abteilung E14, Forschungsreaktor
Senior reporter: Dr. W. Waschkowski
W-8046 Garching/München

Institut für Kernenergetik und Energiesysteme
Director: Prof. Dr. A. Schatz
Senior reporter: Dr M. Mattes
Universität Stuttgart
Pfaffenwaldring 31/35
W-7000 Stuttgart 80 (Vaihingen)

Physikalisch-Technische Bundesanstalt
Abteilung 6, Atomphysik
Director: Prof. Dr. R. Jahr
Bundesallee 100
W-3300 Braunschweig

Fachinformationszentrum Energie, Physik, Mathematik
Directors: Dr. W. Rittberger, E.-O. Schulze
Senior reporter: Dr. H. Behrens
Kernforschungszentrum
W-7514 Eggenstein-Leopoldshafen